Distribution Agreement

In presenting this thesis or dissertation as a partial fulfillment of the requirements for an advanced degree from Emory University, I hereby grant to Emory University and its agents the non-exclusive license to archive, make accessible, and display my thesis or dissertation in whole or in part in all forms of media, now or hereafter known, including display on the world wide web. I understand that I may select some access restrictions as part of the online submission of this thesis or dissertation. I retain all ownership rights to the copyright of the thesis or dissertation. I also retain the right to use in future works (such as articles or books) all or part of this thesis or dissertation.

Signature:

_____ 04.12.2017

Kornelia Galior Date

Protein-based Tension Probes: From Mapping Integrin Adhesion Forces to the Mechanopharmacology of Smooth Muscle Cells

By

Kornelia Galior

Doctor of Philosophy

Chemistry

_____

Khalid Salaita
Advisor

_____

Vince Conticello
Committee Member

_____

David Lynn
Committee Member

Accepted:

_____

Lisa A. Tedesco, Ph.D.
Dean of the James T. Laney School of Graduate Studies

_____

Date

Protein-based Tension Probes: From Mapping Integrin Adhesion Forces to the Mechanopharmacology of Smooth Muscle Cells

By

Kornelia Galior

B.S. Appalachian State University, 2010

Advisor: Khalid Salaita, Ph.D.

An abstract of

A dissertation submitted to the Faculty of the

James T. Laney School of Graduate Studies of Emory University

in partial fulfillment of the requirements for the degree of

Doctor of Philosophy

in Chemistry

2017

Abstract

Protein-based Tension Probes: From Mapping Integrin Adhesion Forces to the Mechanopharmacology of Smooth Muscle Cells

By Kornelia Galior

Cells constantly sense and translate mechanical forces into biochemical signals as part of their normal physiology, thus regulating processes that range from cell adhesion to differentiation and migration. Misregulation in the ability to sense and respond to mechanical cues contributes to a number of diseases including cancer cell invasion and atherosclerosis. While much is known about the identity and spatial localization of proteins within the cell, there is limited knowledge about the mechanical state of proteins. This dissertation presents the development and application of protein-based sensors to map and better understand the forces that regulate mechanotransduction pathways at the single cell level.

Chapter 1 describes the biological motivation for studying mechanical forces in living cells. The chapter also compares different methods that were developed to understand the coupling between mechanical forces and biochemical signaling.

Chapter 2 describes the development of protein-based tension sensors for mapping forces exerted by the cell receptors. These sensors were engineered to measure the high magnitude traction forces applied by integrin receptors. The probes were designed with a I27 titin domain as a spring and this was flanked by a fluorophore and a quencher and immobilized onto a gold nanoparticle substrate. We observed unfolding of titin. In addition, by introducing a molecular disulfide "clamp" within the core of the titin-based sensor and monitoring the kinetics of disulfide reduction, we obtained the first quantitative measurement of integrin forces within mature adhesions.

Chapter 3 describes an application of the protein-based tension sensors for investigating the molecular mechanics associated with asthma. We discovered that asthmatic airway smooth muscle cells have a higher contractile response than normal smooth muscle cells and that this response is further enhanced in the presence of inflammatory inducers. Using the signal generated by the titin tension probe, we demonstrate the first example of conducting a mechanopharmacology measurement that uses pN scale forces as an output. The effective dose for albuterol, a bronchodilator, was quantified for human samples from patients with a history of asthma. The EC_{50} varied as a function of nicotine and NGF treatment in a manner that was patient-dependent. Thus, our approach represents an important step toward personalized mechanomedicine.

Chapter 4 explores the role of integrin-mediated tension in two cellular adhesion structures: focal adhesions and invadopodia using titin-based molecular tension probes. We quantified the integrin tension from cell lung cancer tumor spheroids. Interestingly, cells tagged as being leaders in collective invasion were found to have higher levels of integrin tension. By mapping the integrin forces in invadosomes, we found that the integrin tension is localized around the invadosome rings.

Chapter 5 concludes the thesis with a summary and an outlook for the future design and application of molecular based tension sensors.

Protein-based Tension Probes: From Mapping Integrin Adhesion Forces to the Mechanopharmacology of Smooth Muscle Cells

By

Kornelia Galior

B.S. Appalachian State University, 2010

Advisor: Khalid Salaita, Ph.D.

A dissertation submitted to the Faculty of the

James T. Laney School of Graduate Studies of Emory University

in partial fulfillment of the requirements for the degree of

Doctor of Philosophy

in Chemistry

2017

Acknowledgements

First and foremost, I would like to express my special appreciation and thanks to my advisor, Dr. Khalid Salaita, for not only allowing me to join his amazing lab, but also for his wonderful guidance during my Ph.D. career and for supporting my attendance at various conferences. He is the most enthusiastic and supportive Ph.D. advisor I could have asked for. He guided me through these years with patience, motivation, and immense knowledge and I feel very honored to earn my Ph.D. degree under his guidance. I would also like to thank my thesis committee members, Dr. David Lynn and Dr. Vince Conticello, for their insightful comments and ongoing encouragement over the years! I am thankful for the delightful conversations with Dr. Lynn throughout these years, and grateful that he always kept his office door open and welcomed me with heartwarming enthusiasm! I also wish to express a sincere thank you to my wonderful collaborator, Dr. Cherry Wongtrakool, for giving me her invaluable advice and feedback toward improving my work.

Next, I would like to thank all former and current members of the Salaita lab for making the lab like a second home for me. Special thanks go to Dr. Kevin Yehl, who helped me in the beginning of my academic career, not only with doing experiments but also with improving tennis skills. I would like to thank Victor Ma and Hanquan Su for always being extremely helpful, no matter how busy they were, and for the fun we had over great Chinese food. I would like to thank Roxy Glazier and Josh Brockman (the first BME crew) for always giving their best suggestions throughout my experiments. And of course, big thanks go to the first years, the biggest group of all, for bringing the fresh perspectives and energy into the lab. Especially, I would like to thank Nusaiba Baker for

making my last year the funniest and the most enthusiastic year I have had! I am also grateful for Ann Dasher, who always with a smile, helped me with any questions I had, and Steve Krebs who was always super nice and eager to help.

I would like to give a heartfelt thank you to my wonderful parents in Poland for their unyielding support. Words cannot express how grateful I am to my beloved mom, who always encouraged me to earn a Ph.D. degree and who is the happiest person in the word right now for my accomplishments. To my beloved dad, who was very positive and always made me laugh, thank you for cheering me up!

To Dr. Maya Styner from my previous lab at UNC Chapel Hill, who taught me the laboratory science that provided me with the great start here at Emory, thank you so much! Thank you for helping me with everything, from the moment I finished my undergraduate degree to the moment of being admitted into Mayo Clinic. You had a big impact on my road to scientific success.

And most importantly, to my wonderful boyfriend, Dr. Yang Liu, who not only taught me everything I needed to know, but who was very supportive and caring throughout my Ph.D. career, thank you! You were my extremely talented mentor when I joined the lab, and you were still helpful even after you graduated. I would not have accomplished so much without your mentorship!!

List of Frequently Used Abbreviations

Abbreviation	Full Name
ACP	acyl carrier protein
AFM	atomic force microscopy
ASM	airway smooth muscle
AuNP	gold nanoparticle
BTX	bungarotoxin
DTT	dithiothreitol
EC_{50}	half maximal effective concentration
ECM	extracellular matrix
EGF	epidermal growth factor
EGFR	epidermal growth factor receptor
FA	focal adhesion
FAK	focal adhesion kinase
FN	fibronectin
FRET	förster resonance energy transfer
MLA	methyllycaconitine
MLCK	myosin light chain kinase
MMP	matrix metalloproteinase
mPADs	micropost array detector
MTFM	molecular tension-based fluorescence microscopy
nAChR	nicotinic acetylcholine receptor

NSET	nanometal surface energy transfer
PA	polyacrylamide
PEG	polyethylene glycol
pN	piconewton
QE	quenching efficiency
RGD	Arg-Gly-Asp
REF	rat embryonic fibroblast
RICM	reflection interference contrast microscopy
ROCK	Rho-associated protein kinase
SMFS	single molecule force spectroscopy
sfGFP	superfolder green fluorescent protein
TFM	traction force microscopy
TIRF	total internal reflection fluorescence

Table of Contents

Chapter 1: Current methods for measuring cell-generated contractile forces 1

1.1 Introduction 2

1.1.1 The importance of mechanics in biology 2

1.1.2 Integrin-mediated mechanical sensing 3

1.2 Current techniques to probe cell mechanics 6

1.2.1 Polymer network deformation (TFM and mPADs) 6

1.2.2 Single molecular force spectroscopy (SMFS) 7

1.2.3 Molecular tension fluorescence microscopy (MTFM) 9

1.3 Aim and scope of the dissertation 13

1.5 References 15

Chapter 2: Using protein engineering to map high-magnitude integrin forces 21

2.1 Introduction 22

2.2 Results and discussion 25

2.2.1 Engineering titin as a tension probe to map integrin forces 25

2.2.2 Integrin forces irreversibly unfold sfGFP 28

2.2.3 Integrin forces unfold I27 through RGD in fibronectin 30

2.2.4 Covalently locked I27 resists complete mechanical unfolding by integrin forces 33

2.2.5 Kinetic measurements of S-S reduction to determine integrin forces 36

2.2.6 The rate of I27 unfolding is integrin subtype-dependent 39

2.3 Conclusion 40

2.4 Materials and methods 44

2.4.1 Reagents 44

2.4.2 Cell culture 44

2.4.3 Transfection 45

2.4.4 Antibody blocking 45

2.4.5 Protein engineering 45

2.4.6 Protein expression with UAA incorporation 46

2.4.7 Dye labeling 46

2.4.8 AuNP surface preparation 46

2.4.9 AFM imaging 47

2.4.10 Optical microscopy 47

2.4.11 Data analysis 47

2.4.12 Heat map generation 48

2.4.13 Ensemble fluorescence measurements for calculating quenching efficiency 48

2.5 References 50

2.6 Appendix 56

2.7 Supplementary Note 1 65

Chapter 3: Molecular tension probes as a tool to study the mechanopharmocology of airway smooth muscle cells 67

3.1 Introduction 68

3.2 Results and discussion 71

3.2.1 Myosin dependent contractile forces in human airway smooth muscle cells are transmitted across integrin receptors 71

3.2.2 Human ASM cells isolated from asthmatic patients have an enhanced integrin tension phenotype 74

3.2.3 Nicotine promotes enhancement of integrin forces and stimulates the release of matrix metalloproteinases 77

3.2.4 Role of nicotinic acetylcholine receptor (nAChR) in the transmission of contractile forces 79

3.2.5 Albuterol dose-dependently inhibits contractile forces 82

3.3 Conclusion 85

3.4 Materials and methods 86

3.4.1 Materials 86

3.4.2 Cell culture and transfection 87

3.4.3 Antibody blocking 87

3.4.4 Protein engineering and dye labeling 87

3.4.5 Fabrication of protein-AuNP surfaces 88

3.4.6 Fluorescence immunostaining protocol 89

3.4.7 Drug treatment 89

3.4.8 Kinetic experiment for force measurement 89

3.4.9 Live cell fluorescence microscopy imaging 90

3.5 References 91

3.6 Appendix 100

Chapter 4: Biological applications of MTFM sensors in cancer biology 109

4.1 Introduction 110

4.2 Results and discussion 111

4.2.1 Titin-based MTFM sensor reveals that leader and follower cell lines isolated from a 3D tumor spheroids have different mechanical phenotypes ...111

4.2.2 Leader cell invasion is mediated through focal adhesion signaling pathway 114

4.2.3 Myosin-mediated integrin tension regulates invadosome ring dynamics 116

4.2.4 Invadosome movement in the cytoplasm is highly dynamic and is regulated by the integrins and focal adhesion signaling pathway 120

4.3 Conclusion 121

4.4 Methods and materials 123

4.4.1 Reagents 123

4.4.2 Cell culture 123

4.4.3 Antibody blocking 123

4.4.4 Protein expression and dye labeling 124

4.4.5 Fabrication of protein-AuNP surfaces 124

4.4.6 Live cell fluorescence microscopy imaging 125

4.5 References 126

4.6 Appendix 129

Chapter 5: Conclusions and perspectives 131

5.1 Summary 132

5.2 Future directions 134

5.3 Other contributions 138

5.4 References 139

List of Figures

Figure 1.1 Schematic illustration of the $\alpha_v\beta_3$ integrins in their inactive and active conformations 4

Figure 1.2 Schematic model of integrin-mediated focal adhesions 5

Figure 1.3 Comparison between focal adhesions and invadopodia 6

Figure 1.4 Current strategies to measure mechanical forces 8

Figure 1.5 Schematic illustration of the MTFM sensor and its mechanism of action 10

Figure 1.6 Schematic illustrations and representative images of the first MTFM probes developed in our lab 11

Figure 2.1 I27-based MTFM probes reveal integrin forces within FAs 27

Figure 2.2 Integrin forces irreversibly quench and unfold sfGFP 30

Figure 2.3 Integrin forces unfold I27 through RGD and FN(9-10) ligands 32

Figure 2.4 Covalently locked I27 resists complete mechanical unfolding by integrin forces 35

Figure 2.5 Kinetic measurements of S-S reduction to determine integrin forces ..39

Figure A2.1 Characterization of RGD-ACP(488)-I27 MTFM sensor 56

Figure A2.2 Characterization of RGD-sfGFP-I27 MTFM sensor 57

Figure A2.3 Characterization of RGD-Cy3-I27 MTFM sensor 58

Figure A2.4 Characterization of FN(9-10)-I27 and FN(9-10, RGE)-I27 MTFM sensors 59

Figure A2.5 Characterization of RGD-Cy3-I27G32C-A75C MTFM sensor clamped with disulfide bridge 60

Figure A2.6 Flow chart describing the analysis used for estimating integrin forces from the rate of disulfide reduction 62

Figure A2.7 Inhibition of integrin function by monoclonal antibodies specific for $\alpha_v\beta_3$ and $\alpha_5\beta_1$ 64

Figure 3.1 Mapping human airway smooth muscle cell integrin forces using titin-based probes 73

Figure 3.2 Integrin mediated forces are enhanced in the asthmatic human ASM cells and in the presence of nicotine 76

Figure 3.3 α7 nicotinic acetylcholine receptors mediate the transmission of force through the integrins in ASM cells. 81

Figure 3.4 Albuterol does-dependently inhibits contractile forces in both normal and asthmatic ASM cells treated with and without nicotine 84

Figure A3.1 Tension signals are specifically generated through integrin-RGD interactions and are mediated by the cytoskeleton 100

Figure A3.2 Asthmatic human ASM cells have higher levels of contractile proteins and exert higher magnitude of forces compared to normal human ASM cells ... 102

Figure A3.3 Changes in morphology and gene expression of human ASM cells incubated with and without nicotine for 72 h 103

Figure A3.4 Chronic treatment of human ASM cells with nicotine causes a release of matrix metalloproteinases (MMP) 104

Figure A3.5 Nicotinic acetylcholine receptor (nAChR) is colocalized with the focal adhesion proteins 106

Figure A3.6 Dose dependent curves of integrin mediated tension with and without the chronic treatment of nicotine (50 μg/ml) for 72 h 107

Figure 4.1 Representative confocal microscopy images of H1299 spheroids embedded in a 3D gel and imaged before and after 18 hours 111

Figure 4.2 Representative confocal images of purified H1299 follower and leader cells 112

Figure 4.3 Representative RICM and tension images of H1299 follower and leader cells plated on the RGD-A647-I27 probe for 2 h 113

Figure 4.4 Representative immunofluorescence images of pFAK^{Y397} in H1299 follower and leader spheroids after 24 h of invasion 114

Figure 4.5 Representative RICM and fluorescence images of H1299 purified leader cells plated on the RGD-A647-I27 tension sensor incubated in the presence of either DMSO control or PF-562271 FAK inhibitor 115

Figure 4.6 Representative image and subsequent TFM analysis of podosome ring that is exerting traction stresses on the substrate during movement in the cytoplasm 116

Figure 4.7 Integrin tension around invadosome rings is mediated through the cytoskeleton 119

Figure 4.8 Integrin tension and actin dynamics during invadosome movement in the cytoplasm 122

Figure A4.1 Integrin tension around invadosomes is mediated through cytoskeleton 129

Figure A4.2 Invadosome formation is enhanced in the absence of FAK and is mediated through β_1 integrin subtype.....130

Figure 5.1 Representative single molecule force curves of spectrin dimer and xynalase monomer 135

List of Tables

Table 1.1 Summary of methods for measuring integrin-mediated forces 13

Table 2.1. Values for E_a, Δx and A calculated from Arrhenius kinetic models.....37

Chapter 1: Current methods for measuring cell-generated contractile forces

1.1 Introduction

1.1.1 The importance of mechanics in biology

Mechanical force plays an important role for the survival of many, if not all, living systems. Many fundamental biological processes ranging from embryonic development and cell division to gene expression require mechanical cues. For example, cell-generated forces and changes in matrix mechanics are important for proper tissue development and patterning during embryogenesis[1-2]. Throughout adult physiology, effects of mechanical forces on organ development is prominent in the cardiovascular system, where the morphology and physiology of the heart and vasculature are influenced by stretch and shear stress from circulatory pressure and flowing blood.[3-4] In addition, lung physiology is regulated by stretching forces from air inhalation,[5] whereas mechanical loads from gravity and exercise are crucial for bone growth and maintenance by steering bone marrow stem cells away from the fat lineage.[6-7]

The conversion of mechanical force into biochemical signals that elicit specific cellular responses is called mechanotranduction. Cells sense and respond to the physical cues of the surrounding extracellular matrix (ECM) and neighboring cells by activating intracellular signaling pathways that ultimately regulate adhesion, proliferation and differentiation.[8] Dysfunctional mechanotransduction can contribute significantly to an array of diseases, including heart failure, deafness, atherosclerosis, or asthma. Moreover, cancer progression has been associated with the tissue rigidity or ECM stiffeness.[9] Reciprocally, cells can apply force on their surrounding environment in response to specific chemical signals. For example, a release of transforming growth factor β (TGF-β) causes remodeling of the ECM by the cells which ultimately results in progression of

fibrotic lung disease.[10] Because of the importance of mechanics in human physiology, increasing research has focused on elucidating the mechanotransduction at the molecular level.

1.1.2 Integrin-mediated mechanical sensing

The primary membrane receptors responsible for sensing and transducing mechanical signals from the cell's external environment are integrin receptors, heterodimeric transmembrane glycoproteins.[11-12] Integrins play a tri-finctional role: they bind ligands in the ECM, link internal cytoskeleton to the ECM and regulate intracellular signaling pathways. Integrins are composed of α and β subunits and are paired from a combination of 18 α and 8 β subunits, depending on the cell type.[13] Both α and β subunits contain a short C-terminal cytoplasmic domain, a transmembrane spanning region and a long N-terminal extracellular ligand-binding domain (Figure 1.1).[14] One example of the widely distributed ECM protein that integrins bind to is fibronectin (FN). Specifically, the Arg-Gly-Asp (RGD) sequence motif located on the loop of the FN 10th domain that nearly half of the known integrins recognize. In addition, the 9th domain of fibronectin also contains a short Pro-His-Ser-Arg-Asn (PHSRN) peptide called synergy site that acts together with RGD binding site to enhance integrin-mediated cell adhesion. Integrin signaling between cell-cell and cell-ECM is bidirectional. For the outside-in mode, engagement of integrin receptors with the ligand from the ECM initiates transmission of extracellular signals across the cell membrane and the cell adjusts to those signals with its cytoskeleton; for the inside-out mode, status of actomyosin-derived forces governs the adhesion of the cell to ECM.

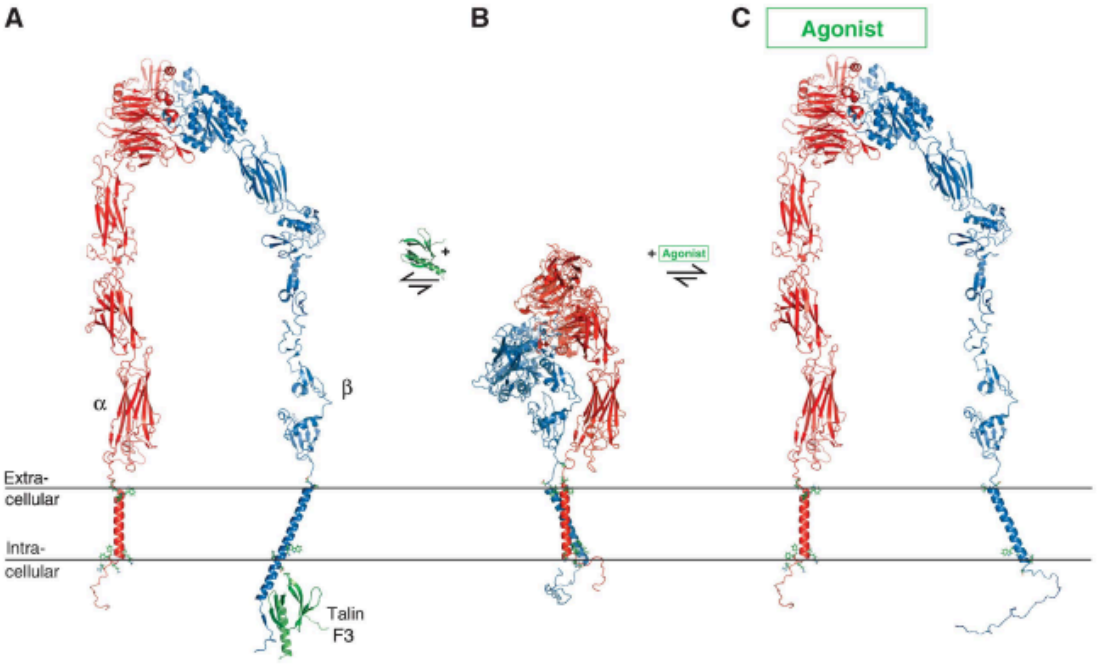

Figure 1.1 Schematic illustration of the $\alpha_v\beta_3$ integrins in their inactive and active conformations. (A) Integrins apply forces to their external environment by inside-out signaling. Talin domain (green) activates integrins by binding to β cytosolic tail which induces conformational change and activates both subtypes of integrins. (B) Integrins in their resting state. (C) Binding of integrins to their cognate ligand causes a conformational change through outside-in signaling. Reprinted from reference 14 with permission of the publisher.

Integrins spontaneously assemble into micro clusters called focal adhesions (FA). Focal adhesions are composed of more than one hundred different proteins that nucleate around integrin receptors and collectively function to physically and chemically link the cytoskeleton to the ECM (Figure 1.2 and 1.3A).[15-16] The cytoplasmic domain of integrins interact with many proteins aggregated at focal contacts, including both signaling (such as focal adhesion kinase, FAK) and cytoskeletal proteins, many of which transmit and respond to mechanical tension (such as talin, vinculin and paxillin).[17] Throughout these structures, cells can sense changes in the environment, such as substrate stiffness, rigidity, and consequently accommodate cell polarization and migration.

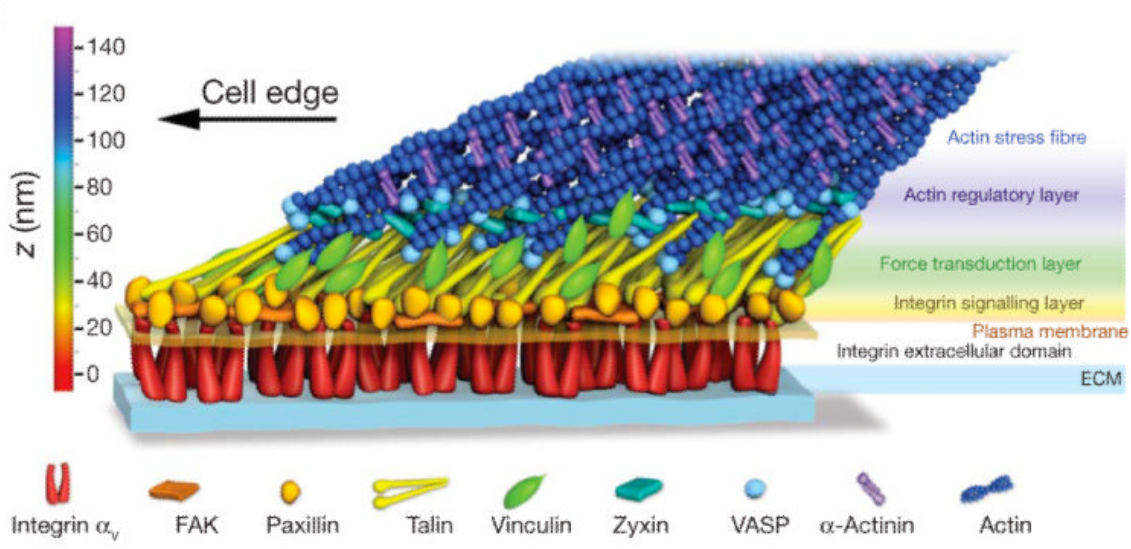

Figure 1.2 Schematic model of integrin-mediated focal adhesions. Reconstructive, super-resolution image showing the architecture of focal adhesions with corresponding proteins that mediate mechanotrasduction. Reprinted from reference 15 with permission of the publisher.

Another form of specialized, mechanosensitive cellular adhesion is called invadopodia. Invadosomes are cellular organelles that form ring-shaped filopodial-like protrusions at the apical site of tumor cells.[18] Invadosomes are highly enriched with the filamentous actin bundles that are surrounded by adhesion and scaffolding proteins and their formation is upregulated when the ECM rigidity is increased.[19-20] β_1, β_3 and β_5 integrin receptors have been identified in invadosomes and these receptors are known to recruit tyrosine kinases (such as focal adhesion kinase, FAK) and adaptor proteins (vinculin and paxillin) that are also found in FA.[21-22] After FA assembly, a release of proto-oncogene tyrosine-protein kinase SRC induces formation of invadopodia that penetrate perpendicularly into the ECM (Figure 1.3B).[23-24] Mature invadosomes mediate cell movement through the tissue microenvironments by releasing matrix metalloproteinases (MMPs) that degrade the ECM and invade surrounding

environment.[25] Invadosome rings are highly dynamic as they can expand in diameter by fusing with each other or completely disappear due to their constant remodeling.

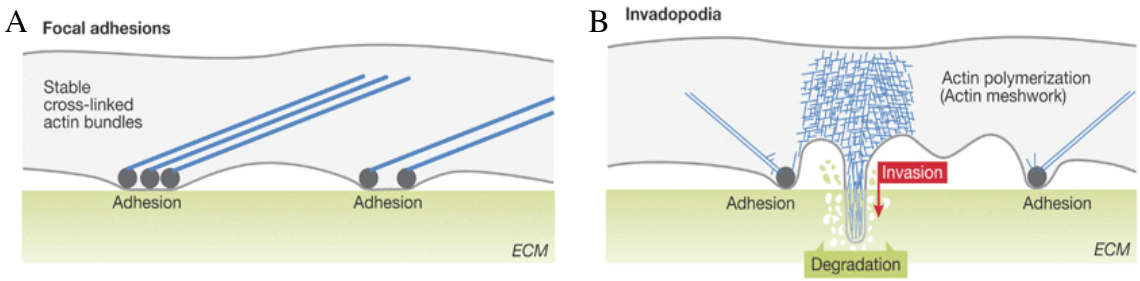

Figure 1.3 Comparison between focal adhesions and invadopodia. (A) Focal adhesions form stable attachments by anchoring long actin bundles at the interface between cell membrane and ECM. (B) Invadopodia are formed from short, disorganized actin cores that form a ring structure and degrade ECM. Reformatted and reprinted from 18 with permission of the publisher.

1.2 Current techniques to probe cell mechanics

1.2.1 Polymer network deformation (TFM and mPADs)

One of the widely-used methods to measure magnitude and directions of cellular forces is called traction force microscopy (TFM). TFM relies on culturing cells on soft compliant polymer substrates coated with ECM proteins that deform under cellular tension (Figure 1.4). Micron sized fluorescence beads are mixed into silicone or polyacrylamide substrates to track substrate displacement using optical microscopy. The maps of deformations are then converted into maps of traction forces at the specific locations using computational finite element analysis.[26] TFM estimates that forces for adhered fibroblasts range from 1 to 2 nN/μm^2, which is approximately 1 – 2 pN per integrin receptor.[27-29] A second method to measure cellular mechanics uses polydimethylsiloxane micropost arrays (mPADs) bend under cellular forces (Figure 1.4). The force can be calculated from using the known spring constant of the posts.[30] Both of

these methods (Table 1) have contributed profoundly in elucidating the mechanical role of focal adhesions in regulating cell processes. However, they have a few limitations. The cross-linked nature of the substrate, and the micrometer size of the beads and micro posts restrict the temporal and spatial details that can be obtained. Calculating the force per single receptor based on the observed deformation of the substrate is challenging because of the complicated analysis that is inherent with these methods. In addition, any small errors in measuring the bead or pillar displacement can result in large errors of force calculations. Also, the topography of the materials itself influence cellular behavior, further convoluting results. Furthermore, given the nN sensitivity of TFM and mPADs, the force resolution needs to be improved to precisely measure the tension experienced by individual integrin receptors.

1.2.2 Single molecular force spectroscopy (SMFS)

Single molecule force spectroscopy (SMFS) is an approach that dissects molecular mechanisms governing force generation at the single-molecule level with high resolution and sensitivity. SMFS employs force spectroscopic methods, such as atomic force microscopy (AFM) and optical and magnetic tweezers (Figure 1.4), to apply external forces to cells to induce cellular signalling.[31-32] AFM uses a cantilever probe to apply mechanical forces to cells and subsequently measures the forces generated by the cells.[33] Optical tweezers move a bead coated with ECM protein bound to a cell using lasers to determine cellular forces. Magnetic tweezers use similar approach as optical tweezers employing a magnetic field to pull or push the bead.[34-35] Using magnetic tweezers, Sheetz and colleagues determined that clustering of $\alpha_5\beta_1$ integrins exerts 6-fold greater forces within the cells compared to $\alpha_v\beta_3$ integrins (0.65 pN and 0.1 pN,

respectively).[36] However, SMFS techniques, though sensitive, do not recapitulate the complex environment of focal adhesions as they only investigate the mechanical event of a single biomolecule and fail to analyze the forces of an entire cell. Furthermore, the low throughput (one molecule at a time) nature of force spectroscopy has made it difficult for the wide-spread adoption.

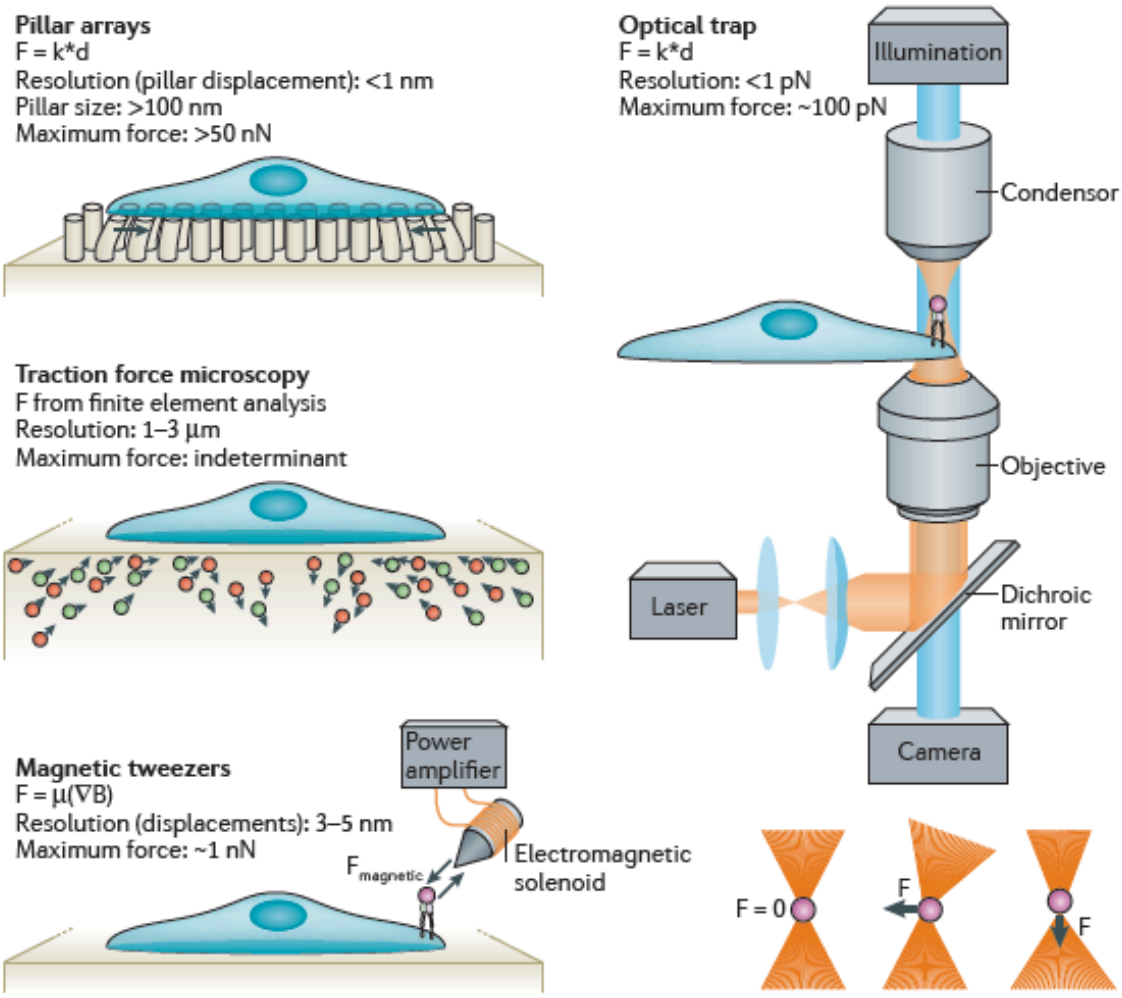

Figure 1.4 Current strategies to measure mechanical forces. Polymer network deformations strategy include pillar arrays and traction force microscopy (TFM). Pillar arrays measure bending of the microposts, whereas TFM monitors the displacement of the fluorescent beads within a hydrogel. Examples of single molecule force spectroscopy include optical and magnetic tweezers. Magnetic tweezers use magnetic beads to apply forces on a receptor, while optical traps use a focused laser beam to move a bead and generate force on the molecule. Reprinted from reference 26 with the permission of the publishers.

1.2.3 Molecular tension fluorescence microscopy (MTFM)

Over the past few years, our group has pioneered the development of molecular tension fluorescence microscopy (MTFM) probes to visualize molecular forces with high specificity in cells with the goal of better understanding the role of mechanical forces in living systems. Our molecular tension probe consists of a molecular spring such as polyethylene glycol (PEG) or oligonucleotides that are covalently conjugated to a biological ligand at one terminus and anchored onto a surface at the other terminus (Figure 1.5). The probe also employs a pair of dyes, a fluorophore and a quencher, that undergo FRET (fluorescence resonance energy transfer) to act as a spectroscopic "ruler". Mechanical tension exerted by a specific cell receptor onto the ligand will stretch the spring from its relaxed conformational state and remove the fluorophore from proximity to the quencher. This results in a turn-on fluorescence signal that provides a map of mechanical tension transduced through a specific receptor. Because the fluorescent reporter can be selected from any range of commercially available dyes that emit in the visible and near-infrared spectra, these probes can simultaneously be used with another fluorescently labeled reporter. This approach can map forces with spatial (~200 nm) and temporal resolution (~msec) in living cells (Table 1). In addition, this strategy is very sensitive with a limit-of-detection down to 1 pN, and by modifying the composition of the molecular spring, the sensor can be tuned to detect tension over a wide range of forces (1~100 pN).

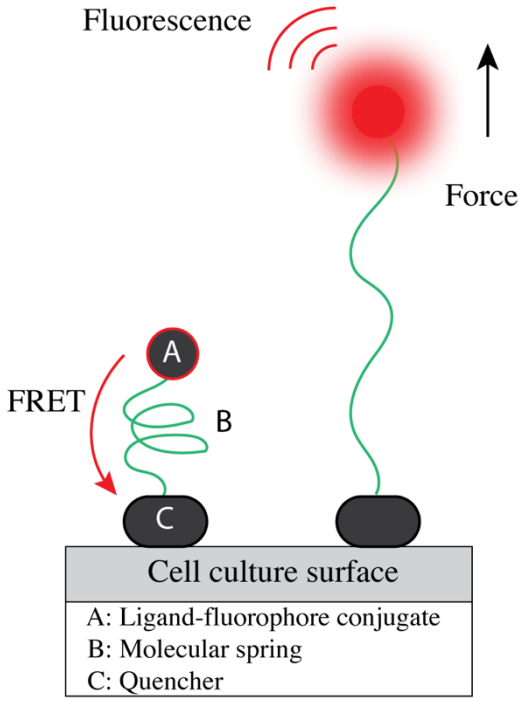

Figure 1.5 Schematic illustration of the MTFM sensor and its mechanism of action. At the resting state, the molecular spring (B) adopts a relaxed conformation, thus placing a ligand-fluorophore conjugate (A) within energy transfer distance from the quencher (C). When a force is applied through the ligand, the molecular springs unfolds, physically separating the fluorophore from proximity to the quencher and resulting in a fluorescent response.

Originally, we employed these force sensors to resolve the role of forces in endocytosis. Internalization is an essential regulatory component in many signaling pathways, and the epidermal growth factor (EGF) receptor pathway is the best studied experimental system for investigating endocytosis. A force sensor was composed of a discrete polyethylene glycol (PEG) chain that adopted a mushroom conformation and reversibly extended in response to mechanical tension. The top of the PEG chain was flanked with the fluorescently labeled EGF protein, where the biotinylated PEG tail was immobilized to a quencher-tagged streptavidin protein. Cellular forces applied to the EGF protein physically separated the fluorophore-quencher pair and displayed increased

fluorescence intensity. Therefore, for the first time, we mapped the forces associated with uptake of EGFR upon binding to its cognate ligand (Figure 1.6A). Our experiments provided the first direct evidence showing that cells exert an average force of ~ 4 pN during clathrin-mediated endocytosis of activated EGFR.[37]

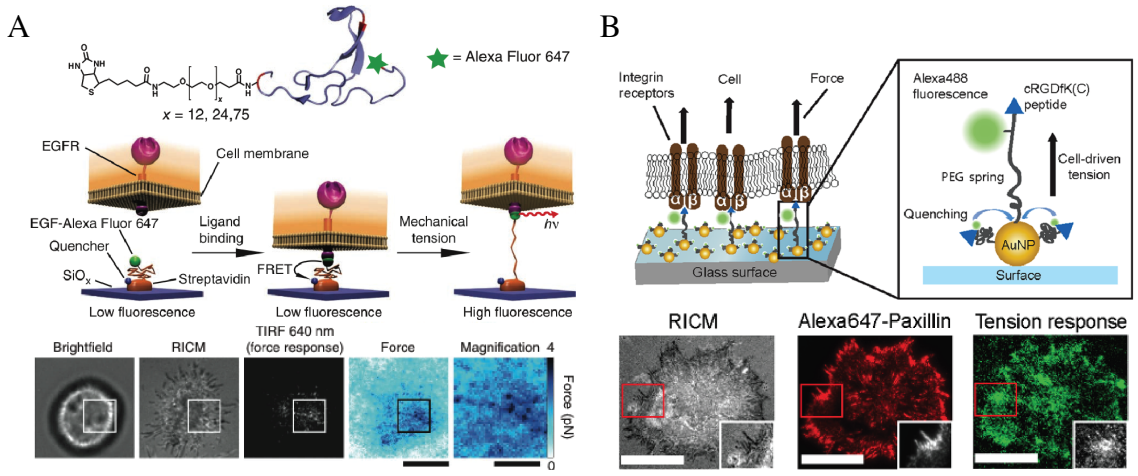

Figure 1.6 Schematic illustrations and representative images of the first MTFM probes developed in our lab. (A) PEG-based MTFM probe was used to measure forces associated with ligand-induced endocytosis of EGFR. (B) AuNP-based MTFM probe was used to measure integrin forces within focal adhesions. Reprinted from references 27 and 28 with the permission of the publishers.

Subsequently, we investigated the role of tension in the activation of integrin receptors, which are primary receptors responsible for sensing and transducing mechanical cues from the extracellular matrix (ECM). We substituted the EGF protein with a cyclized RGD peptide analogue that had been shown to bind $\alpha_v\beta_3$ and $\alpha_5\beta_1$ integrins with high affinity. The linker remained attached to the surface though biotin-streptavidin association, the strongest noncovalent bond in nature. However, when cells were cultured on this probe, integrin-mediated forces caused biotin-streptavidin dissociation, suggesting that integrin forces were significantly higher than previously

thought.[38] These results led us to search for the next generation of tension sensors where we successfully redesigned an integrin sensor by attaching a thiolated PEG polymer onto a AuNP (Figure 1.6B). We chose 15 nm gold nanoparticles because they provided not only a platform to attach the MTFM sensor but also acted as an efficient quencher. AuNP-MTFM probes were more mechanically robust, overcoming the limited stability of biotin-streptavidin. As a result, live cell experiments provided the first real-time molecular maps of integrin tension of focal adhesions measuring over 10 pN,[39-40] which had only been estimated using TFM, a bulk approach three orders of magnitude less sensitive. However, since the PEG polymer was fully extended in response to integrin forces, only the minimal integrin forces (> 10 pN) could be determined. Therefore, we reengineered the MTFM probe by incorporating a DNA hairpin varying GC content. Surprisingly, integrin forces were able to dissociate the DNA hairpin regardless of its force threshold, suggesting that integrin forces were beyond 16 pN.[41-42] Supporting these results, Ha and colleagues determined that integrin forces reach ~ 50 pN.[43] This is based on a method that quantitatively measures detachment of cells. However, this method lacks spatiotemporal resolution. In contrast, Dunn determined that integrin mediated forces are in the range of 1-5 pN.[44-46] In conclusion, multiple research groups have estimated forces exerted by integrin receptors to range over an order of magnitude from 1-50 pN. This discrepancy led us to search for the new tension probe with broader dynamic range, higher sensitivity and improved stability in order to determine the actual forces of integrins in FA.

Table 1. Summary of methods for measuring integrin mediated forces.

	Force range	Spatial resolution	Temporal resolution	Reference
TFM	2 - 120 nN	2 μm	~ sec	27 - 29
Mircopillar	50 pN - 100 nN	1 μm	~ sec	28, 30
Single molecule (AFM/Tweezers)	0.01 pN - 1 nN	1 - 20 nm	~ msec	31 - 36
MTFM	1 pN - 2 nN	200 nm	~ msec	37 - 46

1.3 Aim and scope of the dissertation

Forces generated by the cells are essential drivers of cellular development and homeostasis. Over the past two decades, several new techniques have been developed to investigate mechanical forces at the cellular level. However, current force sensing strategies lack the ability to determine the upper limits of integrin forces at the molecular level. Previous PEG- and DNA-based MTFM probes showed that integrins apply sufficient force to fully extend PEG, denature DNA hairpins, shear DNA duplexes, and dissociate the streptavidin-biotin bond. Therefore, it is necessary to develop more stable spring elements for MTFM probes.

The significance of this dissertation is the development and application of the most stable molecular force probe thus far. It reports on force transmission through a quantitative fluorescence “turn on” response in cellular physiology and pathophysiology. The key questions that can now be addressed include:

- What is the absolute magnitude of integrin forces?
- Can MTFM sensors be used for high-throughput drug screening?
- Can cancer cells be phenotyped using MTFM sensors?
- Are molecular forces exerted around invadosomes?

In brief, Chapter 2 describes the development of focal adhesion-specific mechanosensors that are compatible with forces exerted by integrin receptors. Specifically, we measured cellular transmission of forces using kinetic studies of disulfide reduction to obtain the first quantitative measurement of integrin forces within mature adhesions. Chapter 3 integrates the development of MTFM probes into high-throughput mechano-assays that measure integrin tension of airway smooth muscle cells as a novel phenotypic output for drug discovery of bronchodilators. Finally, chapter 4 describes a mechanobiology study of invadosome using MTFM sensor, where the role of integrin-mediated forces in the formation and regulation of invadsomes is closely examined.

1.4 References

1. Mammoto, T.; Ingber, D. E., Mechanical control of tissue and organ development. *Development* **2010,** *137* (9), 1407-20.

2. Grill, S. W.; Hyman, A. A., Spindle positioning by cortical pulling forces. *Dev Cell* **2005,** *8* (4), 461-5.

3. Chien, S., Mechanotransduction and endothelial cell homeostasis: the wisdom of the cell. *Am J Physiol Heart Circ Physiol* **2007,** *292* (3), H1209-24.

4. Hahn, C.; Schwartz, M. A., Mechanotransduction in vascular physiology and atherogenesis. *Nat Rev Mol Cell Biol* **2009,** *10* (1), 53-62.

5. Tschumperlin, D. J.; Boudreault, F.; Liu, F., Recent advances and new opportunities in lung mechanobiology. *J Biomech* **2010,** *43* (1), 99-107.

6. Rangaswami, H.; Schwappacher, R.; Marathe, N.; Zhuang, S.; Casteel, D. E.; Haas, B.; Chen, Y.; Pfeifer, A.; Kato, H.; Shattil, S.; Boss, G. R.; Pilz, R. B., Cyclic GMP and protein kinase G control a Src-containing mechanosome in osteoblasts. *Sci Signal* **2010,** *3* (153), ra91.

7. Huiskes, R.; Ruimerman, R.; van Lenthe, G. H.; Janssen, J. D., Effects of mechanical forces on maintenance and adaptation of form in trabecular bone. *Nature* **2000,** *405* (6787), 704-6.

8. Hoffman, B. D.; Grashoff, C.; Schwartz, M. A., Dynamic molecular processes mediate cellular mechanotransduction. *Nature* **2011,** *475* (7356), 316-23.

9. Discher, D. E.; Janmey, P.; Wang, Y. L., Tissue cells feel and respond to the stiffness of their substrate. *Science* **2005,** *310* (5751), 1139-43.

10. Leask, A.; Abraham, D. J., TGF-beta signaling and the fibrotic response. *FASEB J* **2004,** *18* (7), 816-27.

11. Schwartz, M. A.; DeSimone, D. W., Cell adhesion receptors in mechanotransduction. *Curr Opin Cell Biol* **2008,** *20* (5), 551-6.

12. Schwartz, M. A., Integrins and extracellular matrix in mechanotransduction. *Cold Spring Harb Perspect Biol* **2010,** *2* (12), a005066.

13. Seong, J.; Wang, N.; Wang, Y., Mechanotransduction at focal adhesions: from physiology to cancer development. *J Cell Mol Med* **2013,** *17* (5), 597-604.

14. Lau, T. L.; Kim, C.; Ginsberg, M. H.; Ulmer, T. S., The structure of the integrin alphaIIbbeta3 transmembrane complex explains integrin transmembrane signalling. *EMBO J* **2009,** *28* (9), 1351-61.

15. Kanchanawong, P.; Shtengel, G.; Pasapera, A. M.; Ramko, E. B.; Davidson, M. W.; Hess, H. F.; Waterman, C. M., Nanoscale architecture of integrin-based cell adhesions. *Nature* **2010,** *468* (7323), 580-4.

16. Humphrey, J. D.; Dufresne, E. R.; Schwartz, M. A., Mechanotransduction and extracellular matrix homeostasis. *Nat Rev Mol Cell Biol* **2014,** *15* (12), 802-12.

17. Parsons, J. T.; Horwitz, A. R.; Schwartz, M. A., Cell adhesion: integrating cytoskeletal dynamics and cellular tension. *Nat Rev Mol Cell Biol* **2010,** *11* (9), 633-43.

18. Gimona, M.; Grashoff, C.; Kopp, P., Oktoberfest for adhesion structures. *EMBO Rep* **2005,** *6* (10), 922-6.

19. Albiges-Rizo, C.; Destaing, O.; Fourcade, B.; Planus, E.; Block, M. R., Actin machinery and mechanosensitivity in invadopodia, podosomes and focal adhesions. *J Cell Sci* **2009,** *122* (Pt 17), 3037-49.

20. Alexander, N. R.; Branch, K. M.; Parekh, A.; Clark, E. S.; Iwueke, I. C.; Guelcher, S. A.; Weaver, A. M., Extracellular matrix rigidity promotes invadopodia activity. *Curr Biol* **2008,** *18* (17), 1295-9.

21. Collin, O.; Na, S.; Chowdhury, F.; Hong, M.; Shin, M. E.; Wang, F.; Wang, N., Self-organized podosomes are dynamic mechanosensors. *Curr Biol* **2008,** *18* (17), 1288-94.

22. Hoshino, D.; Branch, K. M.; Weaver, A. M., Signaling inputs to invadopodia and podosomes. *J Cell Sci* **2013,** *126* (Pt 14), 2979-89.

23. Spuul, P.; Ciufici, P.; Veillat, V.; Leclercq, A.; Daubon, T.; Kramer, I. J.; Genot, E., Importance of RhoGTPases in formation, characteristics, and functions of invadosomes. *Small GTPases* **2014,** *5*, e28195.

24. Murphy, D. A.; Courtneidge, S. A., The 'ins' and 'outs' of podosomes and invadopodia: characteristics, formation and function. *Nat Rev Mol Cell Biol* **2011,** *12* (7), 413-26.

25. Destaing, O.; Petropoulos, C.; Albiges-Rizo, C., Coupling between acto-adhesive machinery and ECM degradation in invadosomes. *Cell Adh Migr* **2014,** *8* (3), 256-62.

26. Iskratsch, T.; Wolfenson, H.; Sheetz, M. P., Appreciating force and shape-the rise of mechanotransduction in cell biology. *Nat Rev Mol Cell Biol* **2014,** *15* (12), 825-33.

27. Sabass, B.; Gardel, M. L.; Waterman, C. M.; Schwarz, U. S., High resolution traction force microscopy based on experimental and computational advances. *Biophys J* **2008,** *94* (1), 207-20.

28. Polacheck, W. J.; Chen, C. S., Measuring cell-generated forces: a guide to the available tools. *Nat Methods* **2016,** *13* (5), 415-23.

29. Schwarz, U. S.; Balaban, N. Q.; Riveline, D.; Bershadsky, A.; Geiger, B.; Safran, S. A., Calculation of forces at focal adhesions from elastic substrate data: the effect of localized force and the need for regularization. *Biophys J* **2002,** *83* (3), 1380-94.

30. Tan, J. L.; Tien, J.; Pirone, D. M.; Gray, D. S.; Bhadriraju, K.; Chen, C. S., Cells lying on a bed of microneedles: an approach to isolate mechanical force. *Proc Natl Acad Sci U S A* **2003,** *100* (4), 1484-9.

31. Tyler, W. J., The mechanobiology of brain function. *Nat Rev Neurosci* **2012,** *13* (12), 867-78.

32. Clausen-Schaumann, H.; Seitz, M.; Krautbauer, R.; Gaub, H. E., Force spectroscopy with single bio-molecules. *Curr Opin Chem Biol* **2000,** *4* (5), 524-30.

33. Marshall, B. T.; Long, M.; Piper, J. W.; Yago, T.; McEver, R. P.; Zhu, C., Direct observation of catch bonds involving cell-adhesion molecules. *Nature* **2003,** *423* (6936), 190-3.

34. del Rio, A.; Perez-Jimenez, R.; Liu, R.; Roca-Cusachs, P.; Fernandez, J. M.; Sheetz, M. P., Stretching single talin rod molecules activates vinculin binding. *Science* **2009,** *323* (5914), 638-41.

35. Jiang, G.; Giannone, G.; Critchley, D. R.; Fukumoto, E.; Sheetz, M. P., Two-piconewton slip bond between fibronectin and the cytoskeleton depends on talin. *Nature* **2003,** *424* (6946), 334-7.

36. Roca-Cusachs, P.; Gauthier, N. C.; Del Rio, A.; Sheetz, M. P., Clustering of alpha(5)beta(1) integrins determines adhesion strength whereas alpha(v)beta(3) and talin enable mechanotransduction. *Proc Natl Acad Sci U S A* **2009,** *106* (38), 16245-50.

37. Stabley, D. R.; Jurchenko, C.; Marshall, S. S.; Salaita, K. S., Visualizing mechanical tension across membrane receptors with a fluorescent sensor. *Nat Methods* **2011,** *9* (1), 64-7.

38. Jurchenko, C.; Chang, Y.; Narui, Y.; Zhang, Y.; Salaita, K. S., Integrin-generated forces lead to streptavidin-biotin unbinding in cellular adhesions. *Biophys J* **2014,** *106* (7), 1436-46.

39. Liu, Y.; Yehl, K.; Narui, Y.; Salaita, K., Tension sensing nanoparticles for mechano-imaging at the living/nonliving interface. *J Am Chem Soc* **2013,** *135* (14), 5320-3.

40. Liu, Y.; Medda, R.; Liu, Z.; Galior, K.; Yehl, K.; Spatz, J. P.; Cavalcanti-Adam, E. A.; Salaita, K., Nanoparticle tension probes patterned at the nanoscale: impact of integrin clustering on force transmission. *Nano Lett* **2014,** *14* (10), 5539-46.

41. Zhang, Y.; Ge, C.; Zhu, C.; Salaita, K., DNA-based digital tension probes reveal integrin forces during early cell adhesion. *Nat Commun* **2014,** *5*, 5167.

42. Blakely, B. L.; Dumelin, C. E.; Trappmann, B.; McGregor, L. M.; Choi, C. K.; Anthony, P. C.; Duesterberg, V. K.; Baker, B. M.; Block, S. M.; Liu, D. R.; Chen, C. S., A DNA-based molecular probe for optically reporting cellular traction forces. *Nat Methods* **2014,** *11* (12), 1229-32.

43. Wang, X.; Ha, T., Defining single molecular forces required to activate integrin and notch signaling. *Science* **2013,** *340* (6135), 991-4.

44. Morimatsu, M.; Mekhdjian, A. H.; Chang, A. C.; Tan, S. J.; Dunn, A. R., Visualizing the interior architecture of focal adhesions with high-resolution traction maps. *Nano Lett* **2015,** *15* (4), 2220-8.

45. Chang, A. C.; Mekhdjian, A. H.; Morimatsu, M.; Denisin, A. K.; Pruitt, B. L.; Dunn, A. R., Single Molecule Force Measurements in Living Cells Reveal a Minimally Tensioned Integrin State. *ACS Nano* **2016,** *10* (12), 10745-10752.

46. Morimatsu, M.; Mekhdjian, A. H.; Adhikari, A. S.; Dunn, A. R., Molecular tension sensors report forces generated by single integrin molecules in living cells. *Nano Lett* **2013,** *13* (9), 3985-9.

Chapter 2: Using Protein Engineering to Map High-Magnitude Integrin Forces

Adapted from Galior, K.; Liu, Y.; Yehl, K.; Vivek, S.; Salaita, K. Titin-based Nanoparticle Tension Sensors Map High-Magnitude Integrin Forces within Focal Adhesions. *Nano Letters* **2016**, *16* (1), 341-348, used with permission.

2.1 Introduction

Cells adhere to the extracellular matrix (ECM) through transmembrane integrin receptors consisting of an α and β subunit.[1] For example, fibronectin (FN) ECM molecules are primarily recognized by $\alpha_5\beta_1$ and $\alpha_v\beta_3$ integrins that bind the Arg-Gly-Asp (RGD) and Pro-His-Ser-Arg-Asn (PHSRN) motifs.[2] Integrin sub-type expression levels are cell type-dependent and dynamic, responding to the chemical and mechanical properties of the ECM.[3] Therefore, determining the magnitude of integrin tension and the spatial and temporal heterogeneity of these forces for different integrin subtypes will help elucidate the role of mechanics in receptor function during cell adhesion and cell migration processes. For example, the existence of heterogeneous distributions of integrin forces within nanoscale domains of a FA is unknown, and it is possible that a subset of integrin receptors experience significant magnitudes of tension that exceed the ensemble average determined by such techniques as traction force microscopy or micropillar array technology.

Integrin activation typically triggers the formation of supramolecular protein assemblies, focal adhesions (FAs), that are comprised of hundreds of different structural and signaling molecules.[4] Collectively, the FA functions to physically and chemically link the cytoskeleton to the ECM.[5] FA assembly/disassembly is highly orchestrated in space and time to accommodate cell polarization and migration activities through inside-out and outside-in signaling mechanisms.[6] While the protein composition of FAs and their dynamics are currently under active investigation, there is limited knowledge about the mechanical forces experienced and transmitted through these structures. For example, except for integrin adhesion receptors[7] and vinculin[8], to the best of our knowledge, there

are no direct measurements of the forces experienced by the hundreds of other proteins making up FAs.

The most common technique to characterize cell adhesion forces is traction force microscopy (TFM), which indicates that forces for adhered fibroblasts range from 1 to 2 nN/μm^2.[9] By estimating the number of bound integrins per unit area (1000 molecules/ μm^2 [10]), the force per receptor was also estimated at 1-2 pN per integrin.[9a] However, the challenge with TFM pertains to its limited spatial resolution (~ 1 μm) and force sensitivity (~nN) because of the crosslinked nature of the polymer. In addition, the deformable TFM substrates influence the cell biology, further convoluting the results.[11]

To address these issues, we pioneered the development of molecular tension fluorescence microscopy (MTFM)[12], which allows for optical imaging of pN-level receptor-mediated forces with high spatial and temporal resolution. MTFM probes consist of an extendable macromolecule such as polyethylene glycol (PEG) or oligonucleotides that are flanked by a fluorophore-quencher pair undergoing resonance energy transfer (RET). MTFM probes are immobilized onto a substrate and modified with a ligand, such that receptor applied tension extends the linker and dequenches the fluorophore, generating a significant increase in donor emission intensity.

To tailor MTFM probes for integrins, we previously modified the PEG_{24} polymer with the cyclic RGDfK peptide and anchored the probe using biotin-streptavidin association.[12f] Fibroblasts cultured on this probe for 45 min caused biotin-streptavidin dissociation, which is surprising because biotin-streptavidin association is often described as the strongest non-covalent bond in nature, suggesting that forces applied by integrins are significant. Nanoparticle-based MTFM probes immobilized using thiol-gold binding,

were more mechanically robust and showed that integrin forces exceed 10-15 pN in magnitude.[12d, 12e] Supporting this result, we and others observed that DNA hairpin tension probes are denatured due to integrin mediated forces, indicating forces in excess of 16 pN.[12c, 13] Likewise, tension gauge tether probes, consisting of DNA duplexes decorated with the cRGDfK peptide indicate that integrin activation is associated with peak forces up to ~50 pN in magnitude.[7] In contrast, Dunn and colleagues determined that integrin-mediated forces are in the range of 1-5 pN based on single molecule imaging of a spidersilk elastin-based tension probe.[14] Therefore, there remains some discrepancy in the reported integrin forces within FAs.

In this report, we investigate the magnitude of integrin tension within mature FAs by engineering the 27th immunoglobulin domain of cardiac titin (I27), which is structurally and mechanically well studied both experimentally[15] and through theoretical modeling[16] and displays highly reversible force-extension curves.[17] Based on single molecule force spectroscopy with constant loading rate (0.4 μm/sec), the most probable unfolding force for I27 is significantly greater (~80-200 pN)[18] when compared to DNA denaturation (~4-50 pN)[7, 12c], and spidersilk elastin extension (~2-6 pN)[14], and therefore investigating integrin forces at ranges that are greater than values studied thus far. In principle, the rate of mechanically driven protein/DNA unfolding is exponentially dependent on the applied force[19] and likewise the cumulative probability of molecular unfolding is also exponentially dependent on the duration of applied force[19] (Supplementary Note 1). Accordingly, this limits the accuracy of inferring a specific magnitude of force from determining the equilibrium distribution of unfolded probes at a given time point. Addressing this limitation, we use the kinetics of titin unfolding rather

than the equilibrium distribution of unfolded domains, to more precisely estimate the values of high-magnitude integrin forces within mature FAs and determine the relative contribution of the $\alpha_5\beta_1$ and $\alpha_v\beta_3$ integrins. In principle, this kinetic approach can be used to determine absolute integrin forces at any time point during FA maturation, thus overcoming a longstanding problem associated with the nascent field of molecular tension sensors. Finally, by employing recombinant protein expression, this work describes a facile and general approach for engineering of virtually any expressible protein ligand within MTFM probes.

2.2 Results and discussion

2.2.1 Engineering titin as a tension probe to map integrin forces

To label the I27 domain with a fluorophore, we initially introduced the acyl carrier protein (ACP)-tag near the N-terminus which can be enzymatically modified at its serine residue with a fluorophore with over 90% yield (Figure 2.1A).[20] The probe displayed the "GRGDS" motif, specific for integrins, at the N-terminus (Figure 2.1B). At the C-terminus, two cysteine residues were introduced for immobilization onto a 9 nm gold nanoparticle (AuNP, see AFM in Figure 2.1C); which serves as an efficient quencher through nanometal surface energy transfer (NSET).[12d] The RGD-ACP-I27 protein was conjugated to Alexa488, which was confirmed by SDS-Page and fluorescence spectrometry. UV-vis indicated a 90% labeling efficiency, and CD spectroscopy confirmed the secondary structure of the I27 construct at 37° C (Appendix, Figure A2.1 A-C). We initially investigated whether integrin-mediated forces would unfold the mechanically stable RGD-ACP(A488)-I27 probe (Figure 2.1B). Protein incubation conditions were optimized to ensure that probes were specifically bound

through the thiol-Au association with minimal non-specific adsorption.[21] This required incubating the AuNP surface with a binary mixture of passivating mPEG, $SH(CH_2\text{-}CH_2\text{-}O)_8COOH$, along with the RGD-ACP(A488)-I27 probe at 1:12 molar stoichiometry for 1 hr at RT. By releasing the sensor from the AuNP, we determined that each 9 nm AuNP presented an average of 5.2 sensors (Appendix, Figure A2.1D).[22] Also note that passivation was important to maintain proper orientation and function of the probe, since cells failed to engage surfaces lacking passivation with the mPEG (data not shown). With these conditions, the quenching efficiency of the ACP-tagged probes was measured at 82%, which was consistent with the dimensions of the ACP and I27 structures, and suggesting a ~7 nm fluorophore-AuNP distance.

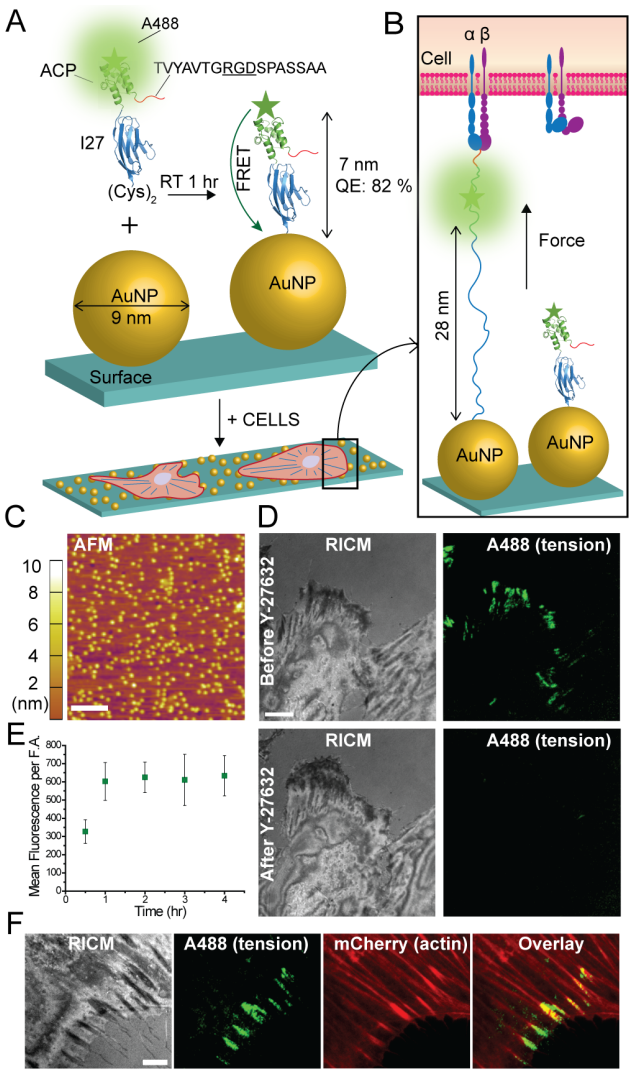

Figure 2.1 I27-based MTFM probes reveal integrin forces within FAs. (A-B) Schematic illustration showing the RGD-ACP(A488)-I27 probe and the mechanism of sensing (PDB ID: 1TIT and 2K92 for I27 and ACP, respectively). The probe is modified at the N terminus with FN binding motif TVYAVTGRGDSPASSAA. The C terminus included two cysteine residues for binding to the AuNP. (C) AFM image of 9 nm AuNPs immobilized on the glass coverslip. Scale bar, 200 nm. (D) Representative RICM and fluorescence images of cells incubated on the tension probe surface before and after treatment with a myosin inhibitor Y-27632 (40 μM) for 30 min. Scale bar, 10 μm. (E) Plot of the average fluorescence tension signal per FA as a function of time. The error bars represent the SEM from n = 5 cells at each time point. (F) Representative RICM and fluorescence images of REF cells that were transfected with mCherry-lifeact to visualize actin and mature focal adhesions. An overlay of the A488 channel with the mCherry channel demonstrates that integrins within FAs apply sufficient tension to unfold RGD-ACP(A488)-I27 sensor. Scale bar, 10 μm.

When rat embryonic fibroblasts (REFs) were incubated on the RGD-ACP(A488)-I27 probe surface for 1 hr, we observed significant signal in total internal reflection fluorescence (TIRF) that coincided with the cell edge as indicated by reflection interference contrast microscopy (RICM) (Figure 2.1D). The increase in fluorescence suggested that integrin-mediated forces unfolded the I27, the ACP domain, or both I27 and ACP domains, thus separating the Alexa488 reporter from the AuNP surface. To confirm that I27/ACP unfolding is driven by the cytoskeleton and specifically myosin II, we treated cells with the Rho-associated protein kinase (ROCK) inhibitor, Y-27632, for 30 min and re-imaged the sample. Following ROCK inhibition, the fluorescence signal was diminished (Figure 2.1D) indicating that signal is reversible and mediated by myosin contractility. Further experiments show colocalization of RGD-ACP(A488)-I27 signal with the termini of F-actin stress fibers (Figure 2.1F). Timelapse analysis of the tension probe signal indicated that fluorescence increased over a period of ~1 hr and then held steady for at least 4 hrs (Figure 2.1E). Beyond 5 hrs, we typically observe a slight decrease in tension signal, likely due to a combination of thiol displacement and protease activity. The results obtained with the RGD-ACP(A488)-I27 nanoparticle probe suggest that this protein engineering strategy is suitable for investigating integrin forces, but the poorly characterized mechanical stability of ACP made it difficult to ascertain which domains mechanically unfolded.

2.2.2 Integrin forces irreversibly unfold sfGFP

We next incorporated superfolder green fluorescent protein (sfGFP) within the I27 MTFM probe, replacing the ACP tag. sfGFP was selected due to its mechanical stability (~100 pN unfolding force[23]), increased brightness when compared to other GFP

reporters[24] and enhanced folding when fused with other proteins. The mass and fluorescence of the RGD-sfGFP-I27 construct were confirmed by SDS-Page and UV-vis (Appendix, Figure A2.2 A-C) and the probe was immobilized onto AuNPs as described above (Figure 2.2A). Surprisingly, when REF cells were cultured onto the RGD-sfGFP-I27 tension probe surface for 3 hrs, sfGFP emission was quenched at the perimeter of the cell (Figure 2.2A). Given that mechanical unfolding of GFP quenches fluorescence, we suspected that integrin-mediated forces were sufficient to unfold the β-barrel of GFP. To verify the source of sfGFP quenching, we labeled free lysine residues of the sfGFP-I27 probe with an amine-reactive Alexa647 (Figure 2.2B). In this case, REF cells showed an increase in Alexa647 signal that coincided with regions of sfGFP quenching. Moreover, treating cells with ROCK inhibitor did not reverse the quenched sfGFP, but did lead to a decrease in Alexa647 emission (Appendix, Figure A2.2D). These experiments demonstrate that integrin-mediated forces denature and irreversibly quench sfGFP, suggesting significant tension, but it remained unclear whether I27 was stable toward integrin tension.

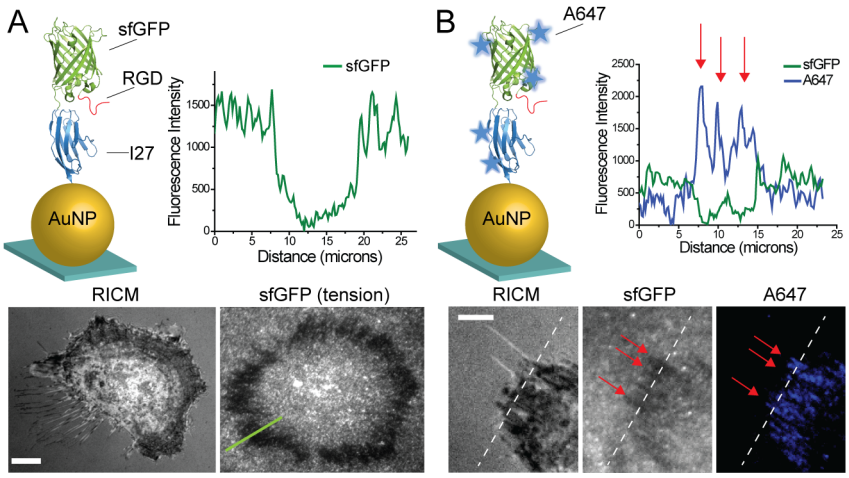

Figure 2.2 Integrin forces irreversibly quench and unfold sfGFP. (A) Schematic illustrating the RGD-sfGFP-I27 probe functionalized onto immobilized AuNPs (sfGFP PDB ID: 2B3P). Representative fluorescence and RICM images of REF cells cultured onto the RGD-sfGFP-I27 sensor surface for 3 hrs. Line scan analysis shows a loss in fluorescence at the cell edge, coinciding with the expected regions of mature FAs. (B) The RGD-sfGFP-I27 probe was non-specifically labeled with Alexa 647, purified and immobilized onto the AuNP surface. Representative RICM, GFP fluorescence and Alexa 647 fluorescence images of cells incubated on the probe surface for 3 hrs. Line scan (dashed white line) analysis through the stress fibers (red arrows) shows anti-correlation between Alexa 647 and sfGFP emission. Scale bar, 10 μm.

2.2.3 Integrin forces unfold I27 through RGD in fibronectin

Unnatural amino acid incorporation was next used to express an I27 MTFM probe labeled with the *p*-azidophenylalanine amino acid. This azide-modified protein was then modified with the Cy3 dye using Cu-free click cycloaddition coupling (Figure 2.3A). The mass of the RGD-I27 construct was confirmed by ESI-MS, the stability of the construct at 37° C was verified using CD spectroscopy and the dye labeling efficiency was confirmed using SDS-Page and UV-vis (Appendix, Figure A2.3 A-E). Quenching efficiency upon AuNP immobilization was calculated to be 92%. This quenching efficiency roughly agrees with the predicted distance between the dye and the AuNP surface (~4 nm). Within 1 hr of incubating REFs on this MTFM probe surface, we

observed Cy3 fluorescence signal at the edges of the cell, suggesting mechanically-driven I27 unfolding at these sites. Following ROCK inhibition with 40 μM of Y-27632 for 30 min, the fluorescence signal was diminished (Appendix, Figure A2.3F) showing that signal is reversible and mediated by myosin contractility. To confirm that tension signal is associated with FAs, we transfected the REFs with GFP-paxillin, a widely accepted FA marker, and found colocalization with Cy3 tension signal (Figure 2.3A). Importantly, this result unambiguously shows that the I27 domain is mechanically unfolded due to integrin forces within 1 hr of cell adhesion.

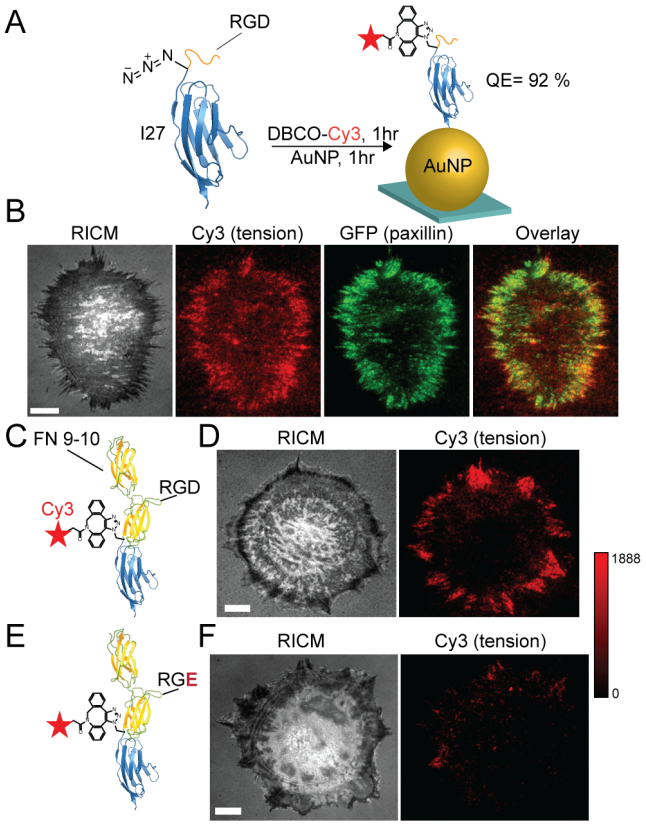

Figure 2.3 Integrin forces unfold I27 through RGD and FN(9-10) ligands. (A) Illustration of the RGD-Cy3-I27 MTFM sensor containing the p-azidophenylalanine amino acid. The dye was conjugated with Cu-free cycloaddition and was subsequently immobilized onto the AuNP surface. The quenching efficiency was 92%. (B) Representative RICM, GFP-paxillin, Cy3 tension and overlay of Cy3/GFP shows colocalization of FAs with tension. (C) Illustration of the FN(9-10)-Cy3-I27 MTFM sensor. (D) Representative RICM and fluorescence images of REF cells that were incubated on FN(9-10)-Cy3-I27 functionalized on the AuNPs for 1 hr. (E) Illustration of the FN(9-10, RGE)-I27 MTFM sensor labeled with DBCO-Cy3 where the highlighted point mutation is indicated in red. (F) Representative RICM and fluorescence images of REFs that were incubated on FN(9-10, RGE)-Cy3-I27 probe functionalized onto AuNPs for 1 hr. The range of fluorescence intensity values for (D) and (F) are identical and the values are displayed using the calibration bar (a.u.). Scale bar, 10 μm.

The RGD sequence derived from FN is widely used in model cell adhesion studies.[25] However, one persistent question is whether the linear RGD sequence recapitulates the properties of more physiologically relevant ECM proteins such as

domains of FN or full length FN. We rationalized that integrin-ligand binding and mechanics may be enhanced for FN domains compared to the RGD peptide fragment. To present more physiologically accurate ligands, the sensor was redesigned to present FN domains 9 and 10 at the N-terminus, providing both the synergy (PHSRN) and GRGDS motifs (Appendix, Figure A2.4A and B). Initial experiments using FN-Cy3-I27 probe showed similar spatial and temporal patterns of fluorescence as the RGD-Cy3-I27 probe (Figure 2.3C and 2.3D). To better understand the specificity of force transmission to the FN tension probe, we generated a control probe presenting RGE rather than the RGD sequence within the FN 10 domain (Figure 2.3E and 2.3F, Appendix, Figure A2.4C). In this case, we found that REF cells spread on the sensor surface but failed to generate a fluorescence response, thus suggesting that the RGD sequence within FN is required for triggering a chemo-mechanical response that generates sufficient tension to unfold I27.

2.2.4 Covalently locked I27 resists mechanical unfolding by integrin forces

Given that I27 unfolds within FAs, we infer that integrin forces range from ~5 pN up to ~1000 pN with the precise value depending on the loading rate and duration of the applied force. We narrowed this range of forces by measuring the initial time point of I27 unfolding following cell spreading (Supplementary Note 1). I27 probes unfold within 4 min of cell spreading over a region of interest, suggesting a minimum force of 36 pN. This value assumes an instantaneous maturation rate of FAs, which underestimates the forces applied by integrins and defines a lower estimate of integrin forces. One approach to define the upper limit of integrin tension is to challenge receptors with a probe that does not mechanically unfold. Therefore, we made use of a modified I27 which has an engineered disulfide bond buried within the core of the protein between the 32nd and

75th residues.[26] Using this reengineered I27, we generated disulfide "clamped" RGD-Cy3-$I27_{G32C-A75C}$ MTFM probe (Appendix, Figure A2.5 A and B). As illustrated in Figure 2.4A, the disulfide bond traps 43 amino acids (green) and leaves the other amino acids unsequestered (blue) under mechanical load. Mechanical extension of this clamped I27 stops at the disulfide bond, placing the dye at a distance of 12 nm, which is predicted to produce a QE of ~80%. Addition of dithiothreitol (DTT) reduction agent leads to disulfide reduction and opening of the clamp. This allows for extension of the dye away from the AuNP surface to fully dequench the fluorophore. Moreover, inhibition of cell-applied force should lead to reversible refolding of I27.

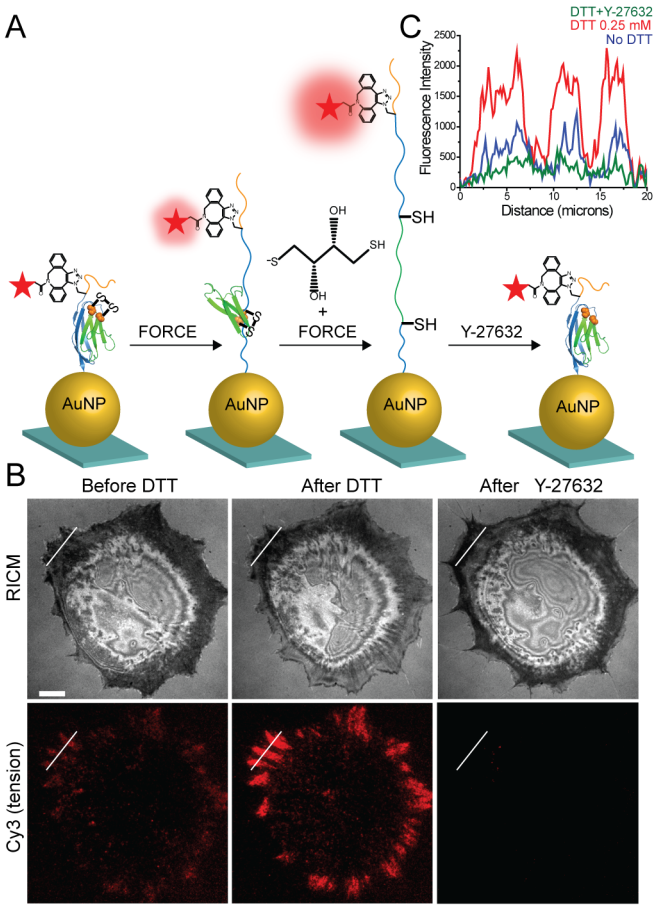

Figure 2.4 Covalently locked I27 resists complete mechanical unfolding by integrin forces. (A) Schematic illustration of disulfide clamped $I27_{G32C\text{-}A75C}$ tension sensor. The disulfide bridge is indicated by orange spheres. The probe was labeled with Cy3 dye and functionalized onto a AuNP surface (QE ~ 92%). When cells apply tension to the clamped MTFM sensor, I27 is stretched to the position of the disulfide clamp, resulting in solvent exposure of the disulfide. I27 can be further mechanically extended only in the presence of reducing agent, such as DTT. Refolding of the sensor is expected after ROCK kinase inhibitor (Y-27632) treatment. (B) Representative RICM and clamped I27 tension signal for REF cells incubated onto the sensor surface for 2 hrs before and after treatment with 0.25 mM DTT for 10 min and then after treatment with Y-27632 (40 μM) for 30 min. Scale bar, 10 μm. (C) Line scan analysis of the region of interest in (B) shows the fluorescence intensity through a FA before and after DTT addition and after Y-27632 treatment.

In a typical experiment testing the clamped RGD-Cy3-I27$_{G32C-A75C}$, REFs were plated on the probe surface for 2 hrs, resulting in a weak fluorescence signal at regions that coincided with FAs (Figure 2.4B). This signal is likely associated with partial unfolding of I27 up to the covalent "lock". Upon addition of 0.25 mM DTT, time lapse movies showed that the signal rapidly increased, suggesting reduction of the disulfide bond and complete mechanical unfolding of the clamped probe (Figure 2.4B and 2.5A). To confirm that opening of the clamped sensor is myosin driven and the signal is reversible, we treated cells with the ROCK inhibitor (Y-27632), and found that the signal was diminished below the original values, prior to DTT incubation (Figure 2.4B and 2.4C). Control experiments indicated that pretreatment of the clamped RGD-Cy3-I27$_{G32C-A75C}$ probe with 1 mM DTT for 10 min, prior to cell plating, did not lead to increase in fluorescence and did not alter probe response following cell plating (Appendix, Figure A2.5D). Treating 50 nM of clamped RGD-Cy3-I27$_{G32C-A75C}$ probe with 10 mM DTT in solution displayed ~10% reduction in emission (Appendix, Figure 2.5D) whereas probe that was immobilized to the AuNPs displayed an average of ~2% decrease in emission upon treatment with DTT. These results confirm that the buried disulfide bridge locks the I27 probe preventing mechanical unfolding, and the reduction of the disulfide bond is dependent on both the cell-applied force, and reducing agent.

2.2.5 Kinetic measurements of S-S reduction to determine integrin forces

Through a series of single molecule experiments[26-27], Fernandez and coworkers found that the rate of disulfide reduction, r, for the clamped I27 was exponentially dependent on force, in accordance with the Bell model, and they showed that r was also linearly dependent on [DTT]. These relations are: $r=k(F)[DTT]$ and $k(F) = A\ exp((F\Delta x_r$-

$E_a)/k_BT)$, where A is a pre-exponential factor, Δx_r is the distance to the transition state of the reaction, and E_a is activation energy for the disulfide bond reduction. By varying the force and [DTT], and measuring r, Fernandez and coworkers determined Δx_r, A and E_a for mechanically catalyzed disulfide reduction in I27. By using these validated constants for I27, we next inferred the magnitude of force experienced by the I27 probe by recording the rate of disulfide reduction as determined from the rate of fluorescence increase (Appendix, Figure A2.6). Although Δx_r, A and E_a were determined in three reports using different mechanical loading conditions (Table 2.1)[27a, 27d, 28], we used fitting values of A = 1.3 x 10^{12} $M^{-1}s^{-1}$, Δx_r = 0.34 Å and E_a = 65 kJ from the most relevant study where *k(F)* was determined by varying DTT concentration.[27a]

Selected Publications	E_a (kJ/mol)	Δx (Å)	A ($M^{-1}s^{-1}$)	Double-pulse force-clamp protocol	
Witta *et al. PNAS*, **2006**	65	0.34	1 x 10^{12}	First pulse at 130 pN for 1 sec, second pulse from 100-400 pN for 5-7 sec.	Varying [DTT] to determine *k(F)*
Ainavarapu *et al. JACS*, **2008**	54	0.34	1 x 10^{12}	First pulse at 150 pN for 0.5 sec or 180 pN for 0.2 sec, second pulse from 100-400 pN for 5 sec.	Constant [DTT] to determine E_a
Liang *et al. JACS*, **2011**	39	0.37	1 x 10^{9}	First pulse at 170 pN for 0.3 sec, second pulse from 100-300 pN.	Constant [DTT] to detrmine E_a and A

Table 2.1 Values for E_a, Δx and A calculated from Arrhenius kinetic models.

We recorded the rate of fluorescence increase for cells treated with DTT concentrations ranging from 0.25 mM up to 25 mM (Figure 5C; n = 25 cells total) at varying sampling frequencies in order to collect enough data points to obtain an accurate fit of the kinetic curves. By fitting the increase of fluorescence versus time, we measured the time constant of disulfide reduction, τ_r, and thus determined the rate of disulfide reduction ($r = 1/\tau_r$) from cell experiments. DTT concentrations greater than 25 mM induced a reduction in cell adhesion, suggesting cell toxicity, which is confirmed by literature studying the effect of DTT on redox signaling in fibroblasts.[29] In contrast,

treating REFs expressing GFP-β_3 with 2.5 mM DTT for 10 min did not lead to any observable change in cell morphology or GFP signal (Appendix, Figure A2.5E). To show the spatial heterogeneity of disulfide reduction rates within a single cell, we generated a heat map of rates (ranging from 0.005 to 0.05 s^{-1}) using the programming software (IDL). As the heat map suggests, there is significant heterogeneity of *r* values within a single cell. Upon closer inspection of *r* values within FAs and overlaying of the final tension signal against *r*, we were not able to identify a correlation between the intensity of the tension signal and the rate of thiol exchange. We next plotted the average r for different DTT concentrations (Figure 2.5D) and then determined *k(F)* from the slope of this plot (Appendix, Figure A2.6). Assuming that the integrin force is constant within the time window of observation (<4 min) with minimal receptor turnover, we estimate that unfolded tension probes experience an average of 110 ± 9 pN (Appendix, Figure A2.6). This assumption is supported by literature showing more stable FA dynamics after 1.5 hrs of REF cell adhesion. [30] Furthermore, the tension signal appears static after the signal saturates reaching maximal thiol exchange, thus suggesting that there is limited FA turnover after cells are allowed to fully adhere on the surface. This value suggests that a subset of integrins experience forces that have been significantly underestimated.

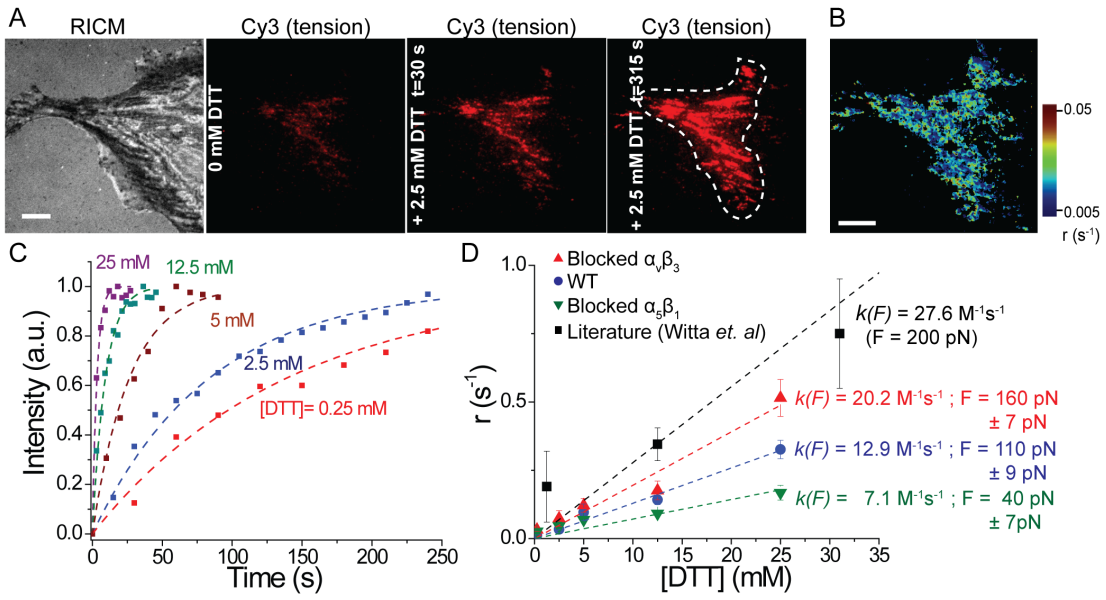

Figure 2.5 Kinetic measurements of S-S reduction to determine integrin forces. (A) Representative RICM and fluorescence images of clamped $I27_{G32C-A75C}$ sensor before and after DTT addition at t = 30 and 315 sec. White dashed line shows the region of interest that was analyzed. Scale bar, 10 μm. (B) Heat map of disulfide reduction rates generated from the fluorescence video of the cell depicted in (A). Scale bar, 10 μm. (C) Representative kinetic plots showing an increase in fluorescence tension signal at different DTT concentrations. Dashed lines represent single-exponential fits used to determine τ_r. (D) Plot of the rate of disulfide reduction ($r = 1/\tau_r$) as function of [DTT] for REF cells (blue), REF cells blocked with αvβ3 (red) and α5β1 antibodies (green). k(F) and F were derived from the linear fit of each data set. Black squares and fit (dashed line) are from Witta et al. PNAS, **2006** where clamped I27 was subjected to a constant force of 200 pN, which generated a slope of 27.6 $M^{-1}s^{-1}$. This previous work included DTT concentration up to 125 mM, but the additional data points were omitted for clarity. Error bars represent the S.E.M. of r obtained from n = 5 cells at each concentration of DTT (0.5 mM, 2.5 mM, 5 mM, 12.5 mM and 25 mM).

2.2.6 The rate of I27 unfolding is integrin subtype-dependent

To investigate force dependence on integrin subtype, we treated the cells with blocking antibodies against $\alpha_v\beta_3$ and $\alpha_5\beta_1$ and repeated the kinetic measurements described above. The efficiency of antibody blocking was confirmed using GFP-β_3 expressing cells (Appendix, Figure 2.7A). Blocking with both antibodies abrogated cell

adhesion, indicating that these two integrins are the primary receptors mediating cell adhesion (Appendix, Figure 2.7B). Cells primarily using $\alpha_v\beta_3$ integrins displayed slowed rates of disulfide reduction indicating a tension of 40 ± 7 pN. This is in contrast to cells employing $\alpha_5\beta_1$ integrins, which showed accelerated rates of disulfide reduction with average forces of 160 ± 7 pN. These values are consistent with precedent indicating greater rupture forces for $\alpha_5\beta_1$ compared to $\alpha_v\beta_3$.[31]

2.3 Conclusion

There is disagreement in the literature regarding the magnitude of integrin-ligand tension within FAs. Dunn and colleagues suggest an integrin-ligand force of 1-5 pN in human foreskin fibroblasts by using single molecule FRET.[14a] In agreement with this estimate, Schwartz et al. calculate cell traction forces of a few pN per integrin receptor in mouse embryo fibroblasts by averaging cell stress over the average number of integrins per unit area.[9a] In contrast, we previously inferred greater integrin forces > 20 pN per receptor based on the observation of mechanically induced biotin-streptavidin dissociation in many cell types.[12f] The tension gauge tether (TGT) technique also suggests greater integrin forces and a peak force of 56 pN for integrin activation.[7]

The I27 tension probes are more mechanically robust than any other sensor tested to date, thus investigating a greater range of integrin tension values. Except for the disulfide clamped RGD-Cy3-$I27_{G32C\text{-}A75C}$, all probes (RGD-ACP(A488)-I27, RGD-sfGFP-I27, RGD-Cy3-I27, FN-A647-I27) were mechanically unfolded by integrin forces displaying a fluorescence response. The sfGFP probe showed mechanically-induced quenching which has been investigated by theory and experiments[32] and is thought to require ~100-200 pN (using a 300 nm/sec loading rate).[23a] This surprising result indicates

that genetically encoded tension probes for cell adhesion proteins are susceptible to mechanical quenching. For example, genetically encoding an integrin tension probe akin to the vinculin tension sensor[8] is not likely to succeed. Although I27 is a highly reversible folder, sfGFP does not recover its full fluorescence after refolding, which may explain why treating cells with the ROCK inhibitor did not lead to full recovery of sfGFP fluorescence.

Importantly, using equilibrium distribution of folded to unfolded tension probes to estimate integrin forces is limited for the following reasons: a) mechanical unfolding is highly dependent on the duration of force (Supplementary Note 1), which is unknown because FA maturation is heterogeneous, b) mechanical unfolding is dependent on the loading rate, which is also unknown during FA maturation, and c) once the applied forces cause unfolding, this defines a minimum tension but not the average tension. Using single molecule techniques can, in principle, overcome the challenges of ensemble averaging to estimate the tension for each receptor. However, single molecule imaging produces a sparse density of reporters since only one receptor is characterized within an area of ~2 μm^2 [14a] and there are hundreds of integrin receptors within such an area. We overcome these limitations by recording the rate of disulfide reduction. Note that a fundamental assumption for force estimates determined by using the kinetics of disulfide reduction are the reaction parameters measured by Fernandez and colleagues. Any significant errors in those measurements will lead to significant deviations in our reported values. Nonetheless, these parameters have been validated in a number of papers investigating different proteins.[26-27]

By blocking REFs with monoclonal antibodies against $\alpha_v\beta_3$ and $\alpha_5\beta_1$ we showed that the cell-generated forces are integrin-subtype dependent. The rate of I27 unfolding by $\alpha_v\beta_3$ integrins is three fold smaller than that for the $\alpha_5\beta_1$ integrins. The mechanism behind differential force levels for different integrin sub-types is likely due to the different functions of each integrins within cell-ECM adhesions. During cell migration, force sensing at the cell edge requires constant recycling of $\alpha_v\beta_3$ integrins that promotes mechanotransduction and reinforcement of other integrins and proteins to the sites of adhesions.[33] However, cells dampen migration by engaging more $\alpha_5\beta_1$ integrins and by generating stable adhesion sites that require stronger integrin-ligand bonds to resist high forces. Sheetz *et al*. found that clustering of $\alpha_5\beta_1$ integrins enhances rupture forces by six-fold compared to the $\alpha_v\beta_3$ integrins.[31] This is consistent with our results.

High magnitude forces reported through the I27 probe likely pertain to a small subset of force bearing receptors. Indeed, the average integrin tension within FAs is 2-4 pN as determined by TFM.[9a] Also DNA- and PEG-based MTFM probes sensitive to ~1-20 pN forces generate signal much more rapidly following cell plating (~10 min compared to ~30 min for I27). Therefore, the results reveal the existence of "hot" receptors that disproportionately carry a greater fraction of cell traction forces compared to the vast majority of integrins recruited to FAs.[10] High magnitude integrin forces exist with FN and RGD ligands as both types of I27 probes display similar signal. Future experiments with multiplexed tension probes will generate a more comprehensive histogram of integrin force distributions within FAs.

In summary, we report a new class of I27-based tension probes that provides many advantages over the previously reported MTFM probes. First, I27 tension probes

are mechanically responsive to a greater dynamic range of forces, and, in principle, the response threshold can range from ~40 pN to ~100 pN by inserting point mutations within the domain. This feature significantly expands the current range of forces detected by MTFM probes. Second, the disulfide bridge clamped sensor circumvents caveats inherent to the transient nature of focal adhesion maturation and the loading rate dependence of mechanical extension, which is a long-standing issue with FRET-based tension sensors. Last, I27-based protein sensors can be easily engineered to incorporate virtually any recombinant protein ligand which provides a general approach that can be adapted for the study of a wide range of mechanotransduction processes.

2.4 Materials and methods

2.4.1 Reagents

The fluorescent dye dibenzocyclooctyne-Cy3 (DBCO-Cy3), dithiothreitol (99%, DTT), (3-aminopropyl) trimethoxysilane (97%, APTMS), 4-(2-hydroxyethyl)piperazine-1-ethanesulfonic acid (≥99.5%, HEPES), potassium phosphate monobasic (≥99.0%), Y-27632 dihydrochloride (>98%), and Hank's balanced salts (#H1387) were purchased from Sigma-Aldrich (St. Louis, MO). For ACP-tag labeling, CoA 488 and SFP synthase were purchased from New England BioLabs (Ipswich, MA) and were used according to manufacturer protocol. The Slide-A-Lyzer™ Dialysis Cassettes and the fluorescent dyes: Alexa647 N-hydroxysuccinimidyl ester and Alexa647 DIBO alkyne were purchased from Life Technologies (Grand Island, NY). 4-Azido-L-phenylalanine was purchased from Chem-Impex International (Wood Dale, IL). Ni-NTA Agarose (#30210) was purchased from Qiagen (Valencia, CA). Number two glass coverslips, 24-well, and 96-well plates were purchased from Fisher Chemical & Scientific (Pittsburg, PA). Dimethyl sulfoxide (99.5%, DMSO) and sodium bicarbonate were purchased from EMD chemicals (Philadelphia, PA). P2 gel size exclusion beads were purchased from BioRad (Hercules, CA). DI water was obtained from a Nanopure water purification system equipped with a UV sterilization unit with a resistivity of 18.2 MΩ.

2.4.2 Cell culture

Rat embryonic fibroblasts (REFs) were cultured in DMEM (Mediatech) supplemented with 10% FBS (Mediatech), penicillin G (100 IU ml-1, Mediatech) and streptomycin (100 μg ml-1, Mediatech) at 37 °C in the presence of 5% CO_2. On the day of the experiment, cells were plated on the functionalized coverslips in a custom-made

chamber with cell media containing 0.5% FBS to minimize nonspecific absorption of serum proteins. Cells were allowed to adhere for: ~30 minutes on RGD-ACP(A488)-I27 and RGD-Cy3-I27 functionalized surfaces; ~2 h on clamped RGD-Cy3-I27$_{G32C-A75C}$ functionalized surfaces; and 3 h on RGD-sfGFP-I27 functionalized surfaces. Kinetic experiments were conducted with adhered cells that were allowed to spread on the surface for 2 h. To initiate the kinetics measurements, DTT was added to the chamber (t=0) and the timelapse video (300 ms exposure time) was collected with the following acquisition frequency: 30 s per frame at 0.25 mM DTT, 15 s per frame at 2.5 mM DTT, 10 s per frame at 5 mM DTT, 3 s per frame at 12.5 mM and 2 s per frame at 25 mM DTT.

2.4.3 Transfection

REF cells were transfected with mCherry-lifeact and GFP-Pax (Addgene plasmid # 15233) using Lipofectamine® LTX (Life Technologies) following the manufacturer protocols. In short, 1 μg of DNA was mixed with Lipofectamine® LTX and Plus™ Reagent per well in a 24-well plate and incubated for 48 h prior to imaging.

2.4.4 Antibody blocking

REF cells were incubated with monoclonal antibodies selective for $\alpha_5\beta_1$ (MAB1969, Millipore) and $\alpha_v\beta_3$ (MAB1976, Millipore) at 10 μg/ml for 30 min. Additionally, each sensor surface prior to REF cell incubation were treated with 10 μg of antibody to ensure complete inhibition of $\alpha_5\beta_1$ and $\alpha_v\beta_3$.

2.4.5 Protein engineering

I27 based constructs were designed with N-terminal ligand (either TVYAVTGRGDSPASSAA or FN type III domains 9-10) and two C-terminal cysteines for attachment onto AuNPs. For kinetic studies, we used a Cys free I27 variant protein in

which Cys^{47} and Cys^{63} were mutated to Ala. A disulfide bond was introduced into this variant by mutating Gly^{32} and Ala^{75} to cysteines. The proteins were purified by Ni^{2+} affinity chromatography and stored at -80 °C in 0.1 M potassium phosphate buffer (pH 7.4) prior to use.

2.4.6 Protein expression with UAA incorporation

The pET22b plasmid encoding MTFM with a TAG codon was co-transformed with pEVOL-pAzF plasmid into electrocompetent BL21(DE3) *E. coli* cells. Cells were grown at 37 °C in the presence of ampicillin, chloramphenicol, and 0.2% glucose to an optical density (OD) of 0.2, at which 1 mM of 4-azido-L-phenylalanine was added. At an OD of 0.4, L-arabinose was added to a final concentration of 0.02% (w/v) and at an OD of 0.8, isopropyl β-D-1-thiogalactopyranoside (IPTG) was added to a final concentration of 1 mM. Cells were shaken for 16 h at 30 °C and purified using His tag chromatography.

2.4.7 Dye labeling

Protein sensors expressing an ACP-tag were incubated with CoA 488 for 1 h at 37 °C, followed by overnight incubation at 4 °C. Protein sensors expressing pAzF were incubated with either DBCO-Cy3 or DIBO-A647 for 1 h at 37 °C, followed by overnight incubation at room temperature. All protein sensors were purified using P2 gel size exclusion beads and the labeling ratio was quantified by UV-Vis absorption (NanoDrop).

2.4.8 AuNP surface preparation

Glass coverslips were piranha etched for 30 min, functionalized with an APTMS solution in acetone for 1 h and thermally annealed at 80 °C for 30 min. Subsequently, the surfaces were passivated with 5% (w/v) mPEG-NHS and 0.5% (w/v) lipoic acid-PEG-

NHS in 0.1 M fresh sodium bicarbonate overnight at 4 °C. After passivation, 12 nM of AuNPs (diameter = 9 nm) were incubated onto the surface for 30 min.

2.4.9 AFM imaging

The atomic force microscope was attached to an anti-vibration stage (Asylum Research, CA). The force constant of the silicon cantilever (MikroMasch) used in our experiment was 5.4-16 N/m. AuNPs (9 nm) were immobilized onto the surface for 30 min and the surfaces were scanned at a rate of 1 Hz at room temperature. Images were generated using IgorPro.

2.4.10 Optical microscopy

A Nikon Eclipse Ti microscope driven by the Elements software package was used for imaging. The microscope is equipped with a TIRF launcher with three laser lines: 488 nm (10 mW), 561 (50 mW), and 638 nm (20 mW), an intensilight Epifluorescence source (Nikon), an Evolve electron multiplying charge coupled device (EMCCD camera, Photometrics), and a CFI Apo 100x (NA 1.49) objective (Nikon). The microscope includes the following filter cubes TIRF 488, TIRF 640, FITC, TRITC, and RICM (reflection interference contrast microscopy) purchased from Chroma (Bellows Falls, VT). The microscope is also equipped with the Nikon Perfect Focus System that maintains focus during timelapse imaging experiments.

2.4.11 Data analysis

Fluorescence analysis was performed using ImageJ (National Institutes of Health) and Origin software (OriginLab Corporation). Based on Witta *et al*., we used the following relation to determine the rate of unfolding: $k(F) = A \exp((F\Delta x_r - E_a)/k_B T)$. The pre-exponential factor $A = 1.3*10^{12}$ $M^{-1}s^{-1}$, the distance to the transition state for the

reaction, Δx_r = 0.34 Å, and the activation energy (E_a) for the disulfide reduction at F=0 was set to 65 kJ/mol. Fernandez *et al*. determined different values for E_a, Δx_r and A using different experimental conditions in three reports[27] (Table 2.1). In our study, we decided to use the values determined from Witta *et al*.[27] because these are the only experiments where *k(F)* was obtained as a function of varying DTT concentration – an identical experimental setup as the one used here. The reported error bars in Figure 5D represent standard error of the mean from each set of rates per DTT concentration (n = 5). The slope of *r* vs DTT and its standard deviation were calculated using the "LINEST" (linear least squares curve fitting routine).

2.4.12 Heat map generation

Heat map of disulfide reduction rates was determined through the following analysis using the programming software Interactive Data Language. Initially, the fluorescence of each pixel was averaged with its neighboring pixel intensity (2x2) for each frame of a fluorescence video and plotted into the equation B(T)=A(0)(1-EXP(-T*A(1))) (where T is time/frame) for all pixels. Rate =A(1) and was displayed as a heat map of rates ranging from 0.005 to 0.05.

2.4.13 Ensemble fluorescence measurements for calculating quenching efficiency

The fluorescence intensities of A488 and Cy3 from AuNPs functionalized protein sensors were calculated using a Biotek Synergy HT plate reader using a filter set with excitation/emission λ = 485 nm/528 nm and λ = 565 nm/610 nm, respectively. Measurements were carried out in triplicate at a volume of 100 μl per well. To dequench the dye, volume of 50 mM KCN was added to the samples at a final concentration of 0.5 mM to dissolve away the AuNP and release the protein into solution. The fluorescence

intensity of the protein sensors were subsequently measured and corrected for the quenching of the dye by KCN and AuNP filter effect as described previously.[12]

2.5 References

1. Hynes, R. O., Integrins: bidirectional, allosteric signaling machines. *Cell* **2002,** *110* (6), 673-87.
2. Redick, S. D.; Settles, D. L.; Briscoe, G.; Erickson, H. P., Defining fibronectin's cell adhesion synergy site by site-directed mutagenesis. *The Journal of cell biology* **2000,** *149* (2), 521-7.
3. Barczyk, M.; Carracedo, S.; Gullberg, D., Integrins. *Cell Tissue Res* **2010,** *339* (1), 269-80.
4. Humphrey, J. D.; Dufresne, E. R.; Schwartz, M. A., Mechanotransduction and extracellular matrix homeostasis. *Nature reviews. Molecular cell biology* **2014,** *15* (12), 802-12.
5. Kanchanawong, P.; Shtengel, G.; Pasapera, A. M.; Ramko, E. B.; Davidson, M. W.; Hess, H. F.; Waterman, C. M., Nanoscale architecture of integrin-based cell adhesions. *Nature* **2010,** *468* (7323), 580-4.
6. Parsons, J. T.; Horwitz, A. R.; Schwartz, M. A., Cell adhesion: integrating cytoskeletal dynamics and cellular tension. *Nature reviews. Molecular cell biology* **2010,** *11* (9), 633-43.
7. Wang, X.; Ha, T., Defining single molecular forces required to activate integrin and notch signaling. *Science* **2013,** *340* (6135), 991-4.
8. Grashoff, C.; Hoffman, B. D.; Brenner, M. D.; Zhou, R.; Parsons, M.; Yang, M. T.; McLean, M. A.; Sligar, S. G.; Chen, C. S.; Ha, T.; Schwartz, M. A., Measuring mechanical tension across vinculin reveals regulation of focal adhesion dynamics. *Nature* **2010,** *466* (7303), 263-6.

9. (a) Sabass, B.; Gardel, M. L.; Waterman, C. M.; Schwarz, U. S., High resolution traction force microscopy based on experimental and computational advances. *Biophysical journal* **2008,** *94* (1), 207-20; (b) Tan, J. L.; Tien, J.; Pirone, D. M.; Gray, D. S.; Bhadriraju, K.; Chen, C. S., Cells lying on a bed of microneedles: an approach to isolate mechanical force. *Proceedings of the National Academy of Sciences of the United States of America* **2003,** *100* (4), 1484-9.

10. Wiseman, P. W.; Brown, C. M.; Webb, D. J.; Hebert, B.; Johnson, N. L.; Squier, J. A.; Ellisman, M. H.; Horwitz, A. F., Spatial mapping of integrin interactions and dynamics during cell migration by image correlation microscopy. *J. Cell Sci.* **2004,** *117* (Pt 23), 5521-34.

11. Engler, A. J.; Sen, S.; Sweeney, H. L.; Discher, D. E., Matrix elasticity directs stem cell lineage specification. *Cell* **2006,** *126* (4), 677-89.

12. (a) Stabley, D. R.; Jurchenko, C.; Marshall, S. S.; Salaita, K. S., Visualizing mechanical tension across membrane receptors with a fluorescent sensor. *Nat Methods* **2012,** *9* (1), 64-7; (b) Jurchenko, C.; Salaita, K. S., Lighting up the Force: Investigating Mechanisms of Mechanotransduction Using Fluorescent Tension Probes. *Mol Cell Biol* **2015**; (c) Zhang, Y.; Ge, C.; Zhu, C.; Salaita, K., DNA-based digital tension probes reveal integrin forces during early cell adhesion. *Nature communications* **2014,** *5*, 5167; (d) Liu, Y.; Medda, R.; Liu, Z.; Galior, K.; Yehl, K.; Spatz, J. P.; Cavalcanti-Adam, E. A.; Salaita, K., Nanoparticle tension probes patterned at the nanoscale: impact of integrin clustering on force transmission. *Nano Lett* **2014,** *14* (10), 5539-46; (e) Liu, Y.; Yehl, K.; Narui, Y.; Salaita, K., Tension sensing nanoparticles for mechano-

imaging at the living/nonliving interface. *Journal of the American Chemical Society* **2013,** *135* (14), 5320-3; (f) Jurchenko, C.; Chang, Y.; Narui, Y.; Zhang, Y.; Salaita, K. S., Integrin-generated forces lead to streptavidin-biotin unbinding in cellular adhesions. *Biophysical journal* **2014,** *106* (7), 1436-46.

13. Blakely, B. L.; Dumelin, C. E.; Trappmann, B.; McGregor, L. M.; Choi, C. K.; Anthony, P. C.; Duesterberg, V. K.; Baker, B. M.; Block, S. M.; Liu, D. R.; Chen, C. S., A DNA-based molecular probe for optically reporting cellular traction forces. *Nat Methods* **2014,** *11* (12), 1229-32.

14. (a) Morimatsu, M.; Mekhdjian, A. H.; Adhikari, A. S.; Dunn, A. R., Molecular tension sensors report forces generated by single integrin molecules in living cells. *Nano Lett* **2013,** *13* (9), 3985-9; (b) Morimatsu, M.; Mekhdjian, A. H.; Chang, A. C.; Tan, S. J.; Dunn, A. R., Visualizing the interior architecture of focal adhesions with high-resolution traction maps. *Nano Lett* **2015,** *15* (4), 2220-8.

15. Botello, E.; Harris, N. C.; Sargent, J.; Chen, W. H.; Lin, K. J.; Kiang, C. H., Temperature and chemical denaturant dependence of forced unfolding of titin I27. *The journal of physical chemistry. B* **2009,** *113* (31), 10845-8.

16. Lu, H.; Isralewitz, B.; Krammer, A.; Vogel, V.; Schulten, K., Unfolding of titin immunoglobulin domains by steered molecular dynamics simulation. *Biophysical journal* **1998,** *75* (2), 662-71.

17. Rief, M.; Gautel, M.; Oesterhelt, F.; Fernandez, J. M.; Gaub, H. E., Reversible unfolding of individual titin immunoglobulin domains by AFM. *Science* **1997,** *276* (5315), 1109-12.

18. Li, H.; Carrion-Vazquez, M.; Oberhauser, A. F.; Marszalek, P. E.; Fernandez, J. M., Point mutations alter the mechanical stability of immunoglobulin modules. *Nature structural biology* **2000,** *7* (12), 1117-20.

19. Szoszkiewicz, R.; Ainavarapu, S. R.; Wiita, A. P.; Perez-Jimenez, R.; Sanchez-Ruiz, J. M.; Fernandez, J. M., Dwell time analysis of a single-molecule mechanochemical reaction. *Langmuir* **2008,** *24* (4), 1356-64.

20. Zhou, Z.; Cironi, P.; Lin, A. J.; Xu, Y.; Hrvatin, S.; Golan, D. E.; Silver, P. A.; Walsh, C. T.; Yin, J., Genetically encoded short peptide tags for orthogonal protein labeling by Sfp and AcpS phosphopantetheinyl transferases. *ACS Chem Biol* **2007,** *2* (5), 337-46.

21. Aubin-Tam, M. E., Conjugation of nanoparticles to proteins. *Methods Mol Biol* **2013,** *1025*, 19-27.

22. Yehl, K.; Joshi, J. P.; Greene, B. L.; Dyer, R. B.; Nahta, R.; Salaita, K., Catalytic deoxyribozyme-modified nanoparticles for RNAi-independent gene regulation. *ACS nano* **2012,** *6* (10), 9150-7.

23. (a) Dietz, H.; Rief, M., Exploring the energy landscape of GFP by single-molecule mechanical experiments. *Proceedings of the National Academy of Sciences of the United States of America* **2004,** *101* (46), 16192-7; (b) Otten, M.; Ott, W.; Jobst, M. A.; Milles, L. F.; Verdorfer, T.; Pippig, D. A.; Nash, M. A.; Gaub, H. E., From genes to protein mechanics on a chip. *Nat Methods* **2014,** *11* (11), 1127-30.

24. Pedelacq, J. D.; Cabantous, S.; Tran, T.; Terwilliger, T. C.; Waldo, G. S., Engineering and characterization of a superfolder green fluorescent protein. *Nat Biotechnol* **2006,** *24* (1), 79-88.

25. Pankov, R.; Yamada, K. M., Fibronectin at a glance. *Journal of cell science* **2002,** *115* (Pt 20), 3861-3.

26. Ainavarapu, S. R.; Brujic, J.; Huang, H. H.; Wiita, A. P.; Lu, H.; Li, L.; Walther, K. A.; Carrion-Vazquez, M.; Li, H.; Fernandez, J. M., Contour length and refolding rate of a small protein controlled by engineered disulfide bonds. *Biophysical journal* **2007,** *92* (1), 225-33.

27. (a) Wiita, A. P.; Ainavarapu, S. R.; Huang, H. H.; Fernandez, J. M., Force-dependent chemical kinetics of disulfide bond reduction observed with single-molecule techniques. *Proceedings of the National Academy of Sciences of the United States of America* **2006,** *103* (19), 7222-7; (b) Ainavarapu, S. R.; Wiita, A. P.; Huang, H. H.; Fernandez, J. M., A single-molecule assay to directly identify solvent-accessible disulfide bonds and probe their effect on protein folding. *Journal of the American Chemical Society* **2008,** *130* (2), 436-7; (c) Wiita, A. P.; Perez-Jimenez, R.; Walther, K. A.; Grater, F.; Berne, B. J.; Holmgren, A.; Sanchez-Ruiz, J. M.; Fernandez, J. M., Probing the chemistry of thioredoxin catalysis with force. *Nature* **2007,** *450* (7166), 124-7; (d) Liang, J.; Fernandez, J. M., Kinetic measurements on single-molecule disulfide bond cleavage. *Journal of the American Chemical Society* **2011,** *133* (10), 3528-34.

28. Koti Ainavarapu, S. R.; Wiita, A. P.; Dougan, L.; Uggerud, E.; Fernandez, J. M., Single-molecule force spectroscopy measurements of bond elongation during a

bimolecular reaction. *Journal of the American Chemical Society* **2008,** *130* (20), 6479-87.

29. Pani, G.; Colavitti, R.; Bedogni, B.; Anzevino, R.; Borrello, S.; Galeotti, T., A redox signaling mechanism for density-dependent inhibition of cell growth. *The Journal of biological chemistry* **2000,** *275* (49), 38891-9.

30. Aroush, D. Z.-B., R.; Bershadsky, A. D.; Wagner, H. D., Temporal evolution of cell focal adhesions: experimental observations and shear stress profiles. *Soft Matter* **2008,** *4* (12), 2410-2417.

31. Roca-Cusachs, P.; Gauthier, N. C.; Del Rio, A.; Sheetz, M. P., Clustering of alpha(5)beta(1) integrins determines adhesion strength whereas alpha(v)beta(3) and talin enable mechanotransduction. *Proceedings of the National Academy of Sciences of the United States of America* **2009,** *106* (38), 16245-50.

32. Saeger, J.; Hytonen, V. P.; Klotzsch, E.; Vogel, V., GFP's mechanical intermediate states. *PLoS One* **2012,** *7* (10), e46962.

33. White, D. P.; Caswell, P. T.; Norman, J. C., alpha v beta3 and alpha5beta1 integrin recycling pathways dictate downstream Rho kinase signaling to regulate persistent cell migration. *The Journal of cell biology* **2007,** *177* (3), 515-25.

2.6 Appendix

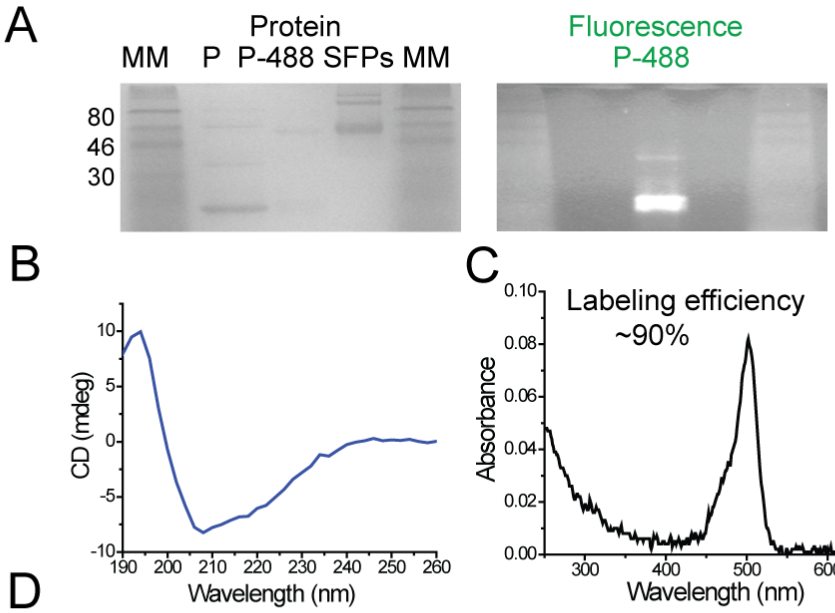

[Protein]=133 nM	[PEG]=1.3 μM	[PEG]=2 μM	[PEG]=2.7 μM
QE	77%	82%	76%
Protein per AuNP	4.4	5.2	4.7

Figure A2.1 Characterization of RGD-ACP(A488)-I27 MTFM sensor. (A) SDS PAGE gel (12%) stained with Coomassie Blue (left) and scanned with UV scanner (right) which indicates a high labeling efficiency of the dye with the ACP tag. From left to right: 1. Prestained protein marker (New England BioLabs); 2. RGD-ACP-I27 protein; 3. RGD-ACP-I27 labeled with CoA 488; 4. SFP synthase; 5. Prestained protein marker. (B) Far UV Circular Dichroism (CD) spectrum of unlabeled RGD-ACP-I27 (40 μM) at 37 °C which displays a mixture of α- helical (ACP) and β-sheet (I27) secondary structures suggesting that the protein remains folded at elevated temperatures. (C) Absorbance spectrum of RGD-ACP(A488)-I27. (D) Table of quenching efficiencies at different mPEG concentrations with the corresponding average number of proteins per nanoparticle.

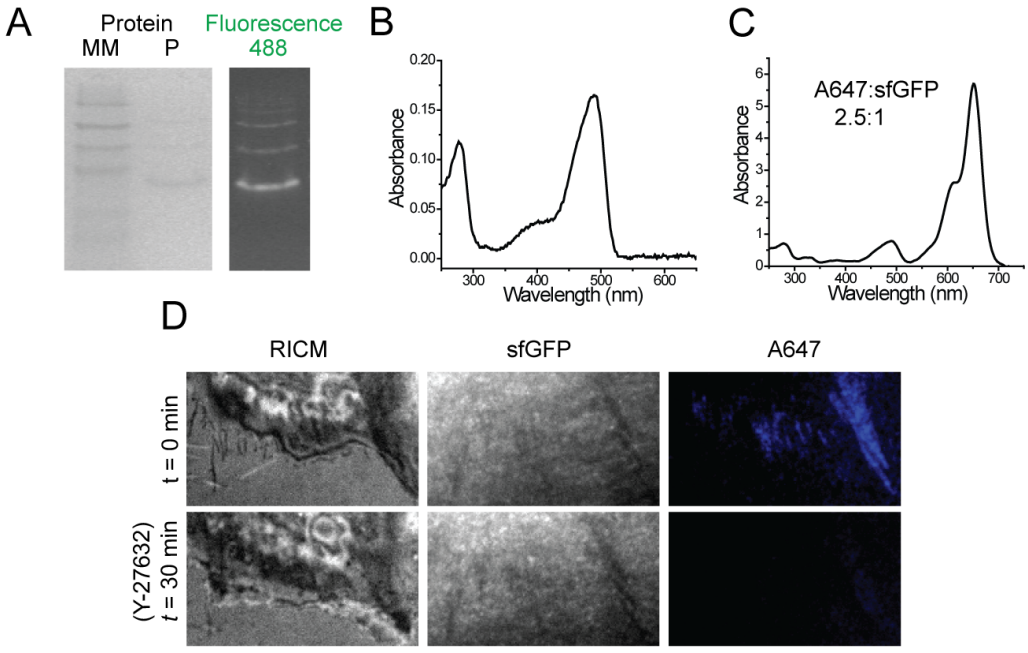

Figure A2.2 Characterization of RGD-sfGFP-I27 MTFM sensor. (A) SDS PAGE gel (12%) stained with Coomassie Blue (left) and scanned with a UV scanner (right). From left to right: 1. Prestained protein marker; 2. RGD-sfGFP-I27 protein; 3. Fluorescence of RGD-sfGFP-I27 protein. (B) Absorbance spectrum of RGD-sfGFP-I27. (C) Absorbance spectrum of RGD-sfGFP-I27 randomly labeled with NHS-A647. The protein sensor was mixed with the dye at an average ratio of ~ 1:20 and was incubated at room temperature for 1 h. Labeled protein sensor was purified from free dye using P2 gel size exclusion beads prior to quantifying the labeling ratio by UV-Vis absorption (NanoDrop). (D) Representative RICM and fluorescence images of REF cells seeded on RGD-sfGFP-I27-A647 sensor surfaces (Protein:Dye =1:2.5) that were treated with 40 μM of ROCK inhibitor (Y-27632) for 30 min. Fluorescence signal declined after 30 min as illustrated in the A647 channel, which indicates the loss of myosin contractility and reversibility of the sensor. However, sfGFP fluorescence was not rescued following refolding of the probe as indicated by the fluorescence images. Scale bar, 10 μm.

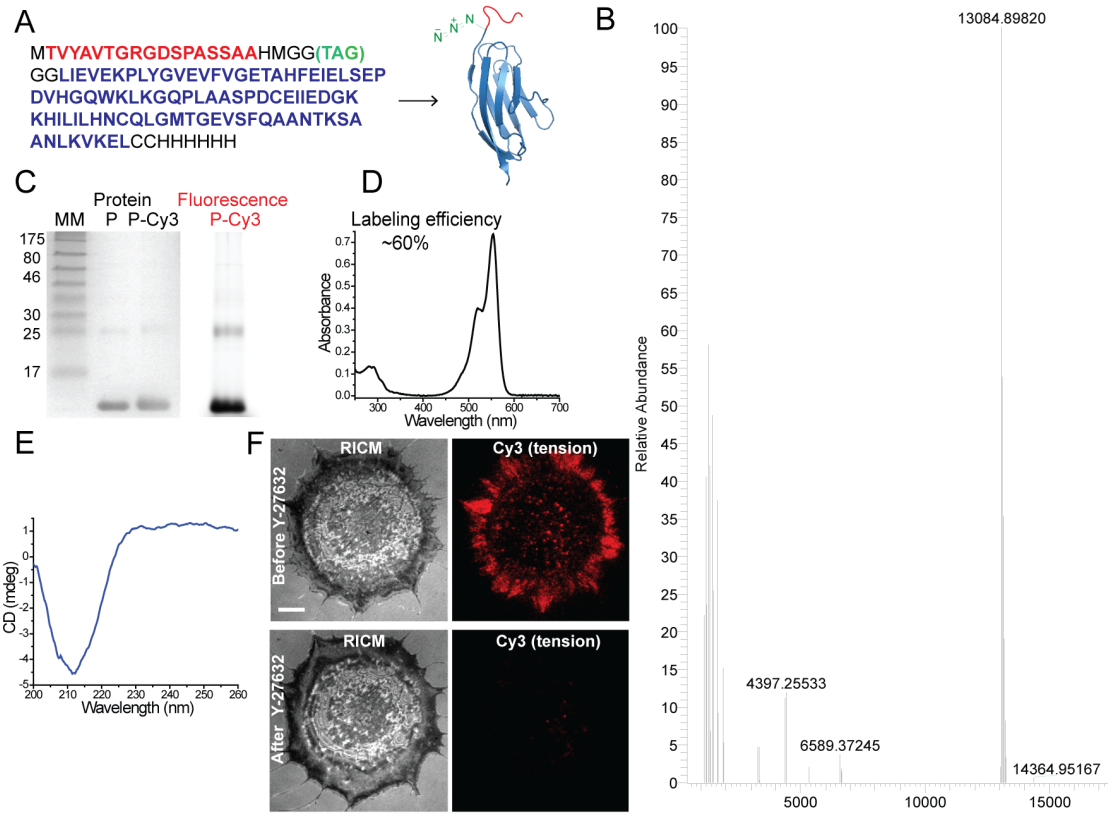

Figure A2.3 Characterization of RGD-Cy3-I27 MTFM sensor. (A) Amino acid sequence of GRGDS-I27 construct including a TAG codon for p-azidophenylalanine incorporation (left) and crystal structure of I27 where the exact position for p-azidophenylalanine is added into the structure in green for clarity (right). The N terminal "GRGDS" motif is necessary for cell recognition. (B) Electrospray ionization (ESI) spectrum of the RGD-Cy3-I27 construct showing a relative abundance of 13084.9 m/z, which corresponds to the + 1 ion of the I27 MTFM sensor (calculated m/z = 13082.8). (C) SDS PAGE gel (18%) stained with Coomassie Blue (left) and scanned with a fluorescence scanner (right). From left to right: 1. Prestained protein marker; 2. RGD-I27; 3. RGD-I27 labeled with DBCO-Cy3; 4. Fluorescence of RGD-Cy3-I27 probe. (D) Absorbance spectrum of RGD-Cy3-I27. (E) Far UV Circular Dichroism (CD) spectrum of unlabeled RGD-I27 (40 μM) at 37 °C which displays a characteristic negative band at 212 nm. This corresponds to β-sheet secondary structure of I27 and suggests that the protein is folded at elevated temperatures. (F) Representative RICM and fluorescence images of REF cells that were treated with 40 μM of ROCK inhibitor (Y-27632) for 30 min. Fluorescence signal declined after 30 min as illustrated in the Cy3 channel indicating the loss of myosin contractility and reversibility of the RGD-Cy3-I27 sensor. Scale bar, 10 μm.

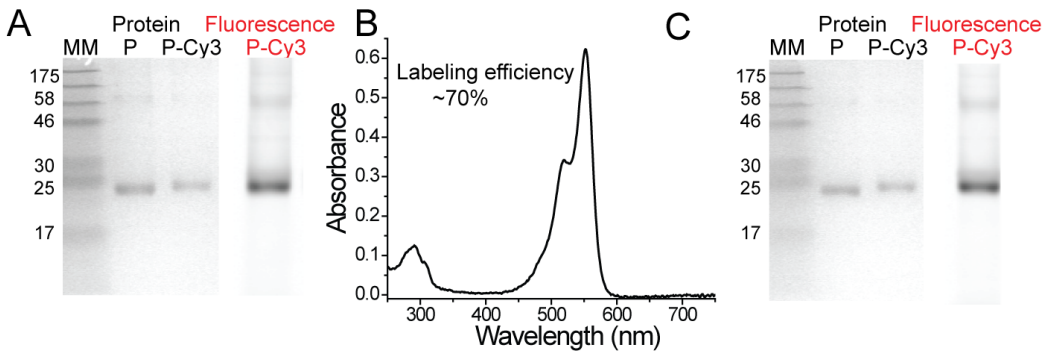

Figure A2.4 Characterization of FN(9-10)-I27 and FN(9-10, RGE)-I27 MTFM sensors. (A) SDS PAGE gel (12%) stained with Coomassie Blue (left) and scanned with a fluorescence scanner (right). From left to right: 1. Prestained protein marker; 2. FN(9-10)-I27 protein; 3. FN(9-10)-I27 labeled with DBCO-Cy3; 4. Fluorescence of FN(9-10)-Cy3-I27 probe. (B) Absorbance spectrum of FN(9-10)-Cy3-I27. (C) SDS PAGE gel (12%) stained with Coomassie Blue (left) and scanned with a fluorescence scanner (right). From left to right: 1. Prestained protein marker; 2. FN(9-10, RGE)-I27 protein; 3. FN(9-10, RGE)-I27 labeled with DBCO-Cy3; 4. Fluorescence of FN(9-10, RGE)-Cy3-I27 probe.

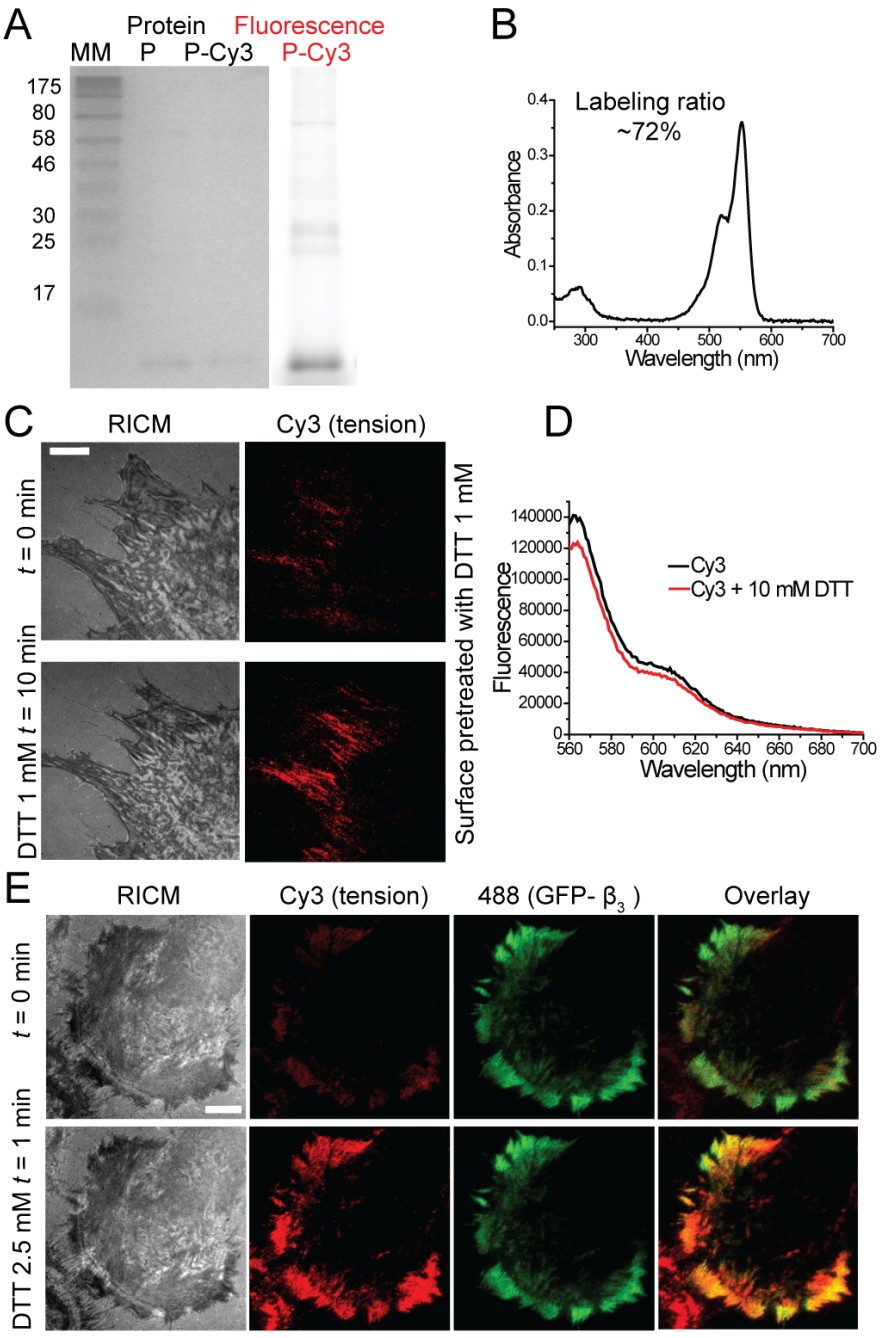

Figure A2.5 Characterization of RGD-Cy3-I27$_{G32C-A75C}$ MTFM sensor clamped with disulfide bridge. (A) SDS PAGE gel (12%) stained with Coomassie Blue (left) and scanned with a fluorescence scanner (right). From left to right: 1. Prestained protein marker; 2. RGD-I27$_{G32C-A75C}$ protein; 3. RGD-I27$_{G32C-A75C}$ protein labeled with DBCO-Cy3; 4. Fluorescence of RGD-Cy3-I27$_{G32C-A75C}$ probe. (B) Absorbance spectrum of RGD-Cy3-I27$_{G32C-A75C}$. (C) AuNP surface functionalized with clamped RGD-Cy3-I27$_{G32C-A75C}$ MTFM sensors was treated with 1 mM DTT for 10 min at room temperature. Surface was

next rinsed with 0.1 M KH_2PO_4 and REFs were added to the surface for 1 h. Cells were then imaged in RICM and fluorescence before and after addition of 1 mM DTT. (D) Fluorescence spectrum of RGD-Cy3-$I27_{G32C-A75C}$ protein [50 nM] treated with 10 mM DTT for 5 min to determine the effects that DTT has on the dye fluorescence. Spectrum indicates that DTT reduces the fluorescence of RGD-Cy3-$I27_{G32C-A75C}$ by ~10% after 30 min of incubation. (E) Representative RICM and fluorescence images of REF cells expressing GFP-β_3 integrins were incubated on the clamped RGD-Cy3-$I27_{G32C-A75C}$ sensor for 1 h and were treated with 2.5 mM DTT. Images were captured before and after 1 min of addition of DTT. Scale bar, 10 μm.

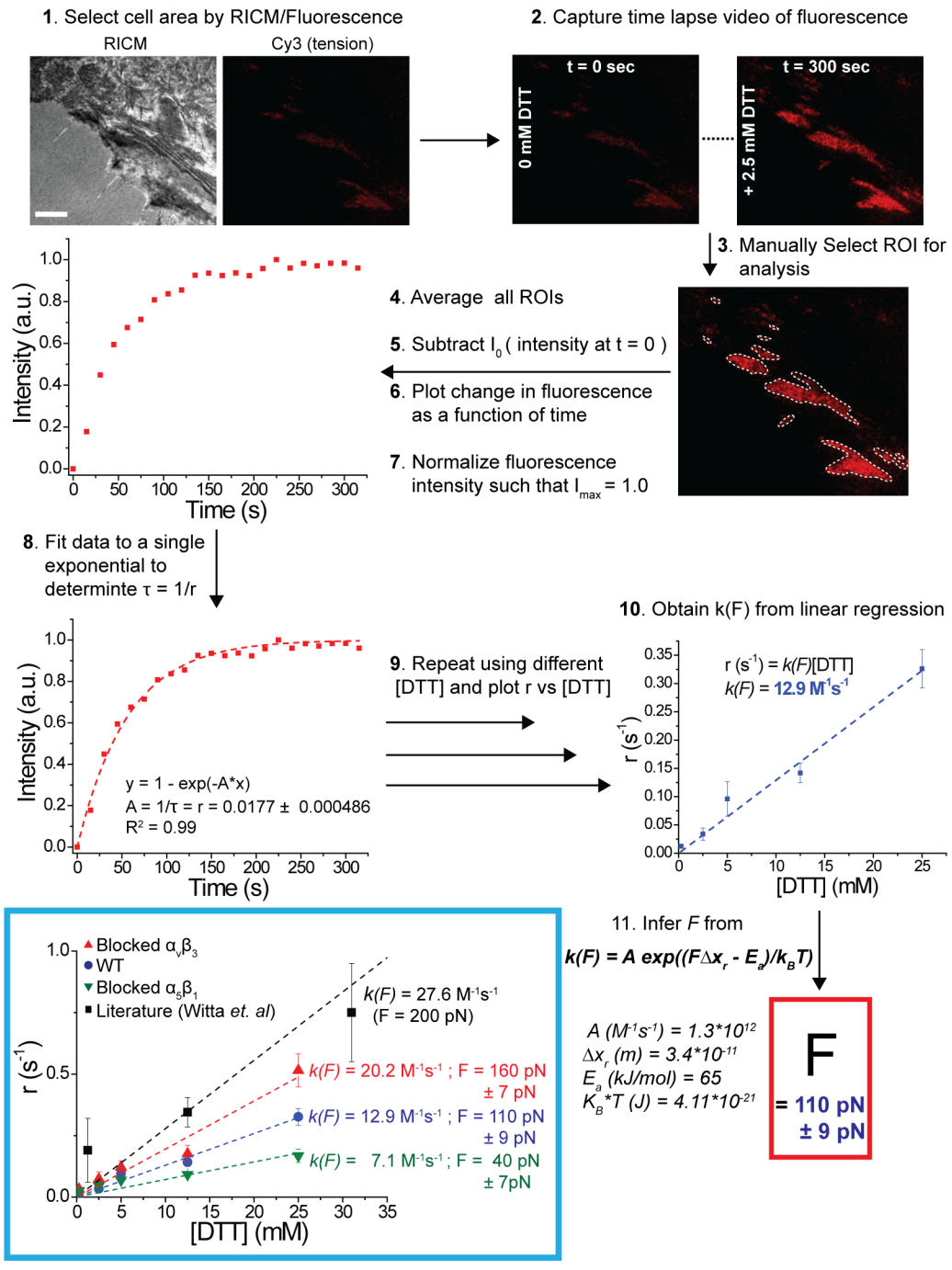
1. Select cell area by RICM/Fluorescence
RICM
Cy3 (tension)
2. Capture time lapse video of fluorescence
t = 0 sec
0 mM DTT
t = 300 sec
+ 2.5 mM DTT
3. Manually Select ROI for analysis
4. Average all ROIs
5. Subtract I0 (intensity at t = 0)
6. Plot change in fluorescence as a function of time
7. Normalize fluorescence intensity such that Imax = 1.0
Intensity (a.u.)
Time (s)
8. Fit data to a single exponential to determinte τ = 1/r
y = 1 - exp(-A*x)
A = 1/τ = r = 0.0177 ± 0.000486
R² = 0.99
9. Repeat using different [DTT] and plot r vs [DTT]
10. Obtain k(F) from linear regression
r (s-1) = k(F)[DTT]
k(F) = 12.9 M-1s-1
r (s-1)
[DTT] (mM)
Blocked αvβ3
WT
Blocked αsβ1
Literature (Witta et. al)
k(F) = 27.6 M-1s-1 (F = 200 pN)
k(F) = 20.2 M-1s-1 ; F = 160 pN ± 7 pN
k(F) = 12.9 M-1s-1 ; F = 110 pN ± 9 pN
k(F) = 7.1 M-1s-1 ; F = 40 pN ± 7pN
11. Infer F from
k(F) = A exp((FΔxr - Ea)/kBT)
A (M-1s-1) = 1.3*10^12
Δxr (m) = 3.4*10^-11
Ea (kJ/mol) = 65
KB*T (J) = 4.11*10^-21
F
= 110 pN ± 9 pN

Figure A2.6 Flow chart describing the analysis used for estimating integrin forces from the rate of disulfide reduction. The plot within the blue box shows a graph containing linear fits of the rate of clamped I27 reduction, r (s^{-1}), as a function of [DTT]. The black squares represent the data obtained from Witta et al.[1], while the red triangle, blue circle, and green inverted triangle represent data collected in this paper. The literature data was collected using a force clamp set at F = 200 pN. This previous work included DTT concentration up to 125 mM, but the additional data points were omitted for clarity. We use the slope of the data to obtain k(F), and then to infer the average force applied by cell receptors. Data was collected using REF cells (blue), cells blocked with $\alpha_v\beta_3$ (red) and $\alpha_5\beta_1$ antibodies (green).

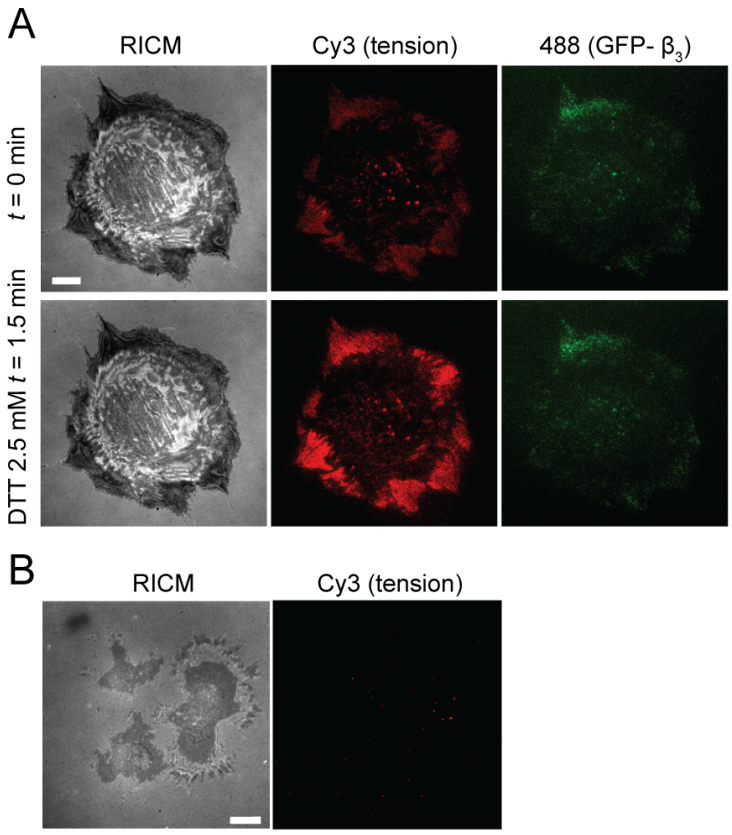

Figure A2.7 Inhibition of integrin function by monoclonal antibodies specific for $\alpha_v\beta_3$ and $\alpha_5\beta_1$. (A) Representative RICM and fluorescence images of REF cells expressing GFP-β_3 integrins that were blocked with antibody against $\alpha_v\beta_3$ for 30 min and then added to a surface coated with clamped RGD-Cy3-$I27_{G32C\text{-}A75C}$ sensors. Blocking $\alpha_v\beta_3$ integrins reveals lower GFP-β_3 localization within the cellular adhesion, which indicates the efficiency of β_3 integrin inhibition. (B) Inhibition of both $\alpha_v\beta_3$ and $\alpha_5\beta_1$ inhibits REF cells adhesion and spreading on the tension surface, which indicates that the majority of integrins employed in RGD binding are $\alpha_v\beta_3$ and $\alpha_5\beta_1$. Scale bar, 10 μm.

2.7 Supplementary Note 1

Timelapse imaging analysis was used to determine the time difference between cell spreading and the onset of tension signal. This minimum time was then used to better estimate the minimum force required to open the I27 protein. To perform this analysis, REF cells were cultured on a RGD-ACP488-I27 probe surface for 5 min and then the timelapse movie was acquired at a rate of 1 frame per min using 300 msec exposure time in TIRFM. To determine the minimum force, we assumed that intial detectable RICM signal corresponded to the initial time point of integrin-ligand binding. We also assumed that FA maturation was instantaneous and that the receptor applied a large and constant force (force clamp) immediately following cell spreading (as determined by RICM). The constants for unfolding rate of I27 at zero force (α_0) and distance to transition state (Δx) are obtained from Carrion-Vazquez et al. Scale bar 2 μm.

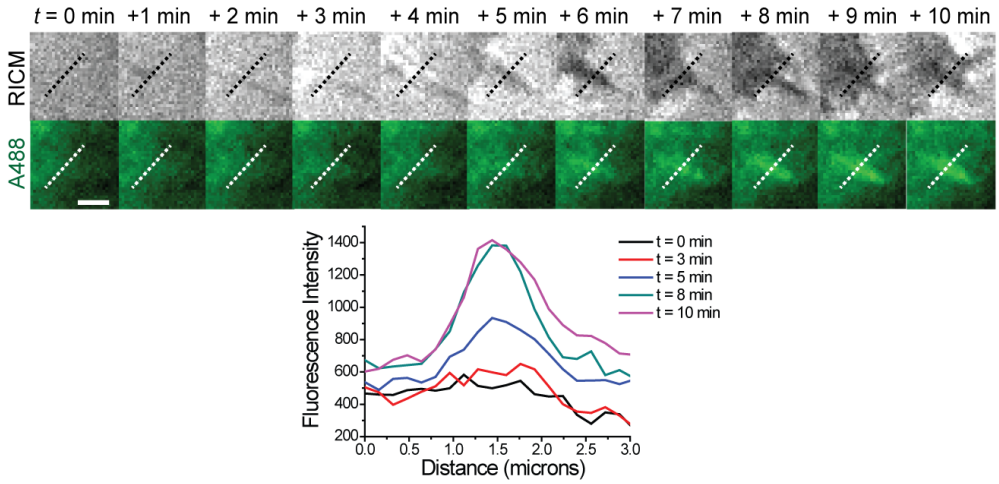

Equations:

$$P = 1 - e^{-(\alpha)\Delta t},$$

where P is the probability of unfolding, α is a rate of unfolding and Δt is time

$$\alpha = \alpha_0 e^{(F\Delta x/kBT)},$$

where α_0 is the unfolding rate of I27 at zero force (3.3×10^{-4} s^{-1}), F is the exerted force, Δx is the distance to the transition state (0.25 nm), k_B is Boltzmann's constant and T is temperature.

at P = 50% and Δt = 4 min, F = 36 pN

Chapter 3: Molecular tension probes as a tool to study the mechanopharmocology of airway smooth muscle cells

Adapted from Galior, K.; Liu, Y.; Ma, VP.; Su, H.; Baker, N.; Panettieri, R.; Wongatrokool, C.; Salaita, K. Molecular tension probes to investigate the mechanopharmacology of asthmatic smooth muscle cells – *manuscript in preparation*

3.1 Introduction

The transition to personalized medicine aims to create a treatment plan that is best for a patient, while simultaneously identifying potential side effects. The typical approach to personalized medicine is using pharmacogenomic molecular technology to determine an individual's genetic makeup, including the presence or absence of specific cellular receptors and enzyme levels, to predict adequate disease maintenance (reviewed in [1-2]). Mechanical phenotypes are rarely used for personalized medicine due to the difficulties in quantifying mechanical phenotype in live cells. Cellular mechanics play a role in disease pathophysiology, such as in asthma, sarcopenia, and metabolic myopathies. Cellular contractility is crucial for proper functioning, and impaired contractile properties significantly alter the quality of life of patients. The main approach used for characterizing the mechanical phenotype of cells is traction force microscopy (TFM). TFM works by measuring the deformation of polymer gels loaded with fiducial markers and calculating the required force fields to drive particle deformation. However, TFM has several limitations. Thus, there is a need to create novel methods for personalized mechanopharmacology that report molecular forces in a high throughput fashion.

Airway smooth muscle cells (ASM) play a fundamental role in lung physiology. ASM cells contract and relax, regulating the airway diameter through force generation and cell shortening.[3-4] Therefore, ASM cell contraction significantly contributes to the development and progression of asthma, a chronic lung disease characterized by the airflow obstruction and bronchoconstriction.[5-6] In asthma, ASM cells display enhanced contraction due, in part, to upregulated inflammatory cytokines and extracellular matrix (ECM) proteins[3] which lead to airway remodeling and narrowing. In addition, asthmatic ASM cells

have increased maximum shortening velocity (v_{max})[7] and capacity[8] which contributes to airway hyperresponsiveness (AHR), or the propensity of an airway to constrict in the presence of specific stimuli. The contractile phenotype of ASM cells is defined by increased levels and activity of myosin light chain kinase (MLCK)[9-10], a protein that phosphorylates myosin light chain in response to changes in cytosolic calcium concentration. These pathological responses are further amplified in the presence of inhaled substances such as nicotine.[11-12] Nicotine stimulates influx of Ca^{2+} in ASMC cells by binding and up-regulating α7-nicotinic acetylcholine receptor (α7-nAChR). This leads to further contraction and a sudden onset of bronchospasm. [13-15]

One of the main therapies to relax airway smooth muscle cells in the event of a bronchospasm is by inhaling short-acting bronchodilators, such as albuterol.[16] Albuterol reduces contractile forces by binding to β2-adrenergic receptors found on the cell membrane thus decreasing intracellular Ca^{2+} concentrations which ultimately inactivates MLCK. However, how bronchodilators reduce force generation at the single cell level is still relatively unexplored because single cell mechanics are difficult to study using conventional techniques used to measure force development. Current tools to study the mechanical phenotype of asthmatic cells rely on measuring intermediate effectors of contraction, such as levels of intracellular messengers[17], protein expression, cytokine release[18], or other phenotypic screening[19] but not the contractile force directly. Therefore, a need exists to develop more sensitive screening assays to measure responses to bronchodilators and contractile agents to accurately interrogate the contractile phenotype of ASM cells.

Contractile forces are transmitted through the cellular cytoskeleton to the external environment through focal adhesions complexes that are comprised of hundreds of signaling and structural proteins that nucleate around integrin receptors.[20] Integrins play an important part in the lung development by regulating various downstream signaling pathways such as ASM phenotype, proliferation, hypertrophy, and cell adhesion and migration.[21-25] Contractile forces of ASM cells have been studied using traction force microscopy (TFM), which relies on culturing the ASM cells on soft polyacrylamide gels that deform under tension.[26-27] However, quantifying these deformations is indirect and the inherent nature of the substrate limits the temporal and spatial information. As a result, how contractile forces are transmitted by integrins in ASM cells at the molecular level has yet to be determined.

To overcome these limitations and to couple ASM contractile forces to a biochemical signaling pathway, we applied an integrin-specific force sensor that was pioneered by our group in a novel experimental technique termed molecular tension fluorescence microscopy (MTFM).[28-36] MTFM maps integrin forces at the single cell with high spatial (200 nm) and temporal resolution (~ms) and pN sensitivity. In general, the force sensor is composed of a molecular spring, either DNA, PEG or protein that is flanked by the fluorophore-quencher pair. The head of the spring is conjugated with the biological ligand of interest while the tail of the spring is anchored to the glass surface. Forces applied to the ligand will physically separate the fluorophore-quencher pair, resulting in dequenching and an observed increase of fluorescence signal intensity.

In this report, we set out to visualize and compare contractile forces of healthy and asthmatic human ASM cells using the titin-based MTFM probe. Titin-based MTFM

provides the most stable probes made thus far because compared to DNA and PEG based MTFM probes, titin unfolding requires greater forces to unfold the molecule. Titin based MTFM probes enabled optical measurement of ASM integrin forces and provided a readout of mechanical phenotype of ASM cells. In addition, we investigated the role of α7-nicotininc acetylcholine receptor in force generation and how addition of nicotine modulates the crosstalk between forces and biochemical signaling at the molecular level. Lastly, we developed a mechano-assay as a potential diagnostic tool for personalized medicine that measures receptor tension as a phenotypic output for drug discovery.

3.2 Results and Discussion

3.2.1 Myosin dependent contractile forces in human airway smooth muscle cells are transmitted across integrin receptors

To visualize contractile forces exerted by the human ASM cells, we used a recently developed protein-based molecular tension fluorescence microscopy (MTFM) sensor that maps piconewton integrin forces with high spatial and temporal resolution.[28] The core of the sensor is comprised of an I27 immunoglobulin domain, a β-sandwich protein with 89 residues, found in the giant sarcomeric protein of striated muscle[37] that exhibits spring-like properties.[37-39] We engineered an I27 domain to display a linear arginine-glycine-aspartate (RGD)-containing peptide at the N-terminus, an integrin-binding sequence found in ECM, followed by a site-specifically incorporated organic dye through unnatural amino acid expression and cysteines at the C-terminus. The cysteine residues allow for immobilization onto 9 nm gold nanoparticles (AuNPs) supported on a glass coverslip (Figure 3.1A). The AuNPs not only serve as a platform to anchor the sensor, but also function as an efficient quencher of the fluorescence through nanometal surface energy transfer (NSET) when I27

is folded into its native β-sandwich structure.[33-34] When ASM cells were cultured on the RGD-Cy3-I27 probe surface for 1 h, we observed an increase in the fluorescence intensity at the sites of adhesion which was observed using total-internal reflection fluorescence (TIRF) and was correlated with the cell perimeter as indicated by reflection interference contract microscopy (RICM) (Figure 3.1B). The increase in the fluorescence signal suggested that integrin-mediated forces mechanically unfolded the I27 domain and separated the Cy3 from the AuNP quencher. To verify that integrins unfolded the protein sensor by engaging RGD ligand, we generated a variant protein sensor in which the structurally conservative RGD was mutated to RGE. This single point mutation prevented cell from adhering to the protein surface, indicating that RGD is required for initiating chemo-mechanical pathway that leads to the unfolding of I27 (Appendix, Figure A3.1A). To confirm that the fluorescence signal coincides with the focal adhesions (FA) proteins, we transfected ASMCs with common FA markers labeled with green fluorescent protein (GFP), such as GFP-vinculin (Figure 3.1B), GFP-actin and GFP-paxillin (Appendix, Figure A3.1B and C) and observed colocalization of FA proteins with the Cy3 tension signal. To further verify that the contractile forces are driven by the cytoskeleton, we incubated the cells with an inhibitor of Rho-associated protein kinase (ROCK) (Y-27632) (Figure 3.1B) and myosin light chain kinase inhibitor (ML-7) (Appendix, Figure A3.1D) for 30 minutes. Following Y-27632 and ML-7 treatment, the fluorescence tension signal dissipated (Figure 3.1B). The loss in Cy3 signal confirms that tension is reversible and driven by the myosin contractility through the integrins engaged to the MTFM I27-based tension sensor. Time-lapse imaging of the same group of cells that were cultured on the tension probe (6 hrs) revealed that tension signals are highly dynamic (Figure, 3.1C).

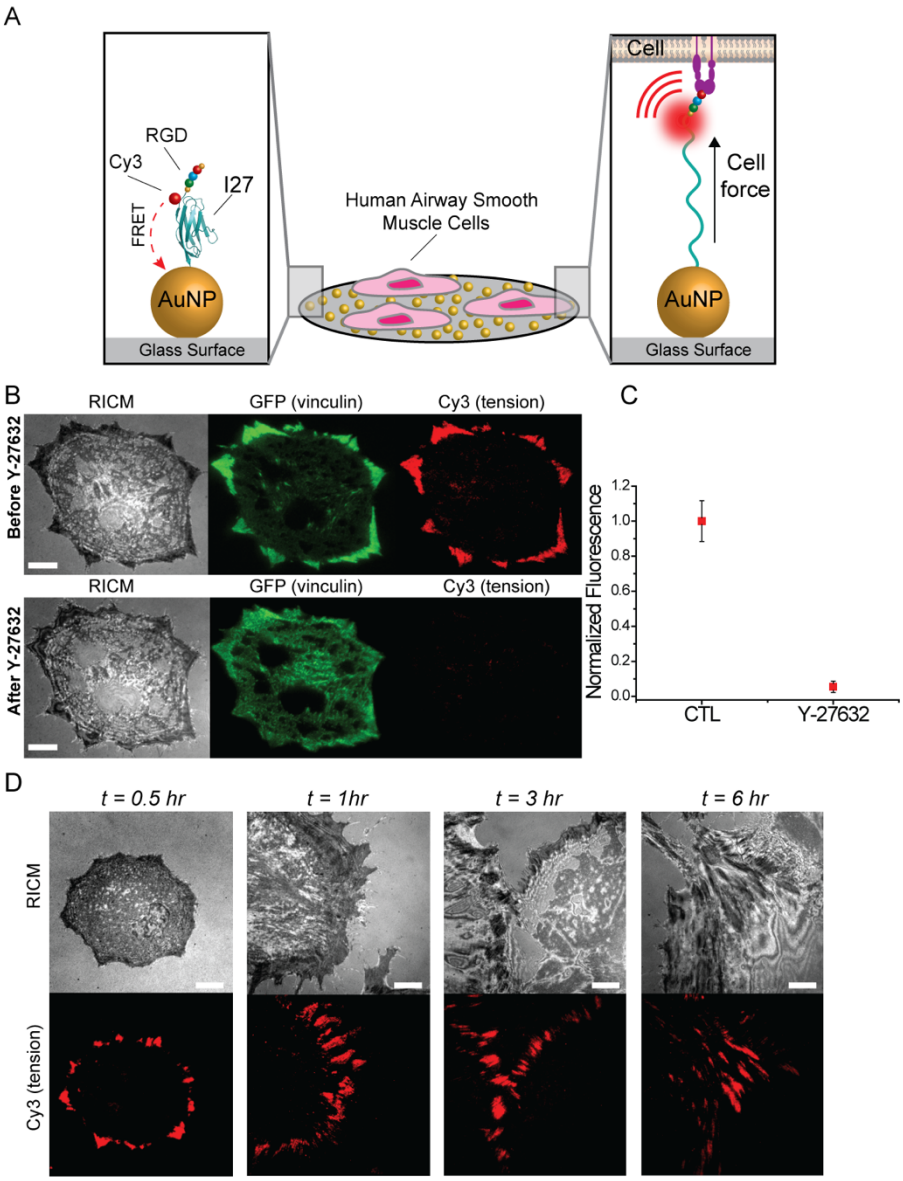

Figure 3.1 Mapping human airway smooth muscle cell integrin forces using titin-based probes. (A) Schematic illustration of the RGD-Cy3-I27 MTFM sensor and its mechanism of reporting integrin forces (PDB ID: 1TIT). (B) Representative RICM and fluorescence images of human ASM cells transfected with GFP-vinculin incubated on the tension sensor before and after treatment with ROCK kinase inhibitor Y-27632 (40 μM) for 30 min. Scale bar, 10 μm. (C) Plot shows the mean tension signal, generated by individual cells before and after ROCK inhibitor treatment. Error bars represents SEM from n = 20 cells from 3 surfaces. (D) Representative time-lapse RICM and fluorescence images of ASM cells cultured on the tension sensor and imaged at the indicated time points. Note the changes in the cell morphology over time. Scale bar, 10 μm.

3.2.2 Human ASM cells isolated from asthmatic patients have an enhanced integrin tension phenotype

Because there are intrinsic differences between asthmatic and healthy airway smooth muscle cells, such as an increase in collagen deposition[40], hypercontractility[7-8, 41-42] and an increase in smooth muscle mass[9, 43-45], we wanted to investigate the mechanical differences between these two cell types. Asthma is characterized by a thickening of airway walls and an enhancement in contractility, but it is unknown whether individuals ASM cells are more contractile at the single cell level. To answer this question, we measured the mechanical tension in ASM cells of healthy individuals and individuals with asthma. ASM cells were harvested from normal individuals and severe asthmatics post mortem and the cells were plated on the AuNP sensor substrates for 1-2 h. The tension was imaged and we found that the fluorescence signal was similarly localized to distal edges of the both normal and asthmatic cells that mirrored the pattern and location of FAs. However, when we integrated the fluorescence intensity of focal adhesions across different patients, we observed that asthmatic cells generated significantly greater levels of integrin tension when compared to normal cells (Figure 3.2C, n = 20 for each cell type). To confirm that the fluorescence signal reflected the different mechanical states of these cells at the protein level, we measured the amounts of total myosin light chain (tMLC) using western blot analysis (Appendix, Figure A3.2A) and verified that asthmatic cells had higher levels of the contractile proteins than normal cells. Next, we measured the magnitude of integrin tension that is applied by normal and asthmatic cells using previously described RGD-Cy3-$I27_{G32C-A75C}$ protein tension sensor clamped with a disulfide bond.[28, 46-47] Normal and asthmatic ASM cells were cultured on the clamped tension probe surfaces for 2 h. By

adding different concentrations of the reducing agent, DTT, and monitoring the kinetics of protein unfolding, we can infer the relative applied tension in each sample. We found that asthmatic ASM cells displayed a second-order rate constant of protein unclamping k_{obs} = 18.9 $M^{-1}s^{-1}$, in contrast to normal cells that displayed a k_{obs} = 25.8 $M^{-1}s^{-1}$. The 25 % increase in integrin tension obtained from kinetics studies is consistent with the data shown in Figure 3.2C. One caveat is that our tension probes do not report forces below the unfolding force of I27. Accordingly, low magnitude tension is ignored. Nonetheless, our data is consistent with ASM cells shortening experiments.[8] Taken together, these results confirmed that ASM cells derived from individuals with asthma not only exerted more integrin tension, but also the magnitude of these forces was greater than that observed for normal individuals.

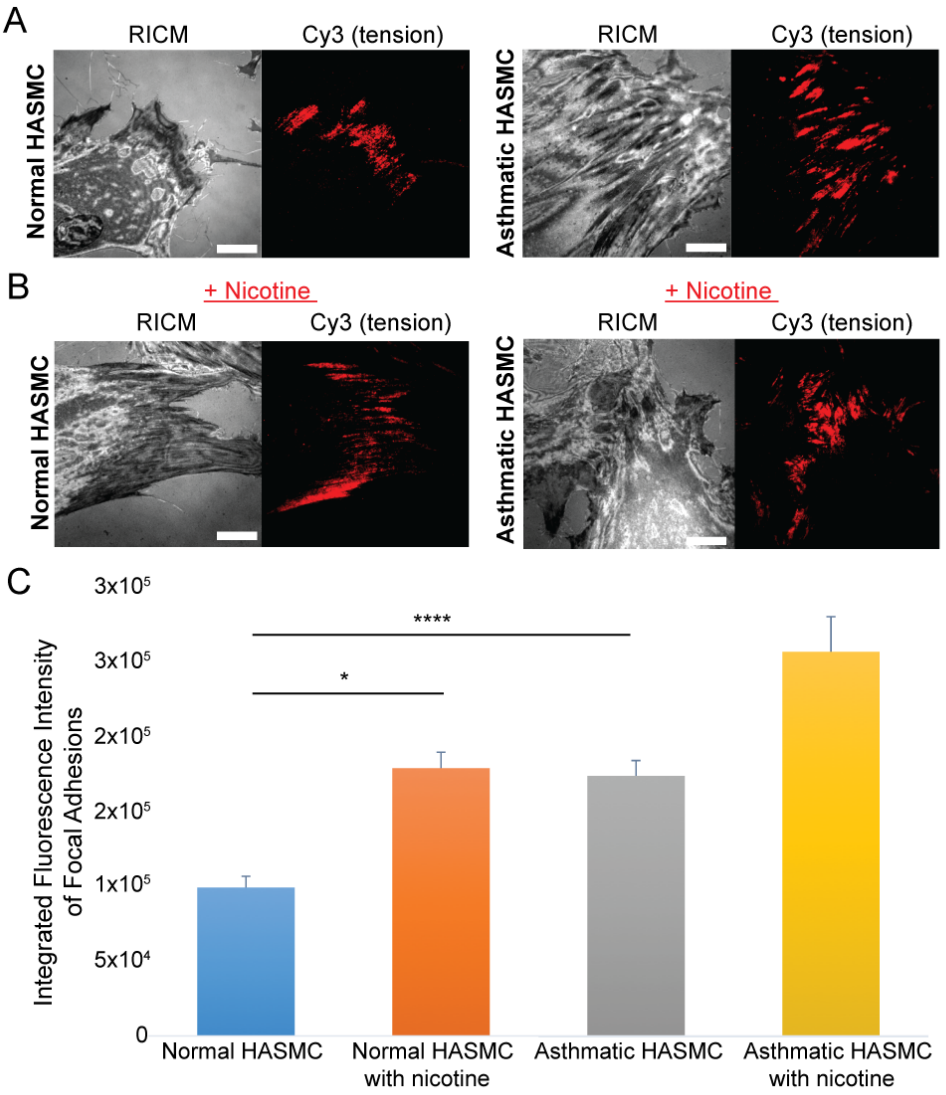

Figure 3.2 Integrin mediated forces are enhanced in the asthmatic human ASM cells and in the presence of nicotine. (A) Representative RICM and integrin-mediated tension images of normal and asthmatic human ASM cells incubated on the RGD-Cy3-I27 tension probe for 2 h. Scale bar, 10 μm. (B) Representative RICM and integrin-mediated tension images of normal and asthmatic ASM cells treated for 72 h with nicotine (50 μg/ml), for 24 h with doxycycline (4 μg/ml) and incubated on the titin-based tension probe for 2 h. Scale bar, 10 μm. (C) Bar graph quantifying the integrated fluorescence intensity of focal adhesions for normal and asthmatic human ASM cells with and without addition of nicotine for 72 h. Error bars represent the standard deviation (S.D.) from n = 10 cells from each group (*$P < 0.05$ and ****$P < 0.0001$).

3.2.3 Nicotine promotes enhancement of integrin forces and stimulates the release of matrix metalloproteinases

Given that certain inhaled substances, such as a cigarette smoke, are known to promote a contractile phenotype of human ASM cells by increasing intracellular calcium concentration and levels of contractile proteins [11, 14, 48-50], we investigated how chronic delivery of nicotine, a major component of cigarette smoke, changes integrin adhesion forces in normal and asthmatic ASM cells. To answer this question, we first treated both normal and asthmatic ASM cells with a daily dose of nicotine at 50 μg/ml for 72 h and measured the changes in the cell morphology using optical microscopy (Appendix, Figure A3.3A). We observed that both cell types became more elongated and aligned when treated with nicotine compared to non-treated cells. This observation suggests changes in cell mechanics. To confirm these observations at the protein level, we measured the amounts of phosphorylated myosin light chain (p-MLC) using western blot analysis (Appendix, Figure A3.3B) and found a significant increase of p-MLC levels in nicotine treated normal ASM cells. These results verified that treatment of ASM cells with nicotine promoted a phenotypic change in the cells that was accompanied by enhanced expression of contraction-promoting markers. To gain further insights into how nicotine affects transmission of traction forces at the molecular level, we plated nicotine treated cells on a surface coated with the RGD-Cy3-I27 tension sensor. Unexpectedly, we found that the fluorescence signal intensity under the perimeter of cells was negative (Appendix, Figure A3.4A). This was only observed in nicotine treated cells. Because previous studies on vascular smooth muscle cells treated with nicotine showed enhanced degradation of extracellular matrix by upregulated matrix metalloproteinase expression (MMPs)[51-53], we

aimed to test whether the negative signal was due to MMP production. MMP release was investigated with surfaces prepared with a binary mixture of RGD-Cy3-I27 and RGE-A647-I27 coincubated on the AuNP surfaces (Appendix, Figure A3.4B). The RGE probes are not engaged by the integrin receptors, so these probes do not experience mechanical unfolding. However, the RGE is sensitive to MMP as it is nearly identical in amino acid sequence to the RGD probes. The results showed that when ASM cells were allowed to spread and engage the binary sensor surface after chronic treatment of nicotine for 72 h, there was a negative fluorescence signal intensity under the distal edges of the cells in both RGD (Cy3) and RGE (A647) fluorescence channels showing that both protein sensors were cleaved by the proteinases. Therefore, the negative signal is mainly due to proteases locally released near mechanically active integrins.

To investigate the dependence of the MMPs release on integrin subtype, we incubated the nicotine-treated cells with monoclonal blocking antibodies specific toward $\alpha_v\beta_3$, $\alpha_5\beta_1$ and $\alpha_v\beta_5$ integrins, the most common subtypes of integrins found in ASM cells for 30 min.[21] When pretreated cells were added to the RGD-Cy3-I27 sensor surfaces and allowed to spread and apply tension for 2 h, we observed a negative signal under the cell perimeter for cells treated with antibodies against $\alpha_v\beta_3$ and $\alpha_v\beta_5$ but not $\alpha_5\beta_1$ (Appendix, Figure A3.4C). These finding are also consistent with the recent work of others that demonstrated that $\alpha_5\beta_1$ integrin tethering to extracellular fibronectin is important in transmitting force throughout the smooth muscle thus leading to cellular contraction.[54]

Further evidence of protease release is revealed by the treatment of ASM cells with doxycycline (4 μg/ml, 24 h), a known inhibitor of MMPs expression[55], before plating cells on tension sensor surfaces (Appendix, Figure A3.4D). The marked increase in Cy3

fluorescence signal and the lack of dark signal at the cell perimeter confirms that ASM cells upregulate protease expression when cultured in the presence of nicotine. Because it has been previously shown that nicotine upregulates MMP-2 and MMP-9 through the α7-nAChR[51, 56], we next examined the role of α7-nAChR in protease expression after chronic treatment with nicotine. When ASM cells were coincubated with nicotine and α-bungarotoxin, an irreversible antagonist of α7- nAChR, for 72 h and plated on the tension surface, there was only a strong fluorescent signal under the cell perimeter and no detectable dark signal (Appendix, Figure A3.4E). Taken together, these findings verify that nicotine drives the release of MMPs and likely MMP-2/-9 at FAs in a α7-nAChR-dependent process.

In order to compare mechanics of normal and asthmatic cells after chronic treatment with nicotine, we cultured the cells with doxycycline (24 h) on the tension sensor to inhibit the release of proteases. Representative cell images are shown in Figure 3.2B and their fluorescence signals were measured and plotted in Figure 3.2C. The data shows that stimulation with nicotine caused the cells to become more polarized and further enhanced integrin tension as measured using the I27 probe by both normal and asthmatic ASM cells.

3.2.4 Role of nicotinic acetylcholine receptor (nAChR) in the transmission of contractile forces

To investigate if α7-nAChR had specific contributions toward integrin mediated mechanical forces, we labeled the α7-nAChR antibody with an amine-reactive Alexa 647 and immunostained ASM cells that had been plated on the sensor surface for 2 h (Figure 3.3A). Surprisingly, an overlay of the immunostained cells with the sensor response showed that tension and α7-nAChR are colocalized at the adhesion sites. Further

experiments indicated that nAChR colocalized with paxillin, a common component of FAs (Appendix, Figure A3.5 A and B). We next pretreated normal ASM cells for 1 h with two antagonists of α7-nAChR: α-bungarotoxin (α-BTX) and methyllycaconitine (MLA) at 2 μM and 10 μM (Appendix, Figure A3.5 C and D), respectively, and added the cells on the RGD-Cy3-I27 substrates. As shown in the RICM, tension and brightfield channels, blocking nicotinic acetylcholine receptors prevented the ASM cells from binding and engaging molecular tension probes on the functionalized surface. Thus, ASM cells were first allowed to spread and generate tension signal at the FA sites followed by the addition of α7-nAChR antagonists. When ASM cells were treated with 5 nM of α-BTX for 30 min which inhibits opening of nicotinic ion channels and calcium flux, we observed that the tension signal under the perimeter of the cells was diminished by ~ 50 % suggesting that integrin tension is mediated in part by the actions of α7-nAChR (Figure 3.3B). We next verified these observations with another potent and specific α7-nAChR antagonist, MLA. After ASM cells generated strong Cy3 fluorescence signal at the edges of the cell, we added 10 μM of MLA for 30 min to block the nicotinic ion channels. We observed a significant decrease at the distal edges of the cells when cells were treated with the MLA (Figure 3.3C). All together, these findings revealed that nicotinic acetylcholine receptor contributes to maintaining the transmission of molecular forces through integrin receptors of FAs.

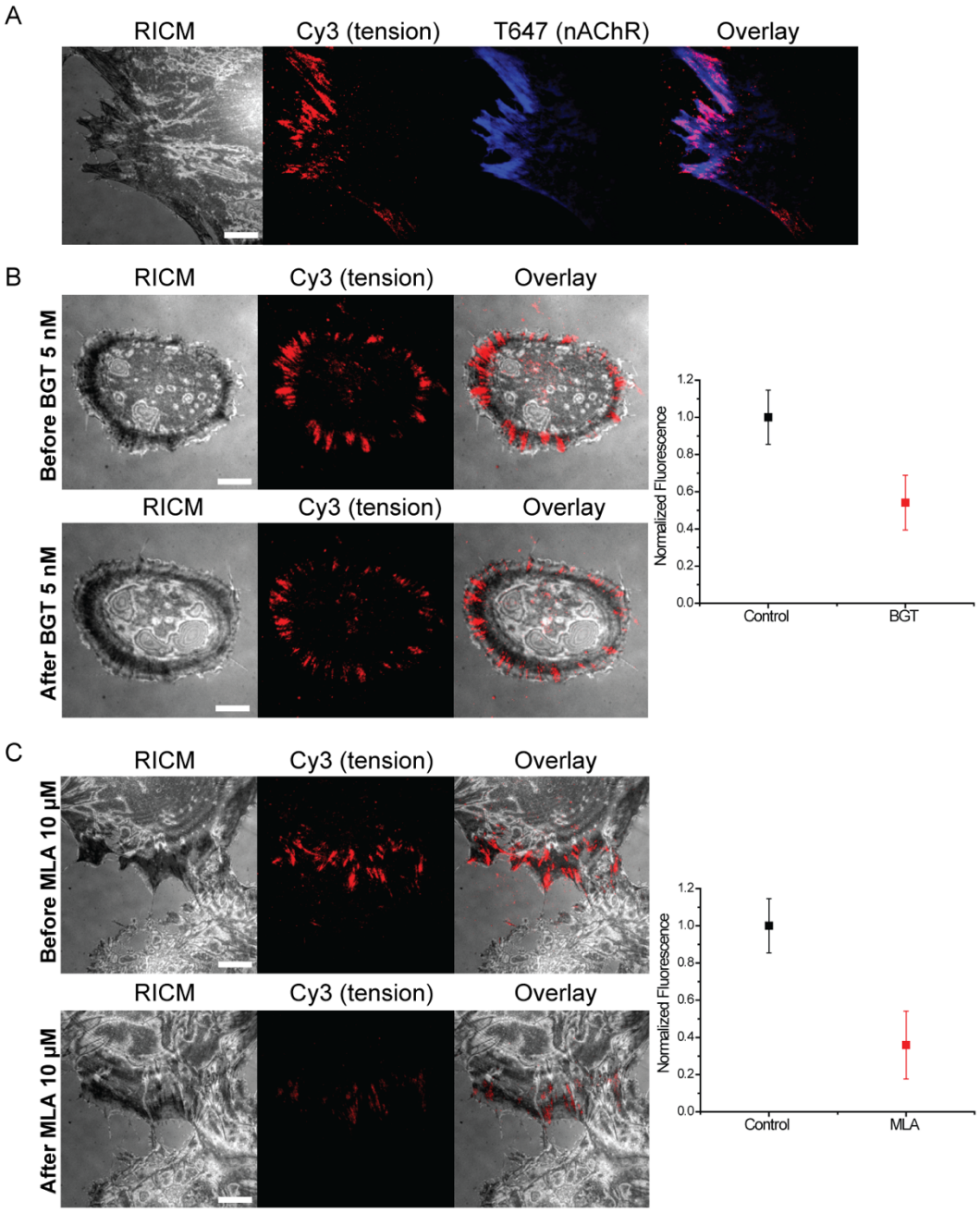

Figure 3.3 α7 nicotinic acetylcholine receptors mediate the transmission of force through the integrins in ASM cells. (A) Representative images of RICM, tension (Cy3), nAChR (T647) and Cy3/T647 overlay images of human ASM cells cultured on the RGD-Cy3-I27 tension sensor for 2 h. Scale bar, 10 µm. (B) Human ASM cells were cultured on the tension sensor for 2 h and treated with 5 nM of α-bungarotoxin (α-BTX), α7 nAChR antagonist, for 30 min. Scale bar, 10 µm. (C) Human ASM cells were cultured on the tension sensor for 2 h and treated with 10 µM of methyllycaconitine (MLA), α7 nAChR inhibitor for 30 min. Scale bar, 10 µm. Error bars represent standard deviation of the mean (SEM) from n = 5 cells from each sample.

3.2.5 Albuterol does-dependently inhibits contractile forces

Our next goal was to extend molecular tension sensors as a diagnostic method to study asthma. We tested the effects of known bronchodilator drugs on integrin tension by plating asthmatic ASM cells on the RGD-Cy3-I27 sensor surface for 2 h and adding albuterol (100 μM) and isoproterenol (100 μM), short acting bronchodilators acting on β2 adrenoceptor for 15 min. Treatment with the bronchodilators rapidly extinguished the fluorescence tension signal (Figure 3.4 A and B). These results suggested that addition of the ASM relaxants led to significant decrease in cell contractility and thus caused the protein sensor to refold and requench the fluorescence.

To titrate the amount of albuterol that was needed to quench the fluorescence signal, we cultured normal ASM cells on the tension sensor substrate for 2 h and then added graded doses of albuterol that ranged from 0.01 nM up to 1 mM. The albuterol was added to the cell media at 5 min intervals (Figure 3.4C). Tension maps in the Cy3 channel showed a gradual decrease of the fluorescence intensity under the cell perimeter. Next, we plotted the integrated tension signal as a function of albuterol concentration for individual cells. Sigmoidal fitting of the data produced a functional EC_{50} for normal cells incubated in the presence and absence of nicotine (Figure 3.4D, for the images of cells treated with nicotine see Appendix, Figure A3.6A). The concentration required for inhibiting 50 % of integrin-mediated tension in ASM cells treated with nicotine (EC_{50} = 198 ± 38 nM) was ~10 fold greater than in untreated ASM cells (EC_{50} = 21 ± 4 nM). These results show that albuterol dose-dependently inhibited contractile force in both normal cells and cells treated with nicotine but a higher concentration of albuterol was required to inhibit 50 % of the tension for the cells pre-treated with nicotine. Herein, the EC_{50} values are more direct

measurements of albuterol effects on contractility and relaxation than has never been measured before. Previous studies reported that the albuterol concentration producing half-maximum attenuation of eosinphill-activating cytokines from human airway smooth muscle cells was 25 ± 3 nM.[18] Another study reported that the concentration of albuterol necessary for driving half-maximum cyclic AMP formation in ASM cells was 0.6 μM.[17] However, there results are readouts of intermediate effectors of contraction, rather than direct and functional readouts of cell mechanics.

Finally, we performed a mechano-assay among the ASM cells derived from the control non-asthmatic patients (n = 3) and asthmatic patients (n = 4) to calculate the EC_{50} for each individual before and after nicotine treatment. We plated ASM cells on the tension probe surface for 2 h to allow for generation of a strong fluorescence signal at the sites of adhesion. Next, we added increasing doses of albuterol and monitored the dissipation of signal (n = 20 cells) and calculated EC_{50} from sigmoidal curves (Figure 3.4E). All together, these findings reveal that 1) asthmatic cells had higher EC_{50} than normal cells and 2) nicotine increased EC_{50} values for both normal and asthmatic. In both cases, higher EC_{50} values suggest a greater contractile, less relaxed phenotype. It is the first mechanopharmacology assay that interrogates how drugs directly modulate pN forces applied by the integrin receptors. The possible applications of this assay include assessing response to therapy, diagnosing diseases characterized by abnormal cellular mechanics, and screening new drugs for effectiveness. As a personalized mechanobiologic assay, this assay may eventually help determine the right treatment and right dose for the right patient with asthma or other disease.

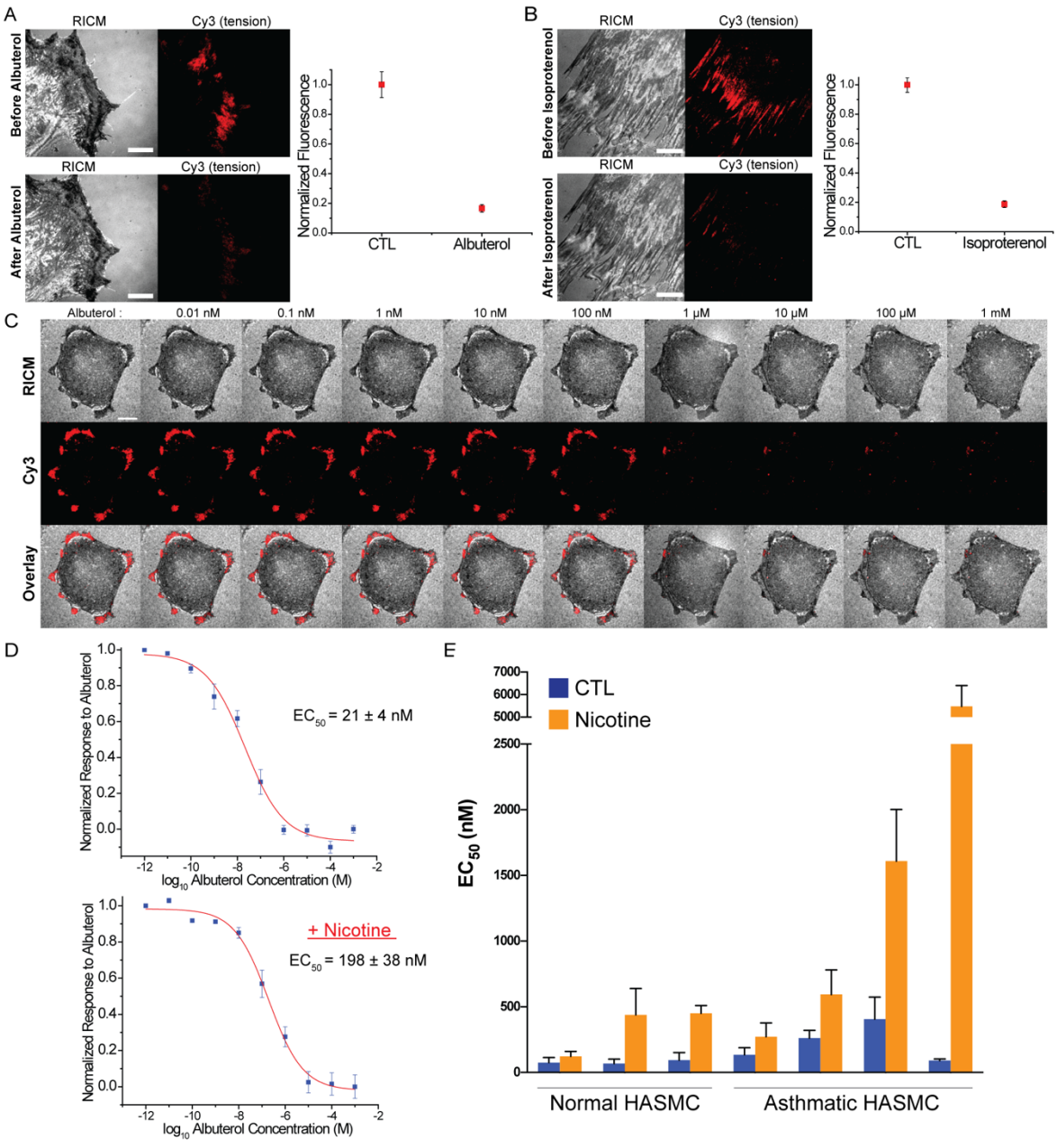
A
RICM
Cy3 (tension)
Before Albuterol
After Albuterol
Normalized Fluorescence
CTL
Albuterol
B
Before Isoproterenol
After Isoproterenol
Isoproterenol
C
Albuterol :
0.01 nM
0.1 nM
1 nM
10 nM
100 nM
1 μM
10 μM
100 μM
1 mM
Cy3
Overlay
D
Normalized Response to Albuterol
EC50 = 21 ± 4 nM
log10 Albuterol Concentration (M)
+ Nicotine
EC50 = 198 ± 38 nM
E
CTL
Nicotine
EC50 (nM)
Normal HASMC
Asthmatic HASMC

Figure 3.4 Albuterol dose-dependently inhibits contractile forces in both normal and asthmatic ASM cells treated with and without nicotine. (A-B) Representative RICM and fluorescence images of asthmatic ASM cells seeded on RGD-Cy3-I27 tension sensor that were treated with 100 μM of albuterol and 100 μM of isoproterenol for 15 min. Scale bar, 10 μm. (C) Representative RICM, integrin tension, and overlay of RICM and tension images for a single, normal ASM cell adhered on the RGD-Cy3-I27 tension surface and treated with a stepwise addition of albuterol (0.01 nM – 1 mM). Scale bar, 10 μm. (D) Representative dose-dependent curves for normal human ASM cells (n = 10 cells) with and without the presence of nicotine (50 μg/ml). R^2 values associated with both fits were >0.98. (E) EC_{50} values were calculated from dose-dependent curves of normal (n = 3 patients) and asthmatic ASM cells (n = 4 patients) stimulated with nicotine (50 μg/ml) for 72 h and doxycycline (4 μg/ml) for 24 h, cultured on the tension sensor and treated with the stepwise addition of the albuterol. Error bars represent the SEM of EC_{50} values obtained from n = 10 cells from each patient.

3.3 Conclusion

In conclusion, we used our recently developed titin-based tension probe to compare integrin-mediated tension in healthy and asthmatic ASM cells. We discovered that asthmatic ASM cells not only generate more traction forces in the cell but also the magnitude of these forces are greater than healthy ASM cells. The contractile response in both phenotypes was further promoted in the presence of nicotine. In addition, we found that there is a link between nicotinic acetylcholine receptor and integrin mediated transmission of molecular forces. However, the physiological importance of this connection remains to be determined. Interestingly, we also discovered that by activating α7-nAChR with nicotine, matrix metalloproteinases MMP-2/-9 are released at the sites of the focal adhesions and that this release was mediated by the $\alpha_5\beta_1$ integrins. Most importantly, using fluorescence signal, we developed a mechano-assay that measures EC_{50}

of a bronchodilator as a readout of the contractile phenotype of the cell. We found that EC_{50} values of albuterol for asthmatic ASM cells were higher than for healthy ASM cells. The highest EC_{50} values were associated with cells that were incubated in the presence of nicotine suggesting that nicotine promoted the contractile phenotype of ASM cells *in vitro*. These findings demonstrate that molecular tension probes can be used as a potential diagnostic tool for personalized mechanopharmacology assay by assessing drug potency and contractile phenotype at the molecular level.

3.4 Materials and methods

3.4.1 Materials

Methyllycaconitine (ML), ROCK inhibitor (Y-27632, ≥98.0%), dimethyl sulfoxide (99%, DMSO), MLCK inhibitor (ML-7), dithiothreitol (99%, DTT), (3-aminopropyl) trimethoxysilane (97%, APTMS), the fluorescent dye dibenzocyclooctyne-Cy3 (DBCO-Cy3), potassium phosphate monobasic (≥99.0%), Y-27632 dihydrochloride (>98%), MLCK inhibitor (ML-7), isoproterenol hydrochloride, α-Bungarotoxin-tetramethylrhodamine, unlabeled α-Bungarotoxin, doxycycline hyclate (≥98%), salbutamol (albuterol) and nicotine (≥99%) were purchased from Sigma-Aldrich (St. Louis, MO). The anit-nicotinic acetylcholine receptor α_7 antibody (ab10096) was obtained from Abcam (Cambridge, United Kingdom). The Slide-A-Lyzer™ Dialysis Cassettes and the fluorescent dyes: Alexa647 N-hydroxysuccinimidyl ester and Alexa647 DIBO alkyne were purchased from Life Technologies (Grand Island, NY). 4-Azido-L-phenylalanine was purchased from Chem-Impex International (Wood Dale, IL). Ni-NTA Agarose (#30210) was purchased from Qiagen (Valencia, CA). Lipofectamine® LTX with Plus™ Reagent

for cell transfection was purchased from Life Technologies (Carlsbad, CA). Number two glass coverslips were purchased VWR (Radnor, PA). Lipoic Acid-PEG-NHS (MW 3400) and mPEG-NHS (MW 2000) were purchased from Nanocs (New York, NY). AuNPs of approximately 9 nm in diameter were purchased from Nanocomposix (San Diego, CA). Sodium bicarbonate was purchased from EMD chemicals (Philadelphia, PA). P2 gel size exclusion beads were purchased from BioRad (Hercules, CA).

3.4.2 Cell culture and transfection

Diseased and healthy human airway smooth muscle (ASM) cells, isolated from asthmatic and healthy patients using endobronchial biopsies, were cultured in DMEM (Mediatech) supplemented with 10% FBS (Mediatech), penicillin G (100 IU ml-1, Mediatech) and streptomycin (100 μg ml-1, Mediatech) at 37 °C in the presence of 5% CO_2. Cells were passaged at ~90 % confluency and plated at a density of 50%. Airway smooth muscle cells (ASMCs) were transiently transfected with either GFP-actin, GFP-vinculin or GFP-paxillin using Lipofectamine® LTX with Plus™ reagent by mixing 1 μg of DNA with Lipofectamine® LTX and Plus™ Reagent for each well in a 24-well plate and incubated for 24-48 h.

3.4.3 Antibody blocking

ASM cells were incubated with monoclonal antibodies selective for $\alpha_5\beta_1$ (MAB1969, Millipore), $\alpha_v\beta_5$ (MAB1961, Millipore) and $\alpha_v\beta_3$ (MAB1976, Millipore) at 10 μg/ml for 30 min. Additionally, 10 μg of antibody was added to each functionalized surface for full inhibition of $\alpha_5\beta_1$, $\alpha_v\beta_5$ and $\alpha_v\beta_3$ integrins.

3.4.4 Protein engineering and dye labeling

I27 protein sensors expressing p-azidophenylalanine were designed with N-terminal ligand (either TVYAVTGRGDSPASSAA or TVYAVTGRGESPASSAA) and two C-terminal cysteines for attachment onto AuNPs. For kinetic studies, we used a I27 variant protein in which Cys^{47} and Cys^{63} were mutated to Ala, and Gly^{32} and Ala^{75} were mutated to cysteines to form disulfide bond as previously described.[28] The proteins were expressed in BL21(DE3) *E. coli* cells, purified by Ni^{2+} affinity chromatography and kept at -80 °C in 0.1 M potassium phosphate buffer (pH 7.4). To label the protein sensors with the dye, I27 protein constructs were incubated with either DBCO-Cy3 or DIBO-A647 for 1 h at 37 °C, followed by overnight incubation at room temperature. To purify protein sensors, P2 gel size exclusion beads were used and the labeling ratio was meaured by UV-Vis absorption (NanoDrop).

3.4.5 Fabrication of protein-AuNP surfaces

Glass coverslips (number 2, 25 mm diameter; VWR) were rinsed with Nanopure water (18.2 mΩ), dried at 80 °C, piranha etched in a 3 : 1 mixture of sulfuric acid and 30% hydrogen peroxide for 30 min and then functionalized with an APTMS solution in acetone for 1 h. The samples were then rinsed in acetone three times and baked in an oven at 80 °C for 30 min. After cooling, the substrates were incubated with a solution of 5% (w/v) mPEG-NHS and 0.5% (w/v) lipoic acid-PEG-NHS in 0.1 M fresh sodium bicarbonate overnight at 4 °C. Subsequently, 12 nM of tannic acid stabilized AuNPs (diameter = 9 nm) were added onto the lipoic acid coated surfaces and incubated for 20 min. Afterwards, AuNP surfaces were rinsed with water and incubated with the binary mixture of mPEG, $SH(CH_2\text{-}CH_2\text{-}O)_8COOH$ and the protein sensor in 0.1 M potassium phosphate buffer (pH 7.4) at 1:10 molar stoichiometry for 1 h at RT. The protein surfaces were rinsed with 0.1 M

potassium phosphate buffer (pH 7.4) to remove unbound protein sensors. Functionalized coverslips were then assembled into a custom-made chamber and filled with cell media containing 0.5% FBS to minimize nonspecific absorption of serum proteins and used within the same day.

3.4.6 Fluorescence immunostaining protocol

ASM cells were gently rinsed with 1 X PBS in the imaging chamber, fixed with 4% paraformaldehyde for 10 min, washed with 1 x PBS and then treated with 0.1% Triton for 10 min. Cells were next rinsed with 1 x PBS and immunostained with 1: 220 dilution of α-Bungarotoxin-tetramethylrhodamine for 2 hours at RT. Before imaging, cell samples were rinsed and imaged in 1 X PBS.

3.4.7 Drug treatment

ASM cells were plated at ~50% density and treated chronically with ± 50 μg/ml of nicotine for 72 hours. A day before cell experiment, smooth muscle cells were incubated with 4 μg/ml of doxycycline to prevent a release of matrix metalloproteinases from the cells. To obtain EC_{50}, ASM cells were allowed to spread on the protein sensor functionalized surfaces for 2 h and generate increase in fluorescence at the sites of adhesion. Next, increasing amounts of salbutamol (albuterol, 0.01 nM – 1 mM) were added every 5 min and the fluorescence dose response curve was generated from which the EC_{50} values were determined using Origin dose response fitting function.

3.4.8 Kinetic experiment for force measurement

Kinetic measurements of S-S reduction to determine integrin forces were performed as previously described.[28] Briefly, normal and human ASMC were cultured on a RGD-Cy3-$I27_{G32C-A75C}$ for 2 h. DTT at different concentrations (0, 0.25 mM, 2.5 mM, 5

mM, 12.5 mM, and 25 mM) was added to the chamber (t=0) and the time lapse video of the fluorescence increase was recorded at the 300 ms exposure time. Next, single-exponential fits were used to determine rates of protein unfolding for each DTT concentration. These rates were subsequently plotted as a function of [DTT] and from the slope of the plot, $k(F)$ was obtained and the average force applied by the integrins was inferred.

3.4.9 Live cell fluorescence microscopy imaging

For live cell imaging at 37 °C, Nikon Eclipse Ti microscope with Elements software was used along with the warming apparatus consisting of an objective warmer and sample warmer. The microscope features a TIRF launcher with three laser lines: 488 nm (10 mW), 561 (50 mW), and 647 nm (20 mW), an Intensilight epifluorescence source (Nikon), an Evolve electron multiplying charge coupled device (EMCCD camera, Photometrics), and the Nikon Perfect Focus system that prevents losing a focus during imaging. The microscope is equipped with TIRF 488, TIRF 640, FITC, TRITC, and RICM (reflection interference contrast microscopy) filter cubes that were purchased from Chroma (Bellows Falls, VT).

3.5 References

1. Relling, M. V.; Evans, W. E., Pharmacogenomics in the clinic. *Nature* **2015,** *526* (7573), 343-50.

2. Weinshilboum, R.; Wang, L., Pharmacogenomics: bench to bedside. *Nat Rev Drug Discov* **2004,** *3* (9), 739-48.

3. Chan, V.; Burgess, J. K.; Ratoff, J. C.; O'Connor B, J.; Greenough, A.; Lee, T. H.; Hirst, S. J., Extracellular matrix regulates enhanced eotaxin expression in asthmatic airway smooth muscle cells. *Am J Respir Crit Care Med* **2006,** *174* (4), 379-85.

4. Fredberg, J. J.; Inouye, D. S.; Mijailovich, S. M.; Butler, J. P., Perturbed equilibrium of myosin binding in airway smooth muscle and its implications in bronchospasm. *Am J Respir Crit Care Med* **1999,** *159* (3), 959-67.

5. Ozier, A.; Allard, B.; Bara, I.; Girodet, P. O.; Trian, T.; Marthan, R.; Berger, P., The pivotal role of airway smooth muscle in asthma pathophysiology. *J Allergy (Cairo)* **2011,** *2011*, 742710.

6. Zuyderduyn, S.; Sukkar, M. B.; Fust, A.; Dhaliwal, S.; Burgess, J. K., Treating asthma means treating airway smooth muscle cells. *Eur Respir J* **2008,** *32* (2), 265-74.

7. Leguillette, R.; Laviolette, M.; Bergeron, C.; Zitouni, N.; Kogut, P.; Solway, J.; Kachmar, L.; Hamid, Q.; Lauzon, A. M., Myosin, transgelin, and myosin light chain kinase: expression and function in asthma. *Am J Respir Crit Care Med* **2009,** *179* (3), 194-204.

8. Ma, X.; Cheng, Z.; Kong, H.; Wang, Y.; Unruh, H.; Stephens, N. L.; Laviolette, M., Changes in biophysical and biochemical properties of single bronchial smooth

muscle cells from asthmatic subjects. *Am J Physiol Lung Cell Mol Physiol* **2002,** *283* (6), L1181-9.

9. Mahn, K.; Hirst, S. J.; Ying, S.; Holt, M. R.; Lavender, P.; Ojo, O. O.; Siew, L.; Simcock, D. E.; McVicker, C. G.; Kanabar, V.; Snetkov, V. A.; O'Connor, B. J.; Karner, C.; Cousins, D. J.; Macedo, P.; Chung, K. F.; Corrigan, C. J.; Ward, J. P.; Lee, T. H., Diminished sarco/endoplasmic reticulum Ca2+ ATPase (SERCA) expression contributes to airway remodelling in bronchial asthma. *Proc Natl Acad Sci U S A* **2009,** *106* (26), 10775-80.

10. Somlyo, A. P.; Somlyo, A. V., Ca2+ sensitivity of smooth muscle and nonmuscle myosin II: modulated by G proteins, kinases, and myosin phosphatase. *Physiol Rev* **2003,** *83* (4), 1325-58.

11. Jiang, Y.; Dai, A.; Zhou, Y.; Peng, G.; Hu, G.; Li, B.; Sham, J. S.; Ran, P., Nicotine elevated intracellular Ca(2)(+) in rat airway smooth muscle cells via activating and up-regulating alpha7-nicotinic acetylcholine receptor. *Cell Physiol Biochem* **2014,** *33* (2), 389-401.

12. Wylam, M. E.; Sathish, V.; VanOosten, S. K.; Freeman, M.; Burkholder, D.; Thompson, M. A.; Pabelick, C. M.; Prakash, Y. S., Mechanisms of Cigarette Smoke Effects on Human Airway Smooth Muscle. *PLoS One* **2015,** *10* (6), e0128778.

13. Wongtrakool, C.; Roser-Page, S.; Rivera, H. N.; Roman, J., Nicotine alters lung branching morphogenesis through the alpha7 nicotinic acetylcholine receptor. *Am J Physiol Lung Cell Mol Physiol* **2007,** *293* (3), L611-8.

14. Wongtrakool, C.; Grooms, K.; Bijli, K. M.; Crothers, K.; Fitzpatrick, A. M.; Hart, C. M., Nicotine stimulates nerve growth factor in lung fibroblasts through an NFkappaB-dependent mechanism. *PLoS One* **2014,** *9* (10), e109602.

15. Rakhilin, S.; Drisdel, R. C.; Sagher, D.; McGehee, D. S.; Vallejo, Y.; Green, W. N., alpha-bungarotoxin receptors contain alpha7 subunits in two different disulfide-bonded conformations. *J Cell Biol* **1999,** *146* (1), 203-18.

16. Cazzola, M.; Page, C. P.; Calzetta, L.; Matera, M. G., Pharmacology and therapeutics of bronchodilators. *Pharmacol Rev* **2012,** *64* (3), 450-504.

17. Scott, M. G.; Swan, C.; Jobson, T. M.; Rees, S.; Hall, I. P., Effects of a range of beta2 adrenoceptor agonists on changes in intracellular cyclic AMP and on cyclic AMP driven gene expression in cultured human airway smooth muscle cells. *Br J Pharmacol* **1999,** *128* (3), 721-9.

18. Hallsworth, M. P.; Twort, C. H.; Lee, T. H.; Hirst, S. J., beta(2)-adrenoceptor agonists inhibit release of eosinophil-activating cytokines from human airway smooth muscle cells. *Br J Pharmacol* **2001,** *132* (3), 729-41.

19. Swinney, D. C.; Anthony, J., How were new medicines discovered? *Nat Rev Drug Discov* **2011,** *10* (7), 507-19.

20. Humphrey, J. D.; Dufresne, E. R.; Schwartz, M. A., Mechanotransduction and extracellular matrix homeostasis. *Nat Rev Mol Cell Biol* **2014,** *15* (12), 802-12.

21. Freyer, A. M.; Johnson, S. R.; Hall, I. P., Effects of growth factors and extracellular matrix on survival of human airway smooth muscle cells. *Am J Respir Cell Mol Biol* **2001,** *25* (5), 569-76.

22. Nguyen, T. T.; Ward, J. P.; Hirst, S. J., beta1-Integrins mediate enhancement of airway smooth muscle proliferation by collagen and fibronectin. *Am J Respir Crit Care Med* **2005,** *171* (3), 217-23.

23. Peng, Q.; Lai, D.; Nguyen, T. T.; Chan, V.; Matsuda, T.; Hirst, S. J., Multiple beta 1 integrins mediate enhancement of human airway smooth muscle cytokine secretion by fibronectin and type I collagen. *J Immunol* **2005,** *174* (4), 2258-64.

24. Tatler, A. L.; John, A. E.; Jolly, L.; Habgood, A.; Porte, J.; Brightling, C.; Knox, A. J.; Pang, L.; Sheppard, D.; Huang, X.; Jenkins, G., Integrin alphavbeta5-mediated TGF-beta activation by airway smooth muscle cells in asthma. *J Immunol* **2011,** *187* (11), 6094-107.

25. Chen, C.; Kudo, M.; Rutaganira, F.; Takano, H.; Lee, C.; Atakilit, A.; Robinett, K. S.; Uede, T.; Wolters, P. J.; Shokat, K. M.; Huang, X.; Sheppard, D., Integrin alpha9beta1 in airway smooth muscle suppresses exaggerated airway narrowing. *J Clin Invest* **2012,** *122* (8), 2916-27.

26. Tolic-Norrelykke, I. M.; Wang, N., Traction in smooth muscle cells varies with cell spreading. *J Biomech* **2005,** *38* (7), 1405-12.

27. Park, C. Y.; Zhou, E. H.; Tambe, D.; Chen, B.; Lavoie, T.; Dowell, M.; Simeonov, A.; Maloney, D. J.; Marinkovic, A.; Tschumperlin, D. J.; Burger, S.; Frykenberg, M.; Butler, J. P.; Stamer, W. D.; Johnson, M.; Solway, J.; Fredberg, J. J.; Krishnan, R., High-throughput screening for modulators of cellular contractile force. *Integr Biol (Camb)* **2015,** *7* (10), 1318-24.

28. Galior, K.; Liu, Y.; Yehl, K.; Vivek, S.; Salaita, K., Titin-Based Nanoparticle Tension Sensors Map High-Magnitude Integrin Forces within Focal Adhesions. *Nano Lett* **2016,** *16* (1), 341-8.

29. Chang, Y.; Liu, Z.; Zhang, Y.; Galior, K.; Yang, J.; Salaita, K., A General Approach for Generating Fluorescent Probes to Visualize Piconewton Forces at the Cell Surface. *J Am Chem Soc* **2016,** *138* (9), 2901-4.

30. Jurchenko, C.; Chang, Y.; Narui, Y.; Zhang, Y.; Salaita, K. S., Integrin-generated forces lead to streptavidin-biotin unbinding in cellular adhesions. *Biophys J* **2014,** *106* (7), 1436-46.

31. Jurchenko, C.; Salaita, K. S., Lighting Up the Force: Investigating Mechanisms of Mechanotransduction Using Fluorescent Tension Probes. *Mol Cell Biol* **2015,** *35* (15), 2570-82.

32. Liu, Y.; Blanchfield, L.; Ma, V. P.; Andargachew, R.; Galior, K.; Liu, Z.; Evavold, B.; Salaita, K., DNA-based nanoparticle tension sensors reveal that T-cell receptors transmit defined pN forces to their antigens for enhanced fidelity. *Proc Natl Acad Sci U S A* **2016,** *113* (20), 5610-5.

33. Liu, Y.; Medda, R.; Liu, Z.; Galior, K.; Yehl, K.; Spatz, J. P.; Cavalcanti-Adam, E. A.; Salaita, K., Nanoparticle tension probes patterned at the nanoscale: impact of integrin clustering on force transmission. *Nano Lett* **2014,** *14* (10), 5539-46.

34. Liu, Y.; Yehl, K.; Narui, Y.; Salaita, K., Tension sensing nanoparticles for mechano-imaging at the living/nonliving interface. *J Am Chem Soc* **2013,** *135* (14), 5320-3.

35. Ma, V. P.; Liu, Y.; Blanchfield, L.; Su, H.; Evavold, B. D.; Salaita, K., Ratiometric Tension Probes for Mapping Receptor Forces and Clustering at Intermembrane Junctions. *Nano Lett* **2016,** *16* (7), 4552-9.

36. Zhang, Y.; Ge, C.; Zhu, C.; Salaita, K., DNA-based digital tension probes reveal integrin forces during early cell adhesion. *Nat Commun* **2014,** *5*, 5167.

37. Carrion-Vazquez, M.; Marszalek, P. E.; Oberhauser, A. F.; Fernandez, J. M., Atomic force microscopy captures length phenotypes in single proteins. *Proc Natl Acad Sci U S A* **1999,** *96* (20), 11288-92.

38. Labeit, S.; Kolmerer, B.; Linke, W. A., The giant protein titin. Emerging roles in physiology and pathophysiology. *Circ Res* **1997,** *80* (2), 290-4.

39. Lu, H.; Isralewitz, B.; Krammer, A.; Vogel, V.; Schulten, K., Unfolding of titin immunoglobulin domains by steered molecular dynamics simulation. *Biophys J* **1998,** *75* (2), 662-71.

40. Bousquet, J.; Lacoste, J. Y.; Chanez, P.; Vic, P.; Godard, P.; Michel, F. B., Bronchial elastic fibers in normal subjects and asthmatic patients. *Am J Respir Crit Care Med* **1996,** *153* (5), 1648-54.

41. An, S. S.; Bai, T. R.; Bates, J. H.; Black, J. L.; Brown, R. H.; Brusasco, V.; Chitano, P.; Deng, L.; Dowell, M.; Eidelman, D. H.; Fabry, B.; Fairbank, N. J.; Ford, L. E.; Fredberg, J. J.; Gerthoffer, W. T.; Gilbert, S. H.; Gosens, R.; Gunst, S. J.; Halayko, A. J.; Ingram, R. H.; Irvin, C. G.; James, A. L.; Janssen, L. J.; King, G. G.; Knight, D. A.; Lauzon, A. M.; Lakser, O. J.; Ludwig, M. S.; Lutchen, K. R.; Maksym, G. N.; Martin, J. G.; Mauad, T.; McParland, B. E.; Mijailovich, S. M.; Mitchell, H. W.; Mitchell, R. W.; Mitzner, W.; Murphy, T. M.; Pare, P. D.; Pellegrino, R.; Sanderson, M. J.; Schellenberg,

R. R.; Seow, C. Y.; Silveira, P. S.; Smith, P. G.; Solway, J.; Stephens, N. L.; Sterk, P. J.; Stewart, A. G.; Tang, D. D.; Tepper, R. S.; Tran, T.; Wang, L., Airway smooth muscle dynamics: a common pathway of airway obstruction in asthma. *Eur Respir J* **2007,** *29* (5), 834-60.

42. Mahn, K.; Ojo, O. O.; Chadwick, G.; Aaronson, P. I.; Ward, J. P.; Lee, T. H., Ca(2+) homeostasis and structural and functional remodelling of airway smooth muscle in asthma. *Thorax* **2010,** *65* (6), 547-52.

43. Trian, T.; Benard, G.; Begueret, H.; Rossignol, R.; Girodet, P. O.; Ghosh, D.; Ousova, O.; Vernejoux, J. M.; Marthan, R.; Tunon-de-Lara, J. M.; Berger, P., Bronchial smooth muscle remodeling involves calcium-dependent enhanced mitochondrial biogenesis in asthma. *J Exp Med* **2007,** *204* (13), 3173-81.

44. Bara, I.; Ozier, A.; Tunon de Lara, J. M.; Marthan, R.; Berger, P., Pathophysiology of bronchial smooth muscle remodelling in asthma. *Eur Respir J* **2010,** *36* (5), 1174-84.

45. Carroll, N.; Elliot, J.; Morton, A.; James, A., The structure of large and small airways in nonfatal and fatal asthma. *Am Rev Respir Dis* **1993,** *147* (2), 405-10.

46. Ainavarapu, S. R.; Brujic, J.; Huang, H. H.; Wiita, A. P.; Lu, H.; Li, L.; Walther, K. A.; Carrion-Vazquez, M.; Li, H.; Fernandez, J. M., Contour length and refolding rate of a small protein controlled by engineered disulfide bonds. *Biophys J* **2007,** *92* (1), 225-33.

47. Wiita, A. P.; Ainavarapu, S. R.; Huang, H. H.; Fernandez, J. M., Force-dependent chemical kinetics of disulfide bond reduction observed with single-molecule techniques. *Proc Natl Acad Sci U S A* **2006,** *103* (19), 7222-7.

48. He, F.; Li, B.; Zhao, Z.; Zhou, Y.; Hu, G.; Zou, W.; Hong, W.; Zou, Y.; Jiang, C.; Zhao, D.; Ran, P., The pro-proliferative effects of nicotine and its underlying mechanism on rat airway smooth muscle cells. *PLoS One* **2014,** *9* (4), e93508.

49. Streck, E.; Jorres, R. A.; Huber, R. M.; Bergner, A., Effects of cigarette smoke extract and nicotine on bronchial tone and acetylcholine-induced airway contraction in mouse lung slices. *J Investig Allergol Clin Immunol* **2010,** *20* (4), 324-30.

50. Takayanagi, I.; Kizawa, Y.; Sone, H., Action of nicotine on guinea-pig isolated bronchial smooth muscle preparation. *Gen Pharmacol* **1984,** *15* (4), 349-52.

51. Li, Z. Z.; Guo, Z. Z.; Zhang, Z.; Cao, Q. A.; Zhu, Y. J.; Yao, H. L.; Wu, L. L.; Dai, Q. Y., Nicotine-induced upregulation of VCAM-1, MMP-2, and MMP-9 through the alpha7-nAChR-JNK pathway in RAW264.7 and MOVAS cells. *Mol Cell Biochem* **2015,** *399* (1-2), 49-58.

52. Gu, Z.; Fonseca, V.; Hai, C. M., Nicotinic acetylcholine receptor mediates nicotine-induced actin cytoskeletal remodeling and extracellular matrix degradation by vascular smooth muscle cells. *Vascul Pharmacol* **2013,** *58* (1-2), 87-97.

53. Wang, Y.; McNiven, M. A., Invasive matrix degradation at focal adhesions occurs via protease recruitment by a FAK-p130Cas complex. *J Cell Biol* **2012,** *196* (3), 375-85.

54. Sundaram, A.; Chen, C.; Khalifeh-Soltani, A.; Atakilit, A.; Ren, X.; Qiu, W.; Jo, H.; DeGrado, W.; Huang, X.; Sheppard, D., Targeting integrin alpha5beta1 ameliorates severe airway hyperresponsiveness in experimental asthma. *J Clin Invest* **2017,** *127* (1), 365-374.

55. Liu, J.; Xiong, W.; Baca-Regen, L.; Nagase, H.; Baxter, B. T., Mechanism of inhibition of matrix metalloproteinase-2 expression by doxycycline in human aortic smooth muscle cells. *J Vasc Surg* **2003,** *38* (6), 1376-83.

56. Dom, A. M.; Buckley, A. W.; Brown, K. C.; Egleton, R. D.; Marcelo, A. J.; Proper, N. A.; Weller, D. E.; Shah, Y. H.; Lau, J. K.; Dasgupta, P., The alpha7-nicotinic acetylcholine receptor and MMP-2/-9 pathway mediate the proangiogenic effect of nicotine in human retinal endothelial cells. *Invest Ophthalmol Vis Sci* **2011,** *52* (7), 4428-38.

3.6 Appendix

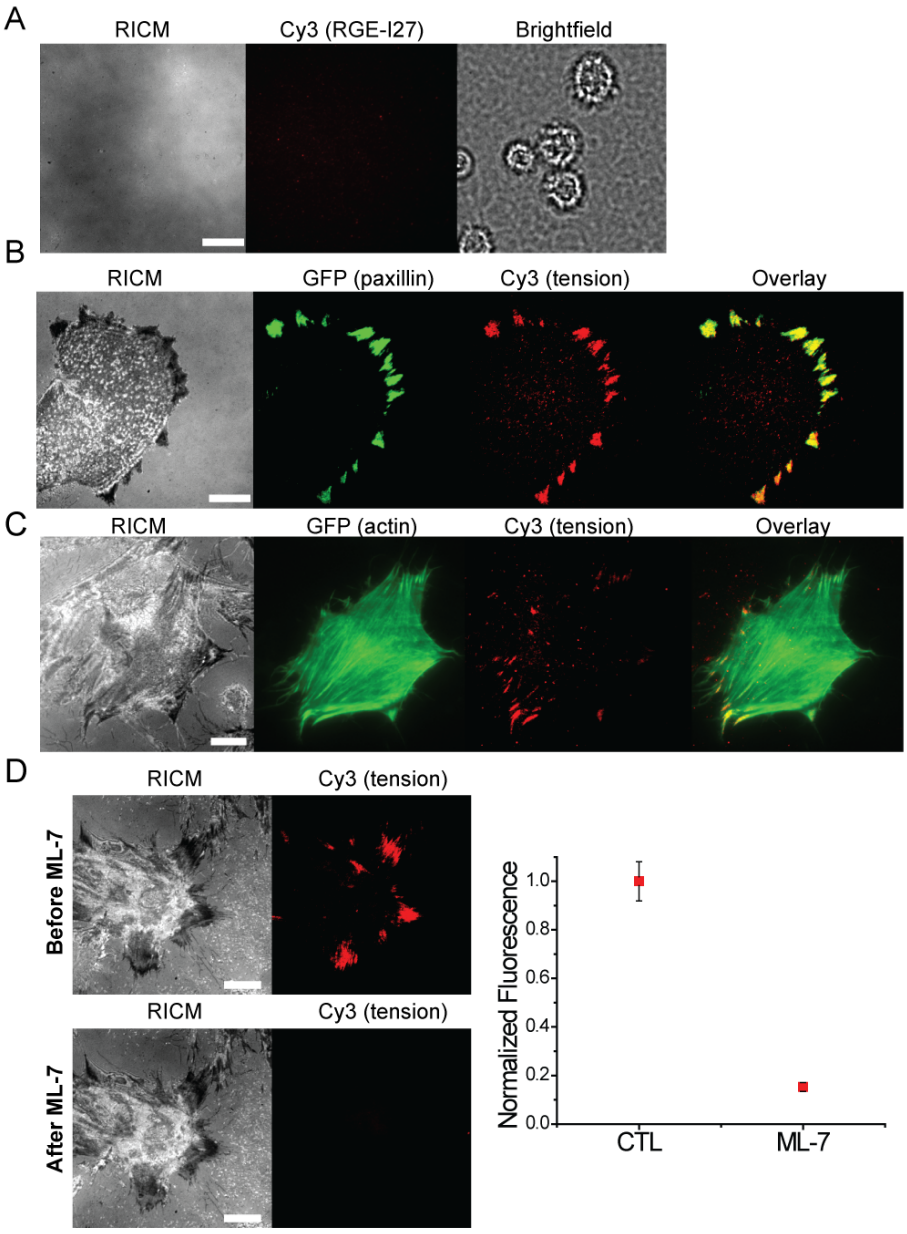
A
RICM
Cy3 (RGE-I27)
Brightfield
B
RICM
GFP (paxillin)
Cy3 (tension)
Overlay
C
RICM
GFP (actin)
Cy3 (tension)
Overlay
D
RICM
Cy3 (tension)
Before ML-7
RICM
Cy3 (tension)
After ML-7
Normalized Fluorescence
1.0
0.8
0.6
0.4
0.2
0.0
CTL
ML-7

Figure A3.1 Tension signals are specifically generated through integrin-RGD interactions and are mediated by the cytoskeleton. (A) Representative RICM, fluorescence and brightfield images of human ASM cells cells plated onto a surface coated with the RGE-Cy3-I27 nanoparticle sensors. Mutating RGD to RGE completely inhibits cell binding and spreading. Scale bar, 10 μm. (B) Representative RICM, GFP-paxillin and Cy3 tension images of human ASM cells incubated on the RGD-Cy3-I27 functionalized on the AuNPs for 1 hr. An overlay of Cy3/GFP demonstrates that tension signal was colocalized with the FA. Scale bar, 10 μm. (C) Representative RICM, GFP-actin, Cy3 tension, and overlay of Cy3/GFP demonstrate that tension signal was colocalized with the cell cytoskeleton. Scale bar, 10 μm. (D) Representative RICM and Cy3 tension images of human ASMCs cultured on the RGD-Cy3-I27 sensor surface for 2 h. Images were captured before and after treatment with MLCK inhibitor: ML-7(40 μM). Scale bar, 10 μm.

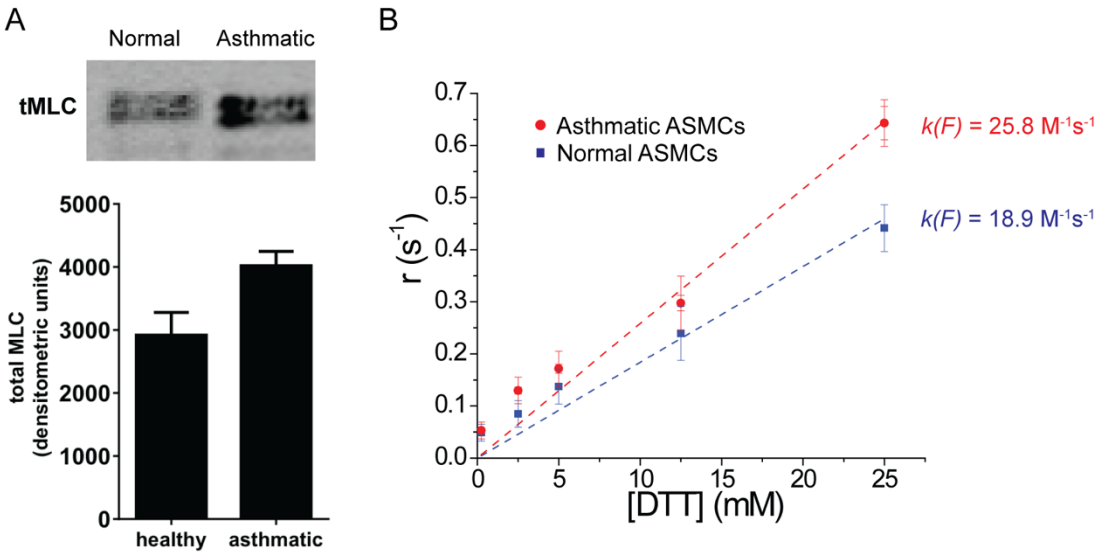

Figure A3.2 Asthmatic human ASM cells have higher levels of contractile proteins and exert higher magnitude of forces compared to normal human ASM cells. (A) Total myosin light chain (total MLC) expression was measured for normal and asthmatic human ASM cells by using western blot analysis with densitometry. (B) Plot of *r* (rate of disulfide reduction) as a function of [DTT] for normal human ASMCs (blue) and asthmatic human ASM cells (red). From *k(F)* which was derived from the slope of the plot, average force *F* was calculated.

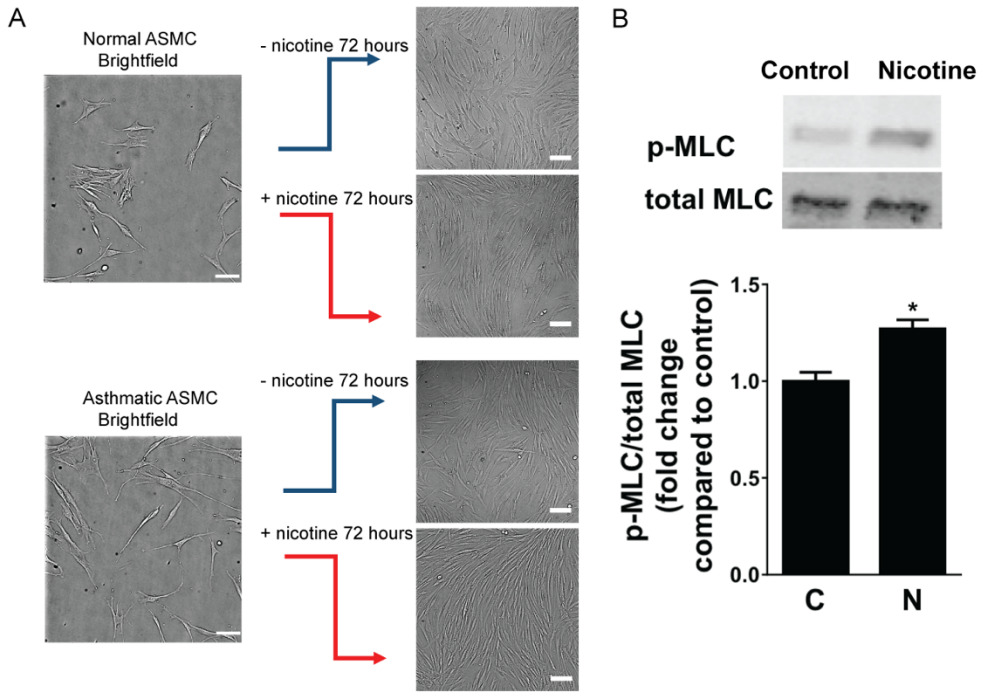

Figure A3.3 Changes in morphology and gene expression of human ASM cells incubated with and without nicotine over 72 h. (A) Representative brightfield images of normal and asthmatic human ASM cells incubated in the presence of 50 μg/ml of nicotine. Scale bar, 100 μm. (B) Total myosin light chain (total MLC) and phosphorylated myosin light chain (p-MLC) expression levels were measured by western blot analysis with densitometry (*$P \leq 0.05$).

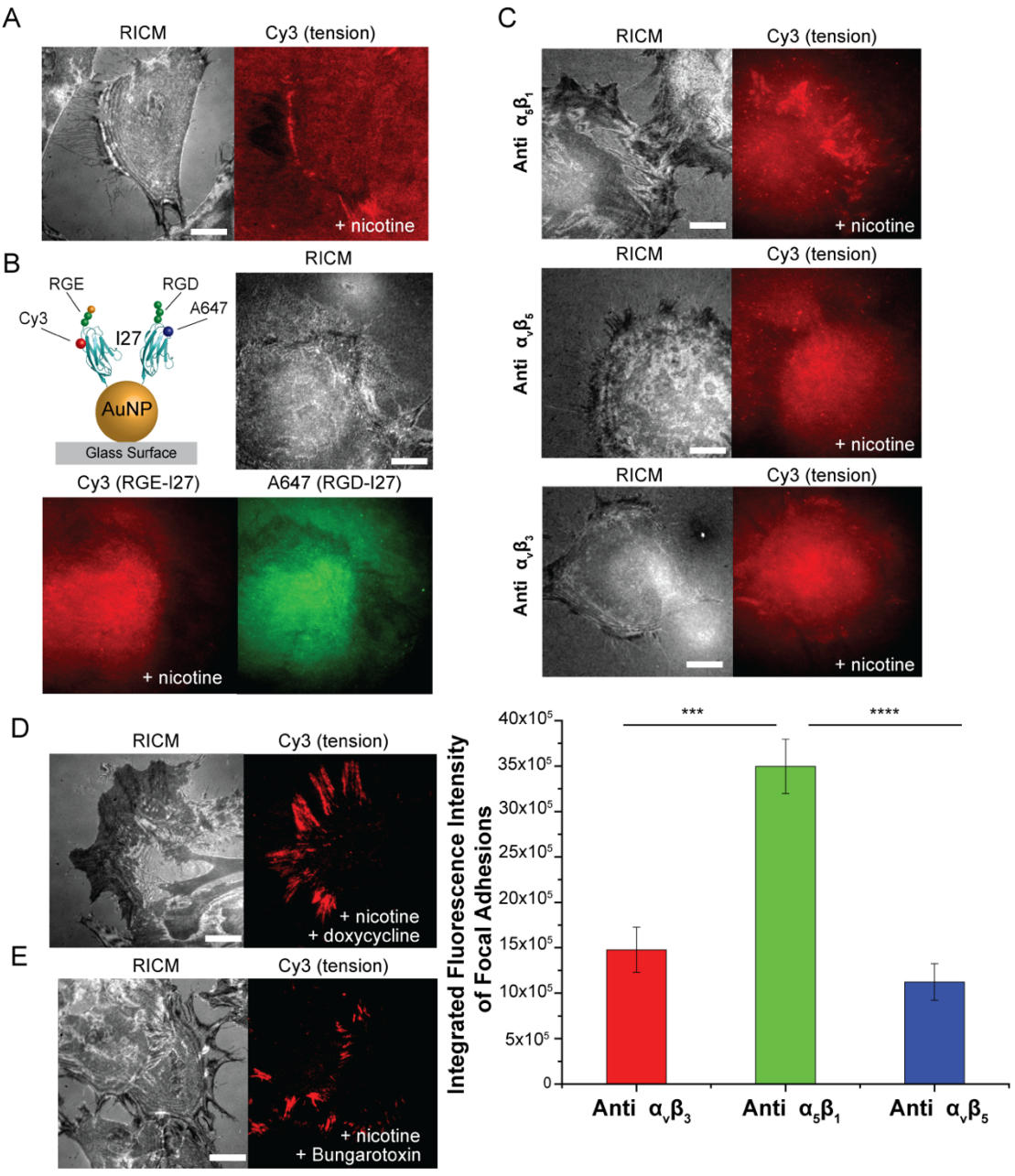
A
RICM
Cy3 (tension)
+ nicotine
B
RGE
RGD
Cy3
A647
I27
AuNP
Glass Surface
RICM
Cy3 (RGE-I27)
A647 (RGD-I27)
+ nicotine
C
RICM
Cy3 (tension)
Anti $\alpha_6\beta_1$
+ nicotine
Anti $\alpha_v\beta_5$
+ nicotine
Anti $\alpha_v\beta_3$
+ nicotine
D
RICM
Cy3 (tension)
+ nicotine
+ doxycycline
E
RICM
Cy3 (tension)
+ nicotine
+ Bungarotoxin
Integrated Fluorescence Intensity of Focal Adhesions
40x10^5
35x10^5
30x10^5
25x10^5
20x10^5
15x10^5
10x10^5
5x10^5
0
***
****
Anti $\alpha_v\beta_3$
Anti $\alpha_5\beta_1$
Anti $\alpha_v\beta_5$

Figure A3.4 Chronic treatment of human ASM cells with nicotine causes a release of matrix metalloproteinases (MMP). (A) Representative RICM and fluorescence images of ASM cells treated with 50 μg/ml of nicotine for 72 h and seeded on the RGD-Cy3-I27 tension sensor for 2 hr. Note dark, negative signal at the sites of adhesion. Scale bar, 10 μm. (B) Human ASM cells were treated with nicotine for 72 h and were seeded on the surface coincubated with the RGD-A647-I27 and RGE-Cy3-I27 sensors for 2 h to visualize protease activity. Both channels showed negative signal which suggested that the proteases were cleaving off the sensors from the AuNPs. Scale bar, 10μm. (C) Representative RICM and fluorescence images of human ASMCs that were treated with 50 μg/ml of nicotine for 72 h, blocked with monoclonal antibodies against $\alpha_v\beta_3$, $\alpha_5\beta_1$, and $\alpha_v\beta_5$ integrins for 30 min before seeding the cells on the RGD-Cy3-I27 sensor surface. The error bars represent SEM from n = 20 cells for each condition (*** $P \leq 0.001$, **** $P \leq 0.0001$). Scale bar, 10μm. (D) Representative RICM and integrin tension images of ASM cells treated with 50 μg/ml of nicotine for 72 h and 4 μg/ml of doxycycline, MMP inhibitor, for 24 h before adding the cells on the RGD-Cy3-I27 sensor surface. Incubating cells with doxycycline inhibited the release of MMPs as observed in a positive fluorescence signal in the fluorescence channel. Scale bar, 10 μm. (E) Representative RICM and RGD-Cy3-I27 tension images of ASMCs treated with 50 μg/ml of nicotine and 5 nM of α-bungarotoxin (BTX), antagonist toward α7-nAChR, for 72 h. Incubating cells with bungarotoxin inhibited the release of MMPs as observed in a positive fluorescence signal in the fluorescence channel. Scale bar, 10 μm.

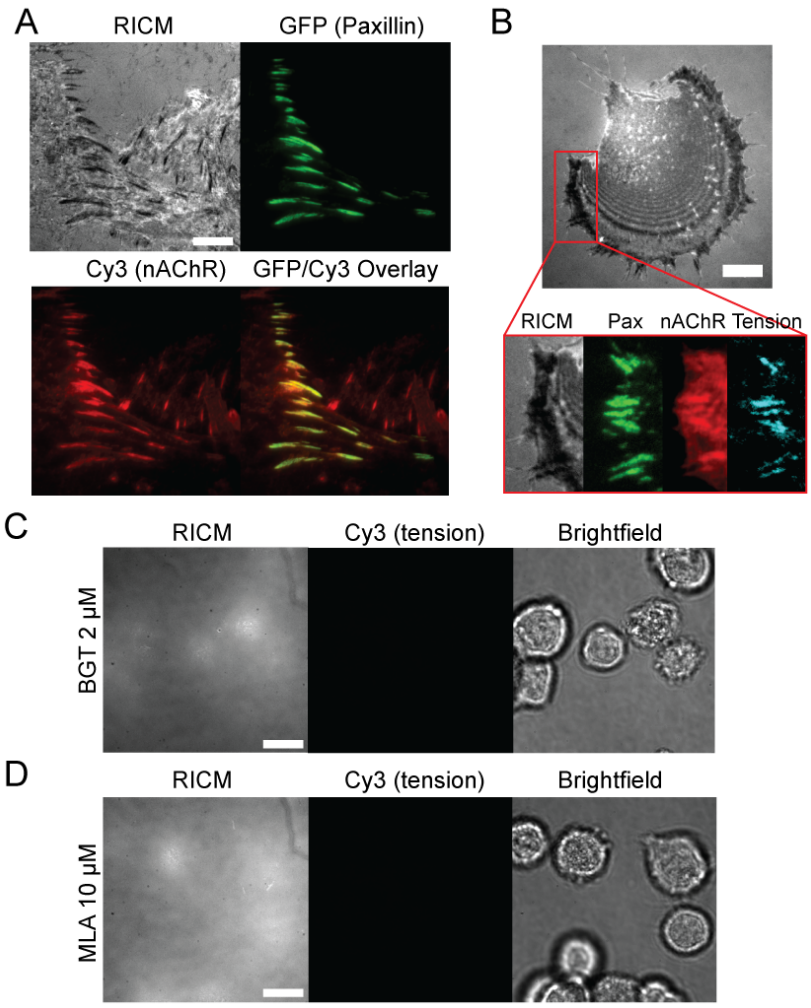

Figure A3.5 Nicotinic acetylcholine receptor (nAChR) is colocalized with the focal adhesion protein and integrin tension signal. (A) Representative RICM, TIRF-488 (GFP-paxillin), TIRF-561 (Cy3-nAChR), and GFP/Cy3 overlay of human ASM cells transfected with GFP-Paxillin and fixed and stained with α-Bungarotoxin-tetramethylrhodamine. Scale bar, 10 μm. (B) Representative RICM, GFP-Paxillin, Cy3-nAChR, and integrin tension images of human ASMCs cultured on the RGD-Cy3-I27 nanoparticle fluorescence sensor. Scale bar, 10 μm. (C-D) Representative RICM, tension and brightfield images of human ASM cells pretreated with selective antagonists toward the α7 nAChR: bungarotoxin (BTX, 2 μM) and MLA (methyllycaconitine, 10 μM) for 1 h. Scale bar, 10 μm.

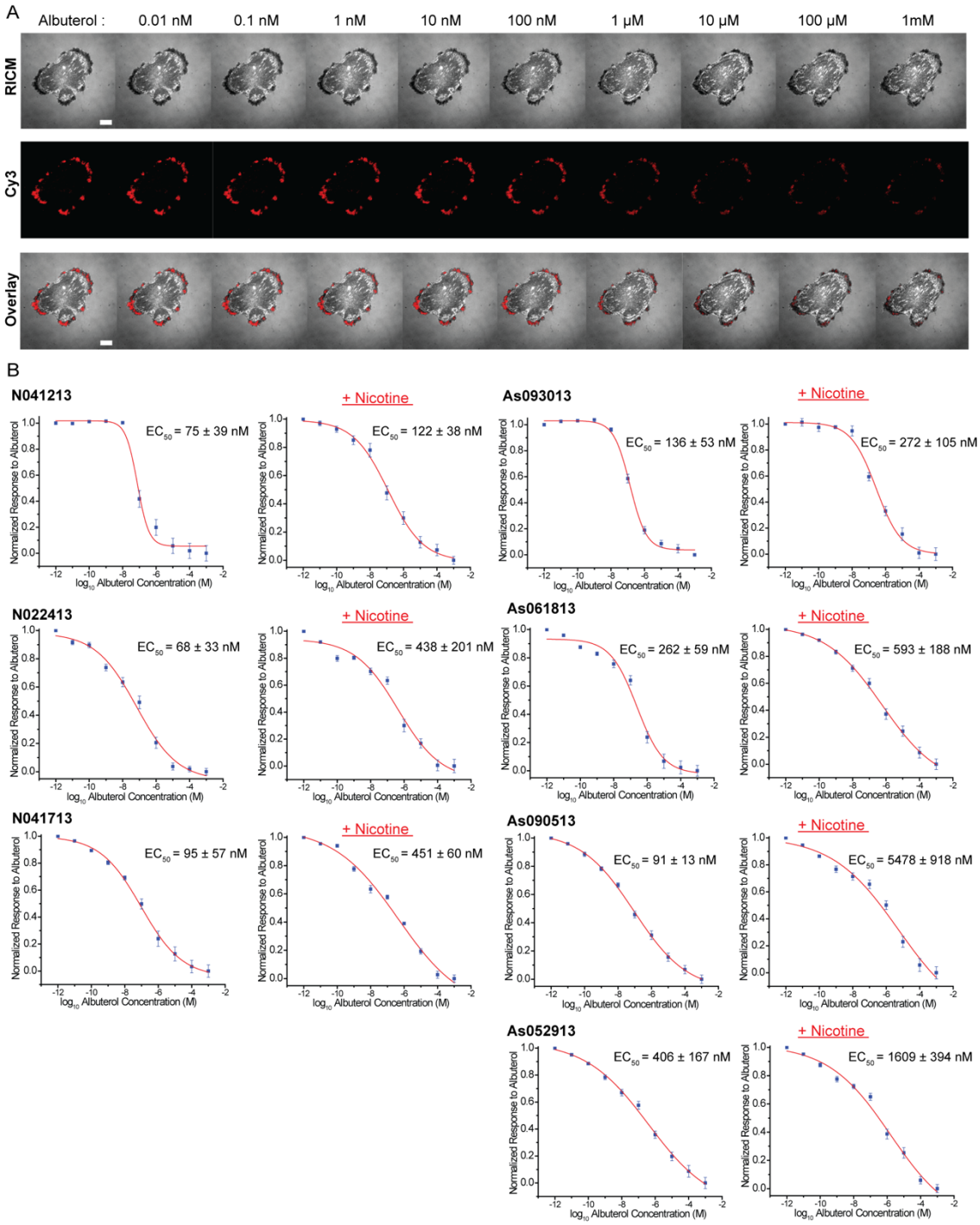
A
Albuterol :
0.01 nM
0.1 nM
1 nM
10 nM
100 nM
1 μM
10 μM
100 μM
1mM
RICM
Cy3
Overlay
B
N041213
EC50 = 75 ± 39 nM
+ Nicotine
EC50 = 122 ± 38 nM
As093013
EC50 = 136 ± 53 nM
+ Nicotine
EC50 = 272 ± 105 nM
N022413
EC50 = 68 ± 33 nM
+ Nicotine
EC50 = 438 ± 201 nM
As061813
EC50 = 262 ± 59 nM
+ Nicotine
EC50 = 593 ± 188 nM
N041713
EC50 = 95 ± 57 nM
+ Nicotine
EC50 = 451 ± 60 nM
As090513
EC50 = 91 ± 13 nM
+ Nicotine
EC50 = 5478 ± 918 nM
As052913
EC50 = 406 ± 167 nM
+ Nicotine
EC50 = 1609 ± 394 nM
Normalized Response to Albuterol
log10 Albuterol Concentration (M)

Figure A3.6 Dose dependent curves of integrin mediated tension with and without the chronic treatment of nicotine (50 μg/ml) for 72 hours. (A) Representative RICM, integrin tension, and overlay of RICM and tension images for a single, nicotine and doxycycline treated, normal ASM cell adhered on the RGD-Cy3-I27 tension surface and treated with a stepwise addition of albuterol (0.01 nM – 1 mM). Scale bar, 10 μm. (B)Normal human ASM cells were harvested from the diseased patients who died from natural causes. These samples are labeled N041213, N022413 and N041713. Asthmatic human ASM cells were harvested from the diseased patients diagnosed with a severe asthma. There samples are labeled As093013, As061813, As090513, and As052913. All the patient samples are age and gender matched. R^2 values associated with all these fits were >0.98

Chapter 4: Biological applications of MTFM sensors in cancer biology

4.1 Introduction

Cell-matrix adhesions, such as focal adhesions (FAs), are crucial in cell migration and invasion.[1-2] In cancer, metastatic cells form a unique structure called invadosome which shares numerous common proteins with FAs but are drastically different in their architecture and dynamics.[3] Invadosomes are composed of an actin-rich core, that penetrates perpendicularly into neighboring tissues, and is surrounded by adhesion and scaffolding proteins.[4-5] In contrast to the more stable elongated morphology of FAs,[6] invadosomes present a life-span between 2 and 20 min[7] and their dynamic is coupled with the local activation and/or exocytosis of matrix metalloproteases (MMPs) for matrix degradation.[8] Thus, these protein structures involved in transmitting mechanical forces play a key role in cancer invasion and metastasis.[9] An understanding of how integrin-transmitted forces regulate invadosome dynamics during cell migration and invasiveness is fundamental to understanding cancer metastasis. However, conventional imaging and biochemical techniques are insufficient to provide the necessary spatial-temporal resolution to investigate the invadosome-associated forces at the molecular level. In this chapter, we will comprehensively compare the morphology and the mechanics of focal adhesions and invadopodia by mapping cell-generated forces with MTFM sensors introduced in chapter 2.

4.2 Results and Discussion

4.2.1 Titin-based MTFM sensor reveals that leader and follower cell lines isolated from a 3D tumor spheroids have different mechanical phenotypes

Cancer cells invade into surrounding tissues through a collective cell invasion, in which cohesive groups of cells remain connected and consequently migrate as one pack.[10-11] Although cell movement appears to be coordinated, the cellular invasion pack is phenotypically heterogeneous in which cells leading the pack, leader cells, exhibit the highest metastatic potential. Despite the importance of leader cells in driving the tumor spread, these cells remain hidden within the tumor. As a result, current methods are not sufficient to separate leader cells from their 3-D environment and perform molecular and genomic analyses. To overcome this limitation, Marcus *et al*. developed spatiotemporal genomic and cellular analysis (SaGa), a novel image-guided genomics technique to specifically extract and amplify phenotypically heterogeneous cancer cells from 3-D cancer cell packs to mechanistically probe rare cancer cell behavior. They investigated

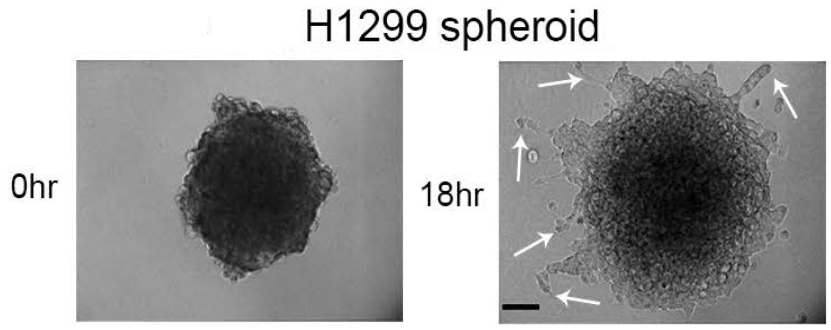

Figure 4.1 Representative confocal microscopy images of H1299 spheroids embedded in a 3D gel and imaged before and after 18 hours. White arrows point at the leader-follower collective chain invasions from which leaders and followers were isolated using SaGA technique. Scale bar, 50 μm. Reprinted from reference 18 with permission of the publisher.

the collective invasion of two lung cancer cell lines, H1299 and H1792 human non-small cell lung cancer (NSCLC) tumor spheroids (Figure 4.1), each labeled with a photoconvertible fluorophore and embedded in a 3-D environment. Next, a region of interest was drawn around the cells of interest, and upon exposure to a specific laser, cells were photo-converted and separated using flow cytometry. Thus, leader and follower cell lines were precisely isolated from collective chain invasions. Purified leader cells were clearly elongated and polarized, whereas purified follower cells demonstrated cuboidal shape. More importantly, leader cells exhibited a more migratory phenotype, raising the question whether leader and follower cells are mechanically distinct and if this mechanical divergence drives the collective migration of invasion packs (Figure 4.2).

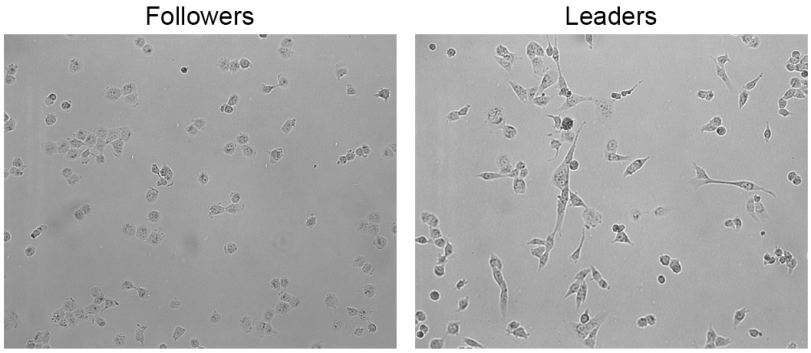

Figure 4.2 Representative confocal images of purified H1299 follower and leader cells.

To address this question of mechanical divergence, we performed MTFM measurements to probe integrin-mediated forces from both leader and follower cells. Prior to fluorescence imaging, each cell line was separately seeded on the AuNP surface decorated with the RGD-A647-I27 protein tension sensor for 2 h. Leader cells generated

significant fluorescence signals that coincided with the cell perimeter as indicated by reflection interference contrast microscopy (RICM). The fluorescence recovery of MTFM sensor indicated that leader cells applied sufficient tension (>36 pN)[12] to unfold I27. In contrast, we did not observe any detectable fluorescence signal on the surface plated with follower cells, suggesting that the adherent follower cells did not generate enough tension to unfold the probe (Figure 4.3).

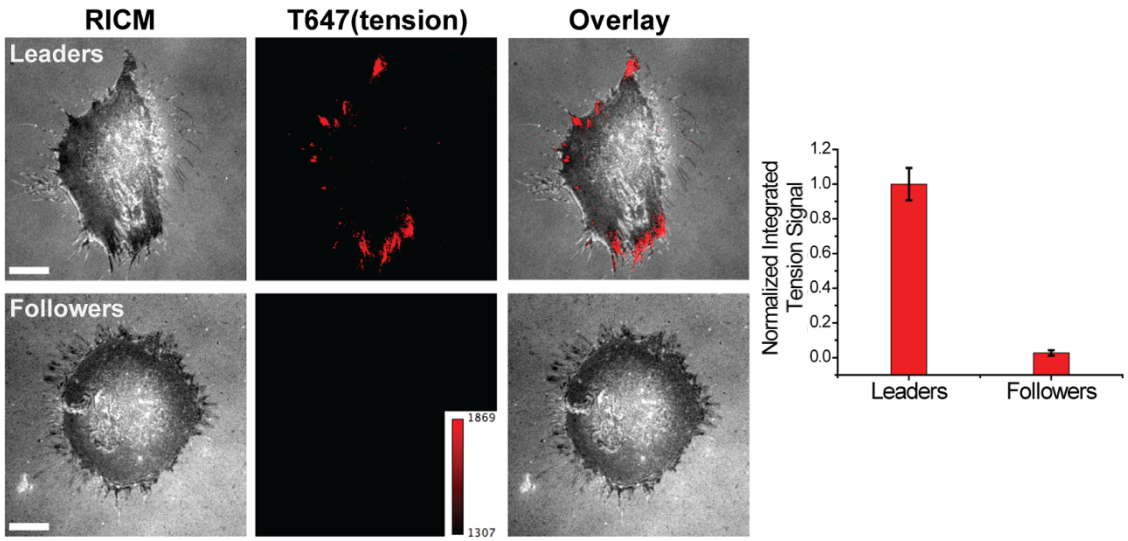

Figure 4.3 Representative RICM and tension images of H1299 follower and leader cells plated on the RGD-A647-I27 probe for 2 h. Scale bar 10 μm. Plot shows the mean tension signal generated by the cells. Error bars represent the standard error of the mean (SEM) from n = 20 cells for each cell line collected from 3 surfaces. Reprinted from reference 18 with permission of the publisher.

4.2.2 Leader cell invasion is mediated through focal adhesion signaling pathway

Focal adhesion kinase (FAK) is one of many proteins that is recruited to focal adhesion sites to regulate adhesion and motility in cells. When leaders and followers were subjected to microarray transcriptome analysis, there was an upregulation of FAK mRNA levels in leader cell spheroids when compared to follower cell spheroids. Comparative immunostaining of purified leader and follower cell lines confirmed an elevated phosphorylation level of FAK (pY397) at the leading edges of leader cells, where larger and polarized adhesion sites were observed (Figure 4.4).

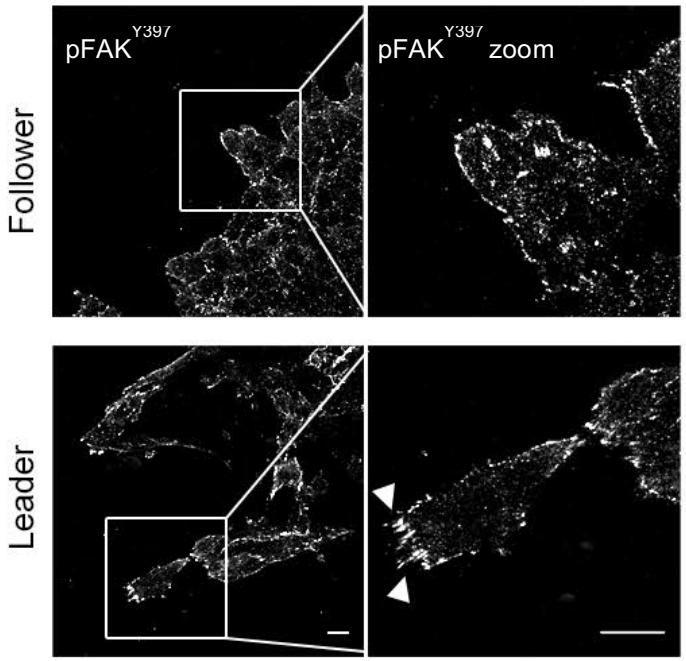

Figure 4.4 Representative immunofluorescence images of pFAK^{Y397} in H1299 follower and leader spheroids after 24 h of invasion. White arrowheads point at the larger adhesion size seen in leader cell population. Scale bar 20 μm. Reprinted from reference 18 with permission of the publisher.

To determine if the invasive phenotype of leader cell spheroids was mediated by focal adhesion kinase (FAK) activity, leader cells were pretreated with 2 μM of FAK inhibitor, and plated on the tension sensor for 2 h (Figure 4.5). As compared to DMSO control, PF-562271 inhibited leader cells displayed significantly reduced tension signal (T640 channel), suggesting not only a positive correlation between elevated FAK activity and integrin tension but also the high invasiveness of leader cells. Subsequent experiments including proliferation and motility assays not described in this chapter, led to conclusion that leader cells utilized FAK-fibronectin signaling to stimulate motility,

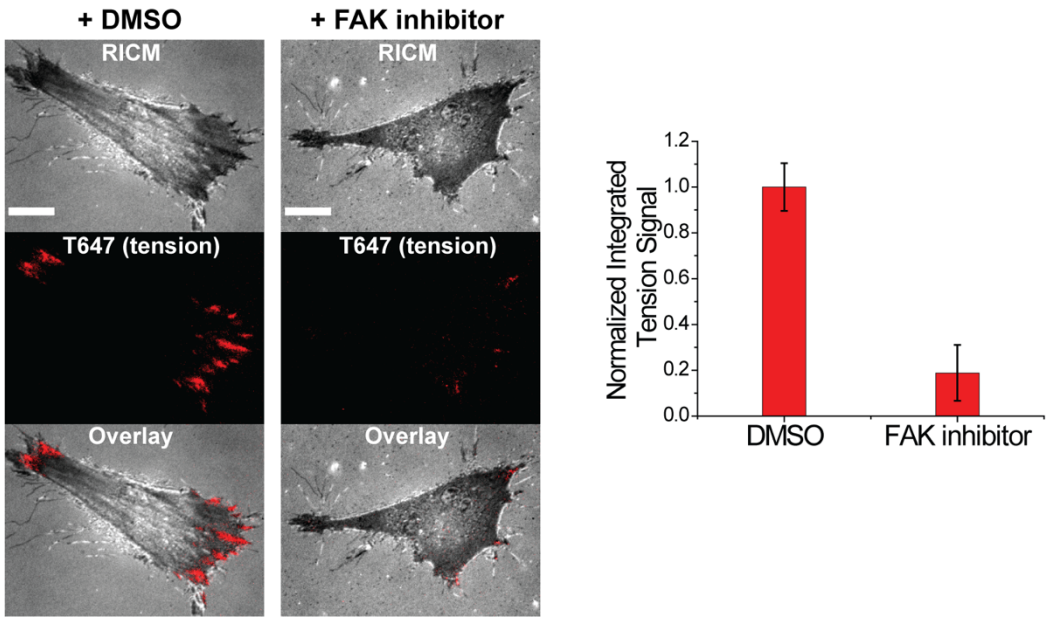

Figure 4.5 Representative RICM and fluorescence images of H1299 purified leader cells plated on the RGD-A647-I27 tension sensor incubated in the presence of either DMSO control or PF-562271 FAK inhibitor. Scale bar 10 μm. Plot shows the mean tension signal generated by the cells. Error bars represent the standard error of the mean (SEM) from n = 20 cells for each cell line collected from 3 surfaces. Reprinted from reference 18 with permission of the publisher.

and as they forged a path to escape, follower cells served to provide leaders with necessary growth and survival benefits.

4.2.3 Myosin-mediated integrin tension regulates invadosome ring dynamics

Invadosomes are dynamic actin-rich structures that adhere to the ECM through integrin receptors (Figure 4.7A).[13-14] Invadosome is a generic term referring either to podosome mostly described during physiological conditions (immune systems, bone remodelling) or to invadopodia mostly described in pathological conditions. In contrast to most of the focal adhesions, invadosomes are also the sites of matrix metalloprotease (MMPs) activity that degrade and remodel their surrounding matrix. Therefore, the

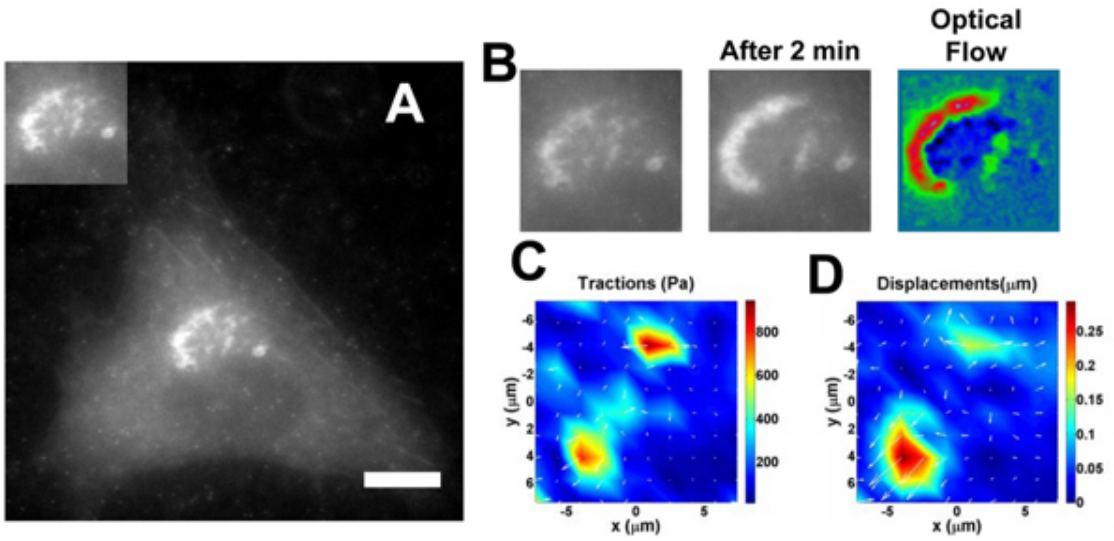

Figure 4.6 Representative image and subsequent TFM analysis of podosome ring that is exerting traction stresses on the substrate during movement in the cytoplasm. (A) Representative image of BHK-RSV cell transfected with mCherry actin cultured on the PA substrate (insert zooms in on the podosome actin ring). (B) Actin ring movement before and after 2 min. Optical flow was used to better visualize ring movement. (C) and (D) Traction forces and gel deformation, respectively. Scale bar 20 μM. Reprinted from reference 8 with permission of the publisher.

formation of invadosomes are considered as a key determinant in cancer cell invasion. Invadosomes are composed of many proteins that are also found in FAs. Besides being a mechanosensor[15], it is unknown if invadosomes transmit mechanical forces like FAs. To answer this question, researchers investigated the force transmission of invadosomes using traction force microscopy (TFM, Figure 4.6).[3, 15] When Rous sarcoma virus transformed-baby hamster kidney cells (BHK-RSV cells expressing a constitutive active mutant of the tyrosine kinase Src) were plated on the polyacrylamide (PA) gels coated with ECM proteins for cell adhesion and embedded with fluorescent microspheres for traction detection (Figure 4.6A and B), cellular force was detected underneath the two extremities of the invadosome semi-ring-like structure (Figure 4.6C and D). These results led to two hypotheses: 1) invadosome rings are not force-sensing structures and cannot exert forces underneath the substrate; 2) TFM is not sensitive enough to visualize invadosome mechanics. Indeed, the group of Maridonneau-Parini used complex inverted atomic force microscopy to show that invadosome cores can generate protrusion forces.[16]

In order to show if other regions of the invadosome could generate integrin forces, we set out to investigate if the integrin tension is distributed under invadosomes using our MTFM probes. When constitutive active Src-transformed mouse embryonic fibroblasts (MEFs) were incubated on the RGD-Cy3-I27 sensor surface for 1 h (Figure 4.7B), we observed a ring structure composed of tiny, individual dot-like actin structures in the GFP channel. Interestingly, the integrin tension signal was primarily found at the periphery of the invadosome structures but not in the center. This data clearly indicates that integrins are spatially distributed around the actin core and transmit forces to the attached matrix. This pattern of tension fits the specific pattern of β_1 integrins in invadosome rings.[17]

These delicate features of integrin forces were simply missed in TFM-based measurements, further suggesting that the pN sensitivity of MTFM probes are required for studying invadosome mechanics. To investigate the role of actin dynamics on the peripheral integrin tension, we treated the cells with 50 μM of Arp2/3 inhibitor, CK-666, that inhibited the actin polymerization in the invadosome core. Following 5 min of CK-666 treatment, the tension signal dissipated and GFP-tagged actin ring rapidly disassembled, supporting that actin-mediated cytoskeletal dynamics plays an important role in the formation and maintenance of invadosome core and producing integrin tension. To further determine whether the unfolding of the I27-based tension sensor is driven by myosin II, we treated the cells with Rho-associated protein kinase inhibitor (Y-27632, 40 μM, 20 min) and myosin light chain kinase inhibitor (ML-7, 40 μM, 10 min), respectively (Appendix, 4.1A and B). Following Y-27632 and ML-7 inhibition, tension signal was attenuated and the invadosome structures dissipated, indicating that the signal is reversible and driven by the myosin contractility. In addition, there was no new formation of invadosome structures once the cells were inhibited with any of the aforementioned drugs, suggesting that integrin tension and invadosome formation is driven entirely by the cytoskeleton.

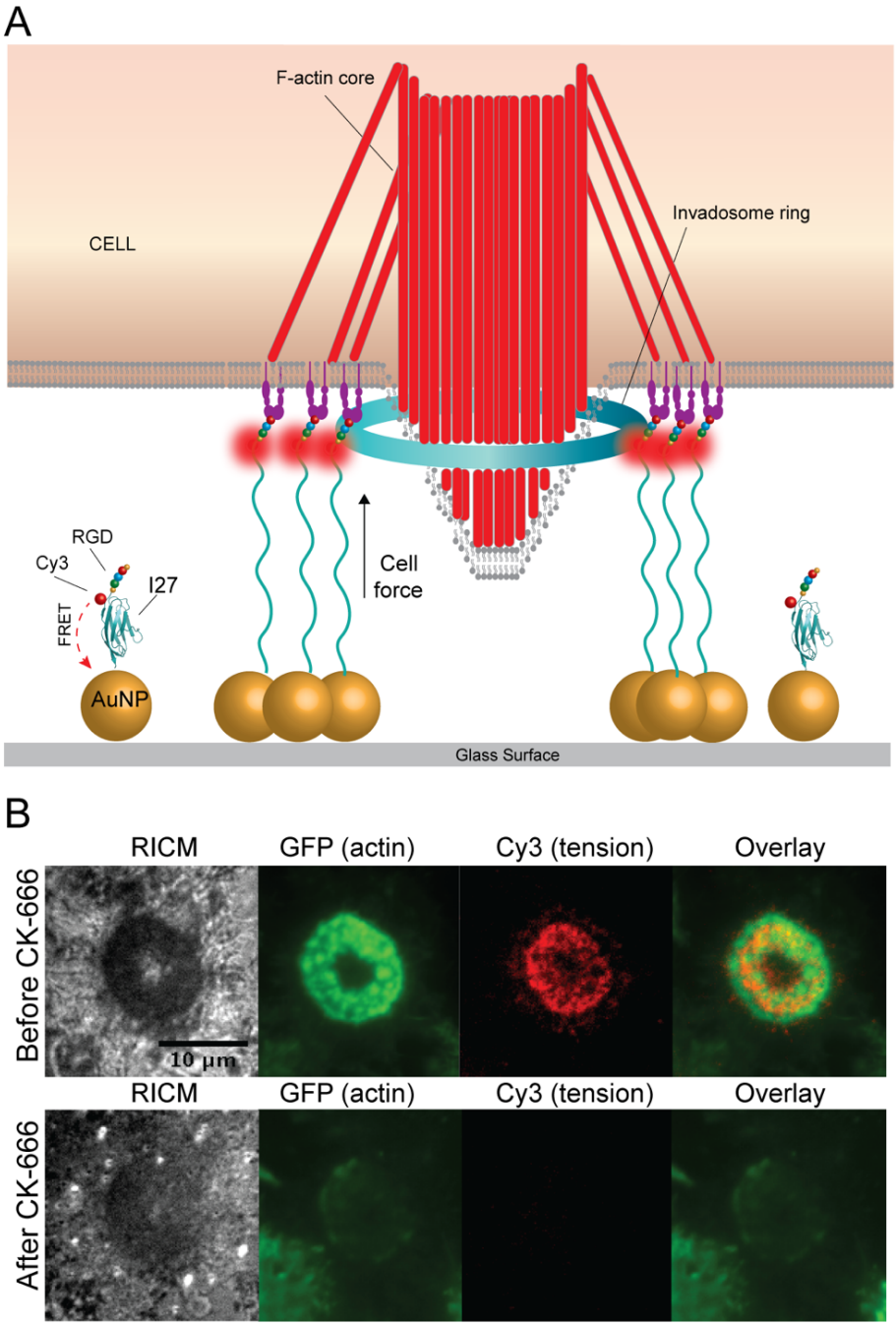

Figure 4.7 Integrin tension around invadosome rings is mediated through the cytoskeleton. (A) Schematic illustration of the I27-based MTFM sensor and its mechanism of unfolding upon integrin binding during invadosome ring formation**.** (B) Representative RICM, GFP-actin and tension images of MEF cells incubated on the RGD-Cy3-I27 sensor and displaying an invadosome ring before and after treatment with Arp2/3 inhibitor (CK-666, 50 μM) for 5 min. Scale bar, 10μm.

4.2.4 Invadosome movement in the cytoplasm is highly dynamic and is regulated by the integrins and focal adhesion signaling pathway

Besides forming small dots units, invadosome structures are highly dynamic and can assemble into a ring-like structure. To better understand the relationship between invadosome dynamics and force transmission, we captured a time-lapse movie of Src-transformed MEF cells plated on the RGD-Cy3-I27 tension sensor for 90 min (Figure 4.8). Fluorescence images of tension sensor and GFP actin show that invadosomes are highly dynamic, and their movement is accompanied by the assembly of surrounding integrin tension. To control invadosome formation, we treated the cells with the monoclonal antibodies selective for $\alpha_5\beta_1$ and $\alpha_v\beta_3$ at 10 μg/ml for 30 min and plated them on the sensor surfaces (Appendix, Figure A4.2B and C). In the agreement with the previous literature, blocking $\alpha_5\beta_1$ inhibited invadosome formation and shifted the cells to form focal adhesions at the distal edges of the cell as visualized by the increase in fluorescence signal in the sensor channel that colocalized with the accumulation of GFP-actin at the sites of adhesion (Appendix, Figure A4.2A). However, blocking the cells with the antibody toward $\alpha_v\beta_3$ integrins enhanced the formation of the invadosome rings. In addition, by incubating the cells with 2 μM of FAK inhibitor, the formation of invadosomes was further promoted. There results confirm that integrin tension at the focal adhesion sites lies directly underneath the adhesions; however in invadosomes, integrin tension is mostly localized around the invadosome structures and generates compression forces by the invadosome core. Thus, it appears that invadosome is based on antagonist and dynamic regimes of tensions inside the same structure.

4.3 Conclusion

Herein, we investigated the integrin tension response of two closely related adhesion structures: FAs and invadosomes. Even though they are alike in physical composition, they differ in structure and function. FAs anchor the cell to the ECM, sense the rigidity of the surrounding environment, and transmit mechanical forces. Our results showed that leader cells, purified from the lung tumor spheroids, generated large, polarized focal adhesions at the leading edge of the cell that corresponded with positive tension signals. On the contrary, follower cell lines did not generate sufficient tension to unfold the I27-based protein sensor. Invadosomes, in contrast, are dynamic structures that play a critical role in matrix degradation and invasion. Our results showed that invadosomes generated integrin tension around the dot-like structures to better control the movement of these structures. In all these studies, the MTFM sensors reported tension dynamics with pN sensitivity and high spatiotemporal resolution that are beyond the capability of TFM, shedding new light on invadosome mechanics at the molecular level.

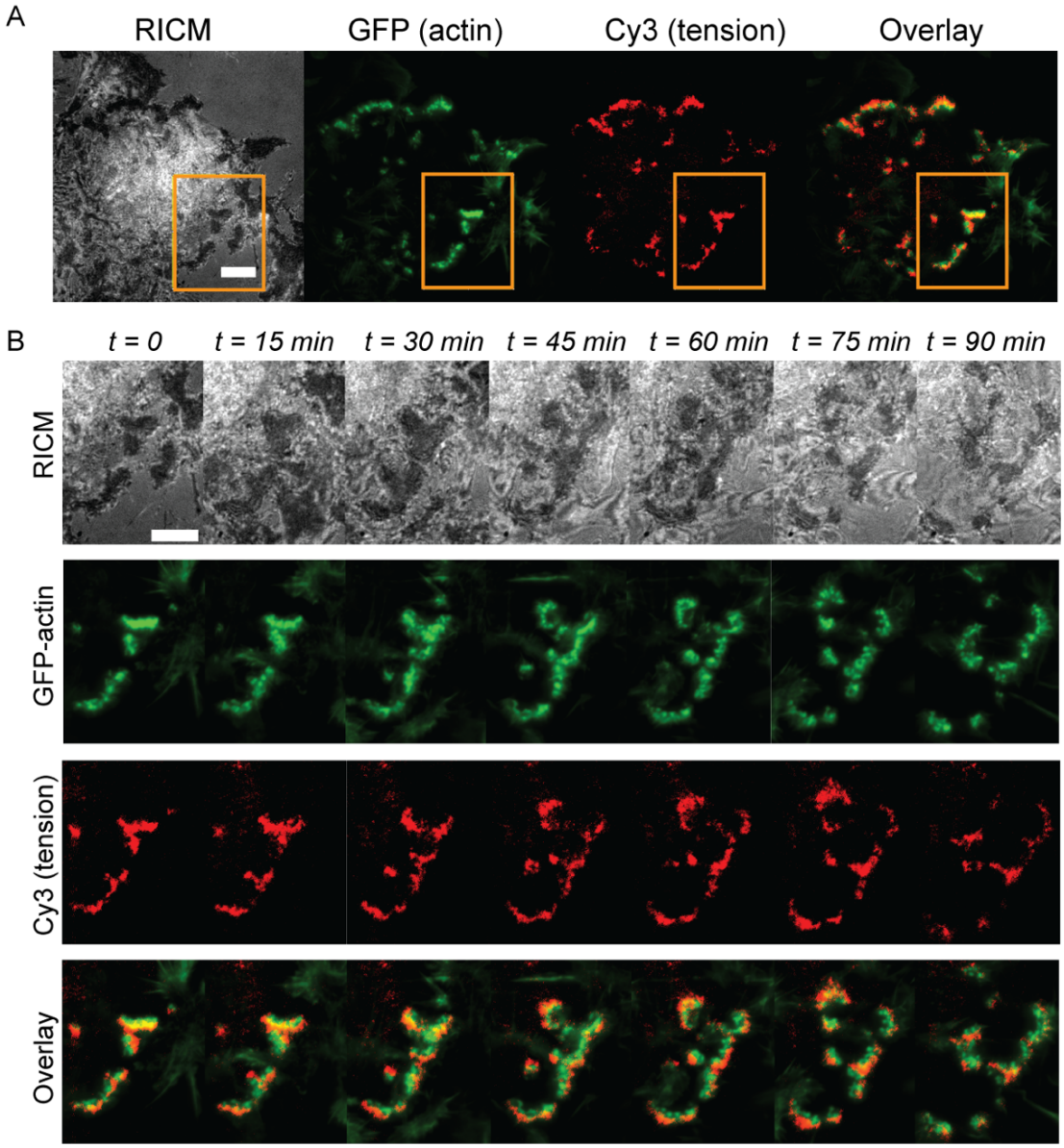

Figure 4.8 Integrin tension and actin dynamics during invadosome movement in the cytoplasm. (A) Representative RICM, GFP-actin and tension images of MEF cells incubated on the RGD-Cy3-I27 sensor. Scale bar, 10μm. (B) Zoom-in timelapse images of RICM, GFP-actin, Cy3 tension and overlay of GFP and tension signals for t = 0 to 90 min.

4.4 Methods and materials

4.4.1 Reagents

FAK inhibitor PF-562271(≥95.0%), ROCK inhibitor (Y-27632, ≥98.0%), dimethyl sulfoxide (99%, DMSO), Arp 2/3 inhibitor (CK-666, ≥98.0%), MLCK inhibitor (ML-7), potassium phosphate monobasic (≥99.0%), sodium bicarbonate and (3-aminopropyl) trimethoxysilane (97%, APTMS) were purchased from Sigma-Aldrich (St. Louis, MO). Fluorescent dye Alexa647 DIBO alkyne was purchased from Life Technologies (Grand Island, NY). 4-Azido-L-phenylalanine was purchased from Chem-Impex International (Wood Dale, IL). Ni-NTA Agarose (#30210) was purchased from Qiagen (Valencia, CA). Number two glass coverslips were purchased VWR (Radnor, PA). Lipoic Acid-PEG-NHS (MW 3400) and mPEG-NHS (MW 2000) were purchased from Nanocs (New York, NY). AuNPs of approximately 9 nm in diameter were purchased from Nanocomposix (San Diego, CA). P2 gel size exclusion beads were purchased from BioRad (Hercules, CA).

4.4.2 Cell culture

H1299 and H1792 human NSCLC cells were cultured in RPMI (Mediatech) supplemented with 10% FBS (Mediatech) and penicillin/streptomycin (100 units/ml, Mediatech) at 37 °C in the presence of 5% CO_2.

Src-transformed MEF cells with stably transfected life-act GFP were cultivated in DMEM (Meditech) supplemented with 10% FBS (Mediatech), L-glutamine (Meditech, 2.5 mM) and penicillin/streptomycin (100 units/ml, Mediatech) at 37 °C in the presence of 5% CO_2.

4.4.3 Antibody blocking

MEF cells expressing invadosomes were incubated with monoclonal antibodies selective for $\alpha_5\beta_1$ (MAB1969, Millipore) and $\alpha_v\beta_3$ (MAB1961, Millipore) at 10 μg/ml for 30 min. Additionally, 10 μg of antibody was added to each functionalized surface for full inhibition of $\alpha_5\beta_1$ and $\alpha_v\beta_3$ integrins.

4.4.4 Protein expression and dye labeling

I27 based construct was designed with N-terminal ligand TVYAVTGRGDSPASSAA and two cysteines at the C-terminal for immobilization onto AuNPs. The pET22b plasmid encoding an I27 based sensor with a TAG codon was co-transformed with pEVOL-pAzF plasmid into electrocompetent BL21(DE3) *E. coli* cells. Cells were grown at 37 °C in the presence of ampicillin, chloramphenicol, and 0.2% glucose to an optical density (OD) of 0.2, at which 1 mM of 4-azido-L-phenylalanine was added. At an OD of 0.4, L-arabinose was added to a final concentration of 0.02% (w/v) and at an OD of 0.8, isopropyl β-D-1-thiogalactopyranoside (IPTG) was added to a final concentration of 1 mM. Cells were shaken for 16 h at 30 °C, purified by Ni^{2+} affinity chromatography and stored at -80 °C in 0.1 M potassium phosphate buffer (pH 7.4). To label the protein sensors with the dye, I27 protein constructs were incubated with DIBO-A647 at the 1 – 5 ratio for 1 h at 37 °C, followed by overnight incubation at room temperature. To purify protein sensors, P2 gel size exclusion beads were used and the labeling ratio was meaured by UV-Vis absorption (NanoDrop).

4.4.5 Fabrication of protein-AuNP surfaces

Glass coverslips were piranha etched for 30 min, functionalized with an APTMS solution in acetone for 1 h and thermally annealed at 80 °C for 20 min. Subsequently, the surfaces were passivated with 5% (w/v) mPEG-NHS and 0.5% (w/v) lipoic acid-PEG-

NHS in 0.1 M fresh sodium bicarbonate overnight at 4 °C. After passivation, 12 nM of AuNPs (diameter = 9 nm) were incubated onto the surface for 20 min. Afterwards, AuNP surfaces were rinsed with water and incubated with the binary mixture of mPEG, $SH(CH_2\text{-}CH_2\text{-}O)_8COOH$ and the protein sensor in 0.1 M potassium phosphate buffer (pH 7.4) at 1:10 molar stoichiometry for 1 h at RT. The protein surfaces were rinsed with 0.1 M potassium phosphate buffer (pH 7.4) to remove unbound protein sensors. Functionalized coverslips were then assembled into a custom-made chamber and filled with cell media containing 0.5% FBS to minimize nonspecific absorption of serum proteins and used within the same day.

4.4.6 Live cell fluorescence microscopy imaging

For live cell imaging at 37 °C, Nikon Eclipse Ti microscope with Elements software was used along with the warming apparatus consisting of an objective warmer and sample warmer. The microscope features a TIRF launcher with three laser lines: 488 nm (10 mW), 561 (50 mW), and 647 nm (20 mW), an Intensilight epifluorescence source (Nikon), an Evolve electron multiplying charge coupled device (EMCCD camera, Photometrics), and the Nikon Perfect Focus system that prevents losing a focus during imaging. The microscope is equipped with TIRF 488, TIRF 640, FITC, TRITC, and RICM (reflection interference contrast microscopy) filter cubes that were purchased from Chroma (Bellows Falls, VT).

4.5 References

1. Moeendarbary, E.; Harris, A. R., Cell mechanics: principles, practices, and prospects. *Wiley Interdiscip Rev Syst Biol Med* **2014,** *6* (5), 371-88.

2. Janmey, P. A.; Miller, R. T., Mechanisms of mechanical signaling in development and disease. *J Cell Sci* **2011,** *124* (Pt 1), 9-18.

3. Block, M. R.; Badowski, C.; Millon-Fremillon, A.; Bouvard, D.; Bouin, A. P.; Faurobert, E.; Gerber-Scokaert, D.; Planus, E.; Albiges-Rizo, C., Podosome-type adhesions and focal adhesions, so alike yet so different. *Eur J Cell Biol* **2008,** *87* (8-9), 491-506.

4. Murphy, D. A.; Courtneidge, S. A., The 'ins' and 'outs' of podosomes and invadopodia: characteristics, formation and function. *Nat Rev Mol Cell Biol* **2011,** *12* (7), 413-26.

5. Albiges-Rizo, C.; Destaing, O.; Fourcade, B.; Planus, E.; Block, M. R., Actin machinery and mechanosensitivity in invadopodia, podosomes and focal adhesions. *J Cell Sci* **2009,** *122* (Pt 17), 3037-49.

6. Kanchanawong, P.; Shtengel, G.; Pasapera, A. M.; Ramko, E. B.; Davidson, M. W.; Hess, H. F.; Waterman, C. M., Nanoscale architecture of integrin-based cell adhesions. *Nature* **2010,** *468* (7323), 580-4.

7. Destaing, O.; Block, M. R.; Planus, E.; Albiges-Rizo, C., Invadosome regulation by adhesion signaling. *Curr Opin Cell Biol* **2011,** *23* (5), 597-606.

8. Mrkonjic, S.; Destaing, O.; Albiges-Rizo, C., Mechanotransduction pulls the strings of matrix degradation at invadosome. *Matrix Biol* **2017,** *57-58*, 190-203.

9. Lange, J. R.; Fabry, B., Cell and tissue mechanics in cell migration. *Exp Cell Res* **2013,** *319* (16), 2418-23.

10. Friedl, P.; Locker, J.; Sahai, E.; Segall, J. E., Classifying collective cancer cell invasion. *Nat Cell Biol* **2012,** *14* (8), 777-83.

11. Wang, X.; Enomoto, A.; Asai, N.; Kato, T.; Takahashi, M., Collective invasion of cancer: Perspectives from pathology and development. *Pathol Int* **2016,** *66* (4), 183-92.

12. Galior, K.; Liu, Y.; Yehl, K.; Vivek, S.; Salaita, K., Titin-Based Nanoparticle Tension Sensors Map High-Magnitude Integrin Forces within Focal Adhesions. *Nano Lett* **2016,** *16* (1), 341-8.

13. Marx, J., Cell biology. Podosomes and invadopodia help mobile cells step lively. *Science* **2006,** *312* (5782), 1868-9.

14. Destaing, O.; Petropoulos, C.; Albiges-Rizo, C., Coupling between acto-adhesive machinery and ECM degradation in invadosomes. *Cell Adh Migr* **2014,** *8* (3), 256-62.

15. Collin, O.; Na, S.; Chowdhury, F.; Hong, M.; Shin, M. E.; Wang, F.; Wang, N., Self-organized podosomes are dynamic mechanosensors. *Curr Biol* **2008,** *18* (17), 1288-94.

16. Labernadie, A.; Bouissou, A.; Delobelle, P.; Balor, S.; Voituriez, R.; Proag, A.; Fourquaux, I.; Thibault, C.; Vieu, C.; Poincloux, R.; Charriere, G. M.; Maridonneau-Parini, I., Protrusion force microscopy reveals oscillatory force generation and mechanosensing activity of human macrophage podosomes. *Nat Commun* **2014,** *5*, 5343.

17. Destaing, O.; Planus, E.; Bouvard, D.; Oddou, C.; Badowski, C.; Bossy, V.; Raducanu, A.; Fourcade, B.; Albiges-Rizo, C.; Block, M. R., beta1A integrin is a master regulator of invadosome organization and function. *Mol Biol Cell* **2010,** *21* (23), 4108-19.

18. Konen J, Summerbell E, Dwivedi B, Galior K, Hou Y, Rusnak L, Chen A, Saltz J, Zhou W, Boise LH, Vertino P, Cooper L, Salaita K, Kowalski J, Marcus A. Image-guided genomics reveals a vascular mimicry within during a symbiotic collective cancer invasion pack. ***Nat. Commun.*** 2017 –in press

4.6 Appendix

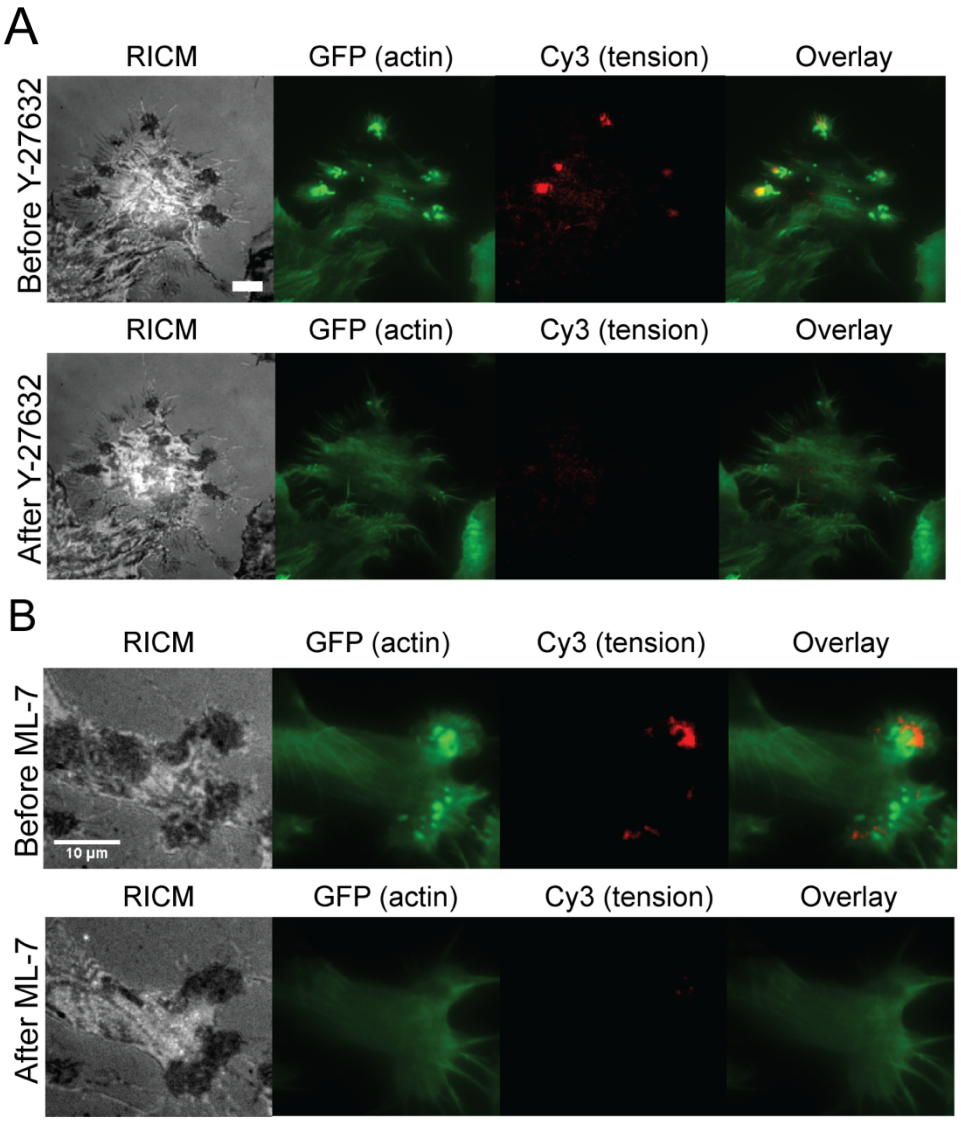

Figure A4.1 Integrin tension around invadosomes is mediated through cytoskeleton. (A) Representative RICM, GFP-actin and tension images of MEF cells incubated on the RGD-Cy3-I27 sensor before and after treatment with ROCK kinase inhibitor Y-27632 (40 µM) for 30 min. Scale bar, 10µm. (B) Representative RICM, GFP-actin and tension images of MEF cells incubated on the RGD-Cy3-I27 sensor before and after treatment with MLCK inhibitor: ML-7(40 µM) for 10 min. Scale bar, 10µm.

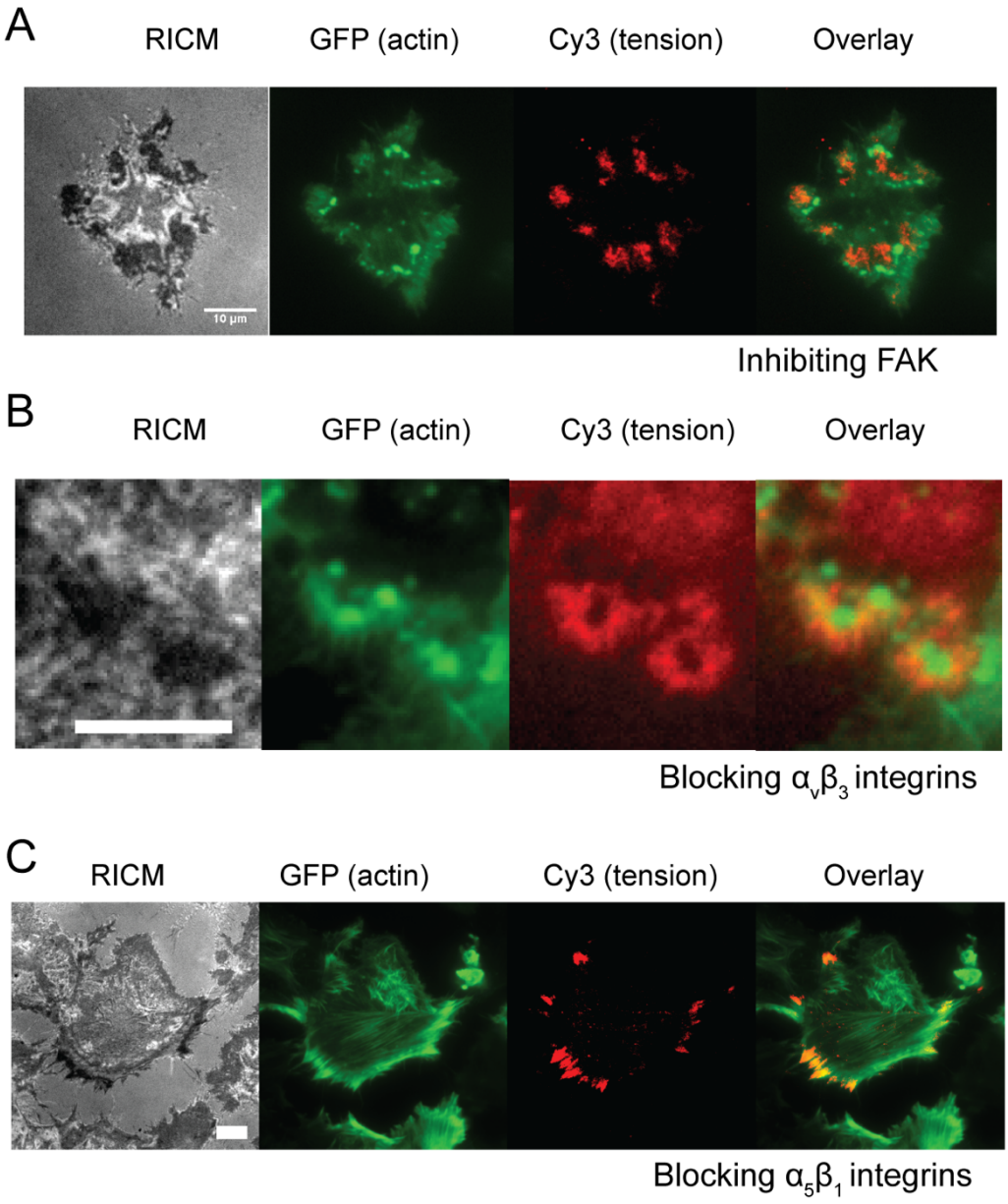

Figure A4.2 Invadosome formation is enhanced in the absence of FAK and is mediated through β_1 integrin subtype. (A) Representative RICM, GFP-actin and tension images of MEF cells pretreated with 2 µM of FAK inhibitor PF-562271 and incubated on the RGD-Cy3-I27 sensor surface. (B) and (C) Representative RICM, GFP-actin and tension images of MEF cells incubated with the monoclonal antibodies against $\alpha_v\beta_3$ and $\alpha_5\beta_1$ integrins, respectively, for 30 min before seeding the cells on the RGD-Cy3-I27 sensor surface. Scale bar, 10µm.

Chapter 5: Conclusions and Perspectives

5.1 Summary

Mechanics are an ever-present physical dimension of a cell and developmental biology. The ability of cells to sense and transduce mechanical forces into biochemical signals is crucial to their survival. Even though cell-generated forces have a profound impact during cell's lifespan, only few methods have been developed to measure these forces. Technologies such as traction force microscopy (TFM) and single molecule force spectroscopy (SMFS) that are described in **Chapter 1** are not able to provide molecular details of forces transmitted by the cells. To better understand the molecular mechanism of mechanotransduction and to quantitatively measure force transmission in living cells, we developed a novel method called MTFM.[1] These MTFM probes are used in measuring tension across the molecular links between primary adhesion receptors (integrins) and their cognate ligands in the ECM. However, Jurchenko et al. and Zhang et al. discovered that integrins apply sufficient force to rupture their probes by dissociating the streptavidin-biotin bond or denaturing DNA hairpins.[2-3] Therefore, I developed and characterized a new generation of mechano-sensitive fluorescent probes that provided greater stability and dynamic range.[4] In addition, I used these probes to investigate integrin mediated force transmission in cancer cells and in pathophysiology of asthma.

Chapter 2 presents step by step development of protein based MTFM sensor. The fundamental discovery in this chapter was that integrins apply forces in the range of hundreds of pN's per molecule – values that are 10 to 100 times greater than previously estimated. We made this discovery through three main innovations. The first was the development of a MTFM sensor based on the elastic domain of titin derived from cardiac muscle. These titin force sensors are the most mechanically stable probes reported to date,

thus mapping an extreme range of forces that were ignored previously. The single molecule force spectroscopy community has studied titin for over two decades, and herein we finally apply the molecular biophysics of this molecule to understand fundamental cell biology. The second innovation is the analysis of titin unfolding kinetics to determine the average integrin-ligand force. We clamped the titin domain with a disulfide bridge and showed that cell forces are insufficient to break the S-S bond. Finally, by adding a reducing agent, DTT, and monitoring the kinetics of disulfide reduction, we obtained the first quantitative measurement of integrin forces within mature adhesions. As a result, by measuring the kinetics of unfolding, we circumvented the inherent limitations in molecular force probe design. The third innovation was the incorporation of extracellular-matrix fibronectin domains into tension probes rather than peptide mimics; thus recapitulating the natural physiology of integrin adhesions.

In **Chapter 3**, we assessed the contractility of normal and asthmatic human ASM cells, by mapping integrin tension using titin-based sensor. Our results also elucidated that the contractile response in both phenotypes is further promoted in the presence of nicotine and that response is mediated by the nicotinic acetylcholine receptor. Most importantly, we demonstrated that we can use molecular tension as a readout for measuring drug potency at a single cell level. We performed the first mechanopharmocology study that interrogates how drugs modulate pN forces applied by integrin receptors. By plating patient samples on the tension probe surfaces and treating them with the gradual amounts of bronchodilator, we captured the relaxation of the cells as determined by the decrease in observed fluorescence and calculated the EC_{50} values of albuterol for each person. These studies

showed that MTFM probes can be used as a potential diagnostic tool for personalized medicine by assessing drug potency and contractile phenotype at the molecular level.

In **Chapter 4**, we expanded the application of the titin-based sensor to investigate the role of integrin-mediated tension in cancer biology. First, in a collaborative work with cancer biology lab, we studied a force response of rare and invasive cells that were extracted from a lung tumor using a novel image-guided technique called SaGa that precisely selected and amplified two cell lines, leaders and followers. We generated force maps for both these cell types and discovered that while leader cells were able to unfold the probe at their focal adhesions, follower cells did not generate sufficient tension to do the same. These results demonstrated that invasiveness of cells correlate with the strength of the forces applied on the tension sensor by the integrin receptors. Second, we provided, for the first time, pN tension maps of integrin forces with high spatial and temporal resolution around another form of adhesions called invadosomes, and we proved that invadosomes are mechanosensitive structures. Our results upend the current understanding of integrin mechanotransduction in invadosomes, and thus underscore the need for new models to explain molecular biophysics in invadosome formation and maturation.

5.2 Future directions

Development of MTFM probes have revolutionized our understanding of mechanical forces in cell biology.[1-9] However, there is number of modifications that could improve the next generation of protein based MTFM probes. One of the advantages of protein based MTFM probe is that it can be easily engineered to incorporate virtually any recombinant protein. As a result, we could incorporate other protein domains that have

been structurally and mechanically studied. For example, we could use spectrin dimer or xynalase monomer to serve as an alpha helical spring (Figure 5.1). Based on single molecule force spectroscopy with constant loading rate (0.8 μm/sec), the unfolding force of spectrin dimer is around 40 pN and the unfolding force of xylanase monomer is around 80 pN.[10] Thus we could have MTFM sensors with two different force thresholds as additional toolset to probe cellular mechanics because not all receptors apply forces with the same magnitude.

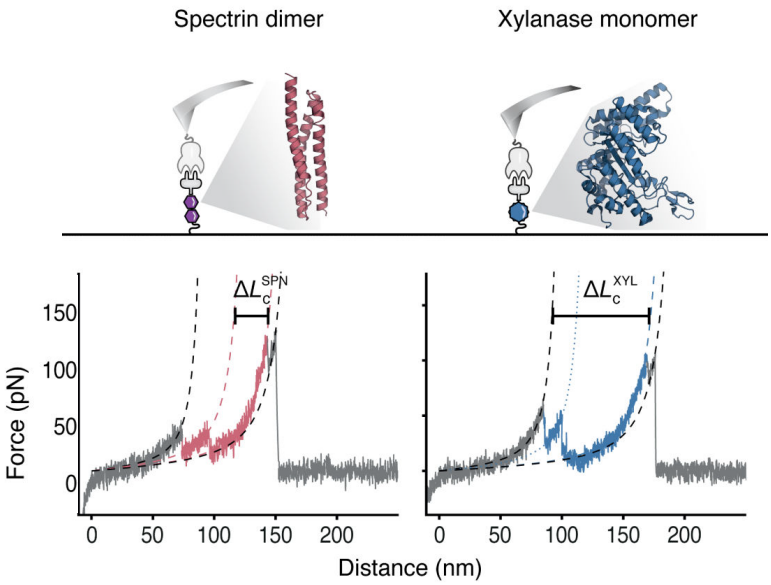

Figure 5.1 Representative single molecule force curves of spectrin dimer and xynalase monomer. Reprinted from reference 10 with permission of the publisher.

One of the disadvantages of the current fluorescence protein sensor is the limited stability of the fluorescence readout due to employment of organic dyes as spectroscopic molecular "rulers'. FRET-based tension probes use organic dyes that are prone to photobleaching, oxidation, and an upper distance limit of ~10-30 nm. As a result, we can

only image tension signal for a limited time before it photo bleaches. To improve and increase MTFM sensor stability is to replace fluorescent organic dyes with quantum dots, nanometer-sized semiconductor crystals. Quantum dots possess much higher brightness, due to their broad absorption and high quantum yields that can be quenched if placed in close proximity to AuNP.[11-12] In addition, they have superior photostability than organic dyes which enables longer exposure. Their size dependent optical properties provide more freedom in designing an optimized FRET/NSET pairs. Furthermore, quantum dots can be easily conjugated to protein by any amine cross-reactive species or click chemistry, thus allowing to develop a fluorescent inorganic QDs-based molecular force sensor. This modification would boost the temporal resolution and force imaging without photobleaching.

A third modification would be to attach protein-based MTFM probes to the surface by a covalent bond instead of thiol-gold attachment. AuNP-MTFM probes overcame the limited stability of biotin-streptavidin that was observed previously.[2] However, thiolated probes are prone to dissociating from the gold surface within 12 hours of cell incubation, likely due to a combination of thiol displacement and protease activity, which prevents from monitoring tension over a long period of time.[4] For example, we could utilize acyl carrier protein tag (ACP) that can be enzymatically modified at its serine residue with Coenzyme A (CoA).[10, 13] After functionalizing amine surfaces with NHS-PEG-CoA, we could covalently attach a protein sensor with the C-terminal ACP tag to the surface via an SFP-synthase-catalyzed reaction. The advantage of this modification would allow for long-term (>12 h) force imaging of processes important to cell development, wound healing or cell differentiation.

Last and probably the most exciting modification of the MTFM sensor would be to incorporate the sensor into a three-dimensional (3D) environment. Currently, we can generate force sensing molecular probes from cells cultured on two-dimensional (2D) glass slides. However, it is still unknown how cellular forces applied in a flat, 2D culture resemble the forces applied in a physiological 3D context. ECM in vivo is a complex environment characterized by a dynamic network of ECM components and mixed population of cells interacting in three dimensions. Many cells lose their phenotype after being taken out of their natural environment and placed into planar cell culture. The ability to recapitulate the forces applied by the cells in 3D extracellular environment with high spatial and temporal resolution would bring an enormous impact in the field of mechanobiology.

5.3 Other contributions

Additional publications that resulted from my PhD work are listed below:

- Liu Y, Ma VP, **Galior K**, Zhang Yun, Chang Yuan, Salaita K. Fluorescence Probes for Molecular Force Imaging in Living Systems. ***Accounts of Chemical Research*** 2016 – *to be submitted*
- Konen J, Summerbell E, Dwivedi B, **Galior K**, Hou Y, Rusnak L, Chen A, Saltz J, Zhou W, Boise LH, Vertino P, Cooper L, Salaita K, Kowalski J, Marcus A. Image-guided genomics reveals a vascular mimicry within during a symbiotic collective cancer invasion pack. ***Nat. Commun.*** 2017 – *in press*
- Liu Y, Blanchfield J, Ma VP, Andargachew R, **Galior K**, Liu Z, Evavold B, Salaita K. DNA-based Nanoparticle Tension Sensors Reveal that T-cell Receptors Transmit Defined pN forces to Their Antigens for Enhanced Fidelity. ***Proc. Natl. Acad. Sci.*** 2016, 113 (20), 5610-5615
- Ma VP, Liu Y, Yehl K, **Galior K**, Zhang Y, Salaita K. Mechanically-induced Catalytic Amplification Reaction for Readout of Receptor-mediated Cellular Forces. ***Angew. Chem. Int. Ed.*** 2016, 55 (18), 5488-5492
- Chang Y, Liu Z, Zhang Y, **Galior K**, Yang J, Salaita K. A General Approach for Generating Fluorescent Probes to Visualize Piconewton Forces at the Cell Surface. ***J. Am. Chem. Soc.*** 2016, 138 (9), 2901-04
- Liu Y, Medda R, Liu Z, **Galior K**, Yehl K, Spatz JP, Cavalcanti-Adam EA, Salaita K. Nanoparticle tension probes patterned at the nanoscale: impact of integrin clustering on force transmission. ***Nano Letters*** 2014, 14 (10), 5539-5546

5.4 References

1. Stabley, D. R.; Jurchenko, C.; Marshall, S. S.; Salaita, K. S., Visualizing mechanical tension across membrane receptors with a fluorescent sensor. *Nat Methods* **2011,** *9* (1), 64-7.

2. Jurchenko, C.; Chang, Y.; Narui, Y.; Zhang, Y.; Salaita, K. S., Integrin-generated forces lead to streptavidin-biotin unbinding in cellular adhesions. *Biophys J* **2014,** *106* (7), 1436-46.

3. Zhang, Y.; Ge, C.; Zhu, C.; Salaita, K., DNA-based digital tension probes reveal integrin forces during early cell adhesion. *Nat Commun* **2014,** *5*, 5167.

4. Galior, K.; Liu, Y.; Yehl, K.; Vivek, S.; Salaita, K., Titin-Based Nanoparticle Tension Sensors Map High-Magnitude Integrin Forces within Focal Adhesions. *Nano Lett* **2016,** *16* (1), 341-8.

5. Liu, Y.; Yehl, K.; Narui, Y.; Salaita, K., Tension sensing nanoparticles for mechano-imaging at the living/nonliving interface. *J Am Chem Soc* **2013,** *135* (14), 5320-3.

6. Liu, Y.; Medda, R.; Liu, Z.; Galior, K.; Yehl, K.; Spatz, J. P.; Cavalcanti-Adam, E. A.; Salaita, K., Nanoparticle tension probes patterned at the nanoscale: impact of integrin clustering on force transmission. *Nano Lett* **2014,** *14* (10), 5539-46.

7. Chang, Y.; Liu, Z.; Zhang, Y.; Galior, K.; Yang, J.; Salaita, K., A General Approach for Generating Fluorescent Probes to Visualize Piconewton Forces at the Cell Surface. *J Am Chem Soc* **2016,** *138* (9), 2901-4.

8. Liu, Y.; Blanchfield, L.; Ma, V. P.; Andargachew, R.; Galior, K.; Liu, Z.; Evavold, B.; Salaita, K., DNA-based nanoparticle tension sensors reveal that T-cell receptors

transmit defined pN forces to their antigens for enhanced fidelity. *Proc Natl Acad Sci U S A* **2016,** *113* (20), 5610-5.

9. Ma, V. P.; Liu, Y.; Blanchfield, L.; Su, H.; Evavold, B. D.; Salaita, K., Ratiometric Tension Probes for Mapping Receptor Forces and Clustering at Intermembrane Junctions. *Nano Lett* **2016,** *16* (7), 4552-9.

10. Otten, M.; Ott, W.; Jobst, M. A.; Milles, L. F.; Verdorfer, T.; Pippig, D. A.; Nash, M. A.; Gaub, H. E., From genes to protein mechanics on a chip. *Nat Methods* **2014,** *11* (11), 1127-30.

11. Resch-Genger, U.; Grabolle, M.; Cavaliere-Jaricot, S.; Nitschke, R.; Nann, T., Quantum dots versus organic dyes as fluorescent labels. *Nat Methods* **2008,** *5* (9), 763-75.

12. Samanta, A.; Zhou, Y.; Zou, S.; Yan, H.; Liu, Y., Fluorescence quenching of quantum dots by gold nanoparticles: a potential long range spectroscopic ruler. *Nano Lett* **2014,** *14* (9), 5052-7.

13. Zhou, Z.; Cironi, P.; Lin, A. J.; Xu, Y.; Hrvatin, S.; Golan, D. E.; Silver, P. A.; Walsh, C. T.; Yin, J., Genetically encoded short peptide tags for orthogonal protein labeling by Sfp and AcpS phosphopantetheinyl transferases. *ACS Chem Biol* **2007,** *2* (5), 337-46.